Dissertation

submitted to the

Combined Faculty of Natural Sciences and Mathematics

of the Ruperto Carola University Heidelberg, Germany

for the degree of

Doctor of Natural Sciences

Presented by

M. Sci. Fai Tsang

born in: Hong Kong, China

Oral examination: 23rd November, 2018.

Towards a Systematic Understanding of the

Neural Circuits of the Periaquedcutal Grey (PAG)

Referees: Dr. Kyung-Min Noh

Prof. Dr. Christoph Schuster

Summary

The midbrain periaqueductal grey (PAG) is commonly recognised as the exit relay for the coordination and execution of a wide range of instinctive behaviours, such as defense, reproduction and predation. In line with its functional diversity, are the range of inputs it receives from higher cortical and subcortical areas as well as ascending spinal pathways, and the various neurotransmitter and neuromodulatory mechanisms active in its different subregions. However, the lack of a comprehensive cell-type classification of the PAG hinders systematic investigations into the intricacies of its many behavioural roles. Here, we applied high-throughput single neuronal nucleus RNA-sequencing to profile transcriptomes of adult mouse PAG neurons. Our data revealed at least 9 distinct PAG neuronal subpopulations, marked by differential expressions of neurotransmitter, neuromodulator and ion channel genes. In addition, using a combination of optogenetic manipulations and a carefully designed defense test battery, we identified separate functions of dPAG vGlut2+, PACAP+ and Tac2+ neurons in triggering and modulating defensive behaviour. We showed that dlPAG vGlut2+ neurons project to the Cuneiform nucleus, and this projection is an output pathway for PAG elicited escape behaviour. Our work supports the existence of molecularly distinct, functionally divergent pathways in the PAG underlying defensive behaviour, and demonstrates a framework towards a systematic dissection of cell-type specific functions of complex brain regions.

Zusammenfassung

Das periaquäduktale Grau (periaqueductal grey, PAG) ist als Integrationszentrum für die Koordinierung und Ausführung einer Reihe instinktiven Verhaltens, wie Verteidigung, Fortpflanzung und Jagd, bekannt. Entsprechend seiner funktionellen Varianz ist es das Ziel vieler Regionen des Cortex, Subcortex, sowie einiger aufsteigenden Bahnen des Rückenmarks. Seine Unterrregionen sind Ort verschiedenster neuromodulatorischer Mechanismen und einer entsprechenden Vielfalt an beteiligten Neurotransmittern. Bisher erschwerte jedoch der Mangel an detaillierter Klassifikation der Zelltypen innerhalb des PAG eine systematische Untersuchung der genauen Rolle, die es in Bezug auf Verhalten spielt. Wir verwendeten high-throughput RNA-Sequenzierung, um Profile des Transkriptoms der PAG Neuronen der erwachsenen Maus zu erstellen. Anhand unterschiedlicher Expressionslevels von Neurotransmitter-, Neuromodulator- und Ionenkanalgenen konnten wir mindestens neun verschiedene Subpopulationen dieser Neuronen identifizieren. Darüber hinaus erlaubte uns die Kombination aus optogenetischer Manipulation und eines sorgfältig entworfenen Protokolls zur Untersuchung defensiven Verhaltens unterschiedliche Funktionen von vGlut2+, PACAP+ und Tac2+ dPAG Neuronen bezüglich seiner Steuerung und Regulierung auszumachen. Wir konnten zeigen, dass vGlut2+ Neuronen in den Nucleus cuneiformis (Cuneiform nucleus, CnF) projezieren und so Fluchtverhalten auslösen. Unsere Erkenntnisse stützen die These der Existenz molekular unterscheidbarer, divergenter Signalwege im PAG und zeigt eine Methode auf um die zellspezifischen Funktionen komplexer Hirnregionen zu entschlüsseln.

Statement of contributions

Some of the data presented in this thesis was acquired with the help of other members of the lab of Dr. Cornelius Gross and the EMBL core facility:

Chapter 3

All libraries were sequenced and initially filtered by the EMBL GeneCore. The setup and optimisation of the data processing pipeline was a collaborative effort between Andreas Buness, Dr. Tallulah Andrews and myself.

Chapter 4

Isabelle Prankerd carried out the Tac2 optogenetic activation experiment while I contributed to the data analysis. Isabelle Prankerd also performed some of the other behavioural experiments.

Chapter 5

Dr. Angelo Raggioli made some of the viruses used.

Acknowledgements

First and foremost, I would like to thank *Dr. Cornelius Gross* for allowing me to pursue a PhD in his lab, and for his continual support and mentoring throughout. Thank you for giving me the opportunity to invent my own project and for believing that I can carry it through.

I would like to thank also the following people:

The members of my thesis advisory committee: *Dr. Christophe Lancrin*, *Dr. Kyung-Min Noh*, and *Prof. Dr. Christoph Schuster*, for their advice and guidance throughout my PhD.

Izzie Prankerd, whom I had the pleasure of supervising and working together with, for her enthusiasm for the project and determination throughout, and for her understanding and encouragment during the stressful times.

None of these experiments could have been completed without the *members of the Gross lab,* past and present. Thanks in particular to: *Piotr Krzywkowski* for my first perfusion; *Maria Esteban Masferrer* for my first surgery; and *Daniel Rossier* and *Violetta La Franca* for my first optogenetics experiment. The welcoming, friendly, and creative lab atmosphere has made the last 4 years a lot easier and more fun.

For the establishment of the single nuclear RNA-seq pipeline, I am indebted to *Cora Chadick*, for her support and expertise during the numerous FACS and iCELL8 trials; *Andreas Buness*, for the bioinformatics discussions; and *Vladimir Benes, Tallulah Andrews*, *Valentine Svensson*, *Leo Chan* and *Marizela Kulisic* for experimental discussions and advice.

Matteo Gaetani, Roberto Voci, Valerio Rossi, Monica Serra and *Rossella Parabeni* for taking care of all the mice used in this project; and *Stefano Tatti* and *Claudia Valeri* for experimental support.

I am grateful for the financial support from the *Croucher Foundation* and *Boehringer Ingelheim Fonds* during parts of the PhD.

Ben Helsen, for proofreading this thesis.

Last but not least, my family, for always being there for me.

List of Abbreviations

Acc	Anterior cingulate cortex
AHN	Anterior hypothalamic nucleus
Aq	Aqueduct
BMA	Basomedial amygdala
CeA	Central nucleus of the amydala
Cb	Cerebellum
ChR2	Channelrhodopsin
CnF	Cuneiform nucleus
CTB	Cholera toxin subunit B
DMH	Dorsomedial hypothalamus
DR	Dorsal raphe nucleus
FACS	Fluorescence-activated cell sorting
GCaMP	Genetically encoded calcium indicators
GC	Griseum Centrale
Hab	Habituation
HVG	Highly variable gene
IC	Inferior colliculus
IL	Infralimbic cortex
LA	Lateral amygdala
LS	Lateral septum
LHA	Lateral hypothalamic area
LPB	Lateral parabrachial nucleus
MEA	Medial amygdala
mPFC	Medial prefrontal cortex
MLR	Midbrain locomotor region
MPN	Medial preoptic nucleus
NGS	Next generation sequencing
PAG	Periaqueductal grey
PC	Principal component
PL	Paralimbic cortex
PMD	Dorsal premammillary nucleus
PMV	Ventral premammillary nucleus
PPN	Pedunculopontine nucleus
PVH	Paraventricular hypothalamus
SC	Superior colliculus
SCN	Suprachiasmatic nucleus
Stim	Stimulation
VMH	Ventromedial hypothalamus
VMM	Ventromedial medulla
USV	Ultrasonic vocalisation
ZI	Zona incerta

List of Figures

Supplementary Figures

List of Tables

Supplementary tables

Table of Content

1 Introduction

1.1 Probing neural circuits underlying behaviour

> "Further, it is pointed out that although behaviourism exerts an emotional appeal because it appears radical, modern and simple, we shall find it recondite, difficult, but we may hope, scientific."
>
> - Purposive behaviour in Animals and Men, E. C. Tolman (1932)

Rene Descartes, 17th century French Philosopher, was amongst the first people to challenge the divinity of the soul. Through his observation of fountains and statues in the royal gardens of St. Germaine, he suggested that human bodies were "mere machines", lacking in soul and consciousness. Instead, he hypothesised (along with his "dualistic" contemporaries) that the soul existed separately, but could control the body through mediation of the pineal gland, which was filled with animal spirits (Weckowicz and Liebel-Weckowicz 1982).

Fast-forward 400 years (and 2000 since Aristotle and Plato, whose ideas Cartesian dualism stemmed from), we have understood that our behaviour is not controlled entirely by our pineal glands but mostly by our brains. Descartes's most important legacy, in my opinion, is the inspiration to apply rationalism and scientific methods in the study of behaviour. Behaviourists like Watson and Skinner, for example, proposed that "all behaviours are lawful and open to experimental analysis" (Skinner 1950). Tinbergen laid out a general framework of four categories of questions: function, evolution, mechanism and ontogeny, for understanding behaviour (Tinbergen 1951).

In parallel, we have known since the 19th century that the brain is composed of networks of nerves; Ramon y Cajal and Golgi described neurons, their morphologies and their connections; Hodgkin and Huxley modelled action potentials, while Katz and Fatt discovered quantal releases of neurotransmitters at synapses. The brain we know is no longer a homogeneous grey mass, but is composed of circuits of connected neurons, receiving and sending electrical and chemical signals.

While it is obvious, perhaps already from the time of Descartes, that the studies of behaviour and of the brain are linked, it is important to recognise that, historically, their immediate

motivations, and hence their levels of understanding have been very different. This led to the use of different experimental approaches, and as we dissected and parcellated the neural substrates of behaviours, simulated and described larger neural networks, we have reached a point where bridging the gap between the two seems possible.

In this section, I aim to provide a brief review of the efforts made to bridge the gap from neurons to behaviour, the experimental approaches and the techniques involved. I will highlight recent technological advances which together represent a sufficiently strong foundation to comprehensively study the neural substrates underlying specific behaviours.

1.1.1 A historical perspective

One of the first key insights into brain "components" underlying behaviour came from the studies of Phineas Gage, who famously suffered damage to his frontal lobe from a railroad accident; while he survived the accident, he became rude and impatient, completely opposite to his pre-accident polite, quiet self. It lent support to the then emerging theories of the localisation of brain functions, and implicated the frontal lobe in personality. Since then, different parts of the brain in animals have been lesioned and broad functions have been mapped to regions, e.g. the amygdala's involvement in affective and social behaviour, the ventromedial hypothalamus's role in ingestion (Wheatley 1944; Dicks, Myers, and Kling 1968). Another main technique used in the mid-20th century was electrical stimulation, which, as opposed to lesions studies, is a gain-of-function approach, which allows for investigations into the capability of the brain region. Stimulation of the mesencephalon, for example, causes freezing or running, depending on the intensity of the stimulation (Bandler, Carrive, and Depaulis 1991).

Using these two techniques together, neuroscientists gleaned insights into the "hierarchy" of brain regions in regulating behaviours; that one structure sends information to another, and lesioning downstream areas would annul the effects of stimulating an upstream region. Tract tracing experiments using anterograde and retrograde tracers, such as Phaseolus vulgaris-leucoagglutinin (PHA-L) and wheat germ agglutinin (WGA), became crucial in understanding how regions are connected with each other. This forms the foundations of the idea of behavioural circuits.

The discovery of neurotransmitters and neuromodulatory systems prompted investigations into their behavioural through local injections of agonists and antagonists of receptor systems,

neurotransmitter analogies, etc. In conjunction with electrophysiological recordings, these shed light on the finer aspects of controls of behaviours.

The above techniques have a common limitation: they are invasive, hence causing certain damage that may affect the resulting behavioural or anatomical measurement. The identification of C-fos and other immediate early genes in response to neuronal activation presented a way to label neurons involved in the behaviour of interest post-mortem, facilitating non-invasive functional mapping essentially down to single neuron level (Bullitt 1990). Coupled with tract tracing, immunostaining and/or in situ hybridisation, neuroscientists can go beyond location and anatomy, and can understand the connectivity and identity of neurons involved in a certain behaviour.

While these approaches provide insight into gross anatomical composition of behavioural neural circuits, they give little information on how behaviours are regulated or computed on a neuronal or synaptic level. This demands the use of simpler nervous systems with easily identifiable neurons and quantifiable behavioural outputs. Applying single neuron ablations, paired-recordings, patch clamp and connection mapping in invertebrate system such as aplysia, lobsters (somatogastric nervous system), and lamprey, neuroscientists gained precious knowledge on synaptic mechanisms, network motifs and pattern generators, and how these work together to compute simple behaviours (Selverston, Russell, and Miller 1976; Grillner and Matsushima 1991; Harris-Warrick and Marder 1991; Dale, Schacher, and Kandel 1988; Getting 1989). These results laid the foundations for modelling larger neural circuits and understanding the regulation of more complex behaviours.

1.1.2 Modern Techniques

The recent technological advancements in neural circuit research have two main goals: better specificity and larger scales; these are crucial for furthering studies of complex behavioural systems.

Specificity is pivotal especially for manipulation studies. The use of transgenic animals and engineered viruses made cell type specific targeting possible, thus facilitating the dissection of neural circuits beyond anatomical regions. This becomes particularly powerful in mouse and drosophila research, where efforts have been made to generate an entire transgenic toolbox, comprising knockouts/knock-ins, Cre-driver lines and Cre-dependent reporter lines and viruses. For example, the combination a Cre-driver line with a Cre-dependent retrograde virus allows the labelling and manipulation of inputs of a specific genetic identity to a specific region

of interest. Temporal specificity in manipulation studies has been greatly improved by the invention of optogenetics; neurons can be activated and deactivated instantaneously and reversibly, providing intra-subject control for behavioural experiments, which was almost impossible before (lesions are irreversible, and pharmacogenetic substrate effects last for several hours).

To understand computation in a complex circuit, one has to be able to observe and record responses from multiple regions/neurons simultaneously. This is made possible by the development of large scale recording tools, such as multielectrode arrays, that allow long term recordings of neurons across a large area of the brain. Another breakthrough came with the development of genetically encoded calcium indicators (GCaMPs), which can be stably expressed in the region and/or cell type of interest. With two-photon microscopy, and recently also an implantable microendoscope, this allowed the recording of the activities of hundreds and even thousands of neurons at the same time in live, behaving animals. The advantages of GCaMP over large scale single unit electrophysiology recording are that one can selectively record from a certain genetically marked neuronal population, and the same neurons can be repeatedly identified and recorded from across behavioural sessions and days, something that was previously only achievable in simple model organisms with several hundreds of neurons in total.

Finally, large scale connectivity mapping coupled with transcriptome information is made possible by the developments in next generation sequencing and viral tracing technologies. A well-described circuit (with each neuron's firing properties and connections comprehensively described) was exclusive to primitive model organisms like molluscs and lampreys. As an example, the Allen Brain Atlas (Lein et al. 2007), which will be referred to countless times in the subsequent sections, comprises large databases of *in situ* hybridisation and viral tracing experiments; it represents a major effort towards generating a comprehensive description of the mouse, primate and human brains.

1.1.3 Top-down vs bottom-up: what does "understanding a neural circuit" mean

Animal behaviour is the result of sequential muscular contractions, which are in turn controlled by the sequential firing of neurons connected with each other. Neuron firing is triggered by the reception of appropriate signal from an input neuron, and controlled by ion channels. It hence follows that if one can exhaustively describe all responses of every neuron to all possible signals from all its inputs, then all of behaviour could be explained. A strong proponent of this school of

thinking is Allen Selverston, who in his seminal article titled "Are Central Pattern Generators Understandable?" outlined the minimal criteria for understanding a neural circuit: (1) a characterisation of its components (neurons and their synaptic connections, (2) identification of their functional properties and (3) delineation of how these properties influence the flow of activity through the circuit, thus the circuit output and associated behaviour (Selverston 1980; Parker 2006) As mentioned in the last section, high-throughput assaying of single neuron properties in complex nervous systems, such as that of the mouse, is now technologically possible. In particular, large scale neuronal transcriptome profiling provide a quantitative, functionally relevant characterisation of a large number of neurons by essentially describing the components of the neurons, meeting the first of Selverston's criteria. Such description of the circuit components would also allow one to hypothesize their functional properties at a circuit level and how they influence the information flow through the circuit, or in other words, how they compute to produce the corresponding behaviour.

At the same time, the highly specific modern day manipulation tools facilitates finer and finer dissections of behavioural neural circuits in complex nervous systems. Many of behavioural experiments carried out nowadays involves the activation or inhibition of a molecularly defined cell type (e.g. vGlut2+) in a small brain region with certain connectivity. With a robust behavioural paradigm, circuit level functions of specific molecularly defined groups of neurons can be identified. The key to success is to make use of a robust phenotype: one that is reliable, sensitive and measurable/quantifiable such that small behavioural changes can be observed.

The mouse instinctive defensive response is an example of such behaviour. Instinctive behaviours are behaviours that do not require learning; they are often considered as hardwired and have a fixed pattern. Instinctive defense, for example, are responses against threats such as predators, and in mice includes flights and freezing (more in the following section). These are well described in the literature, and tests have been designed to measure specific aspects of the response. The brain regions, neuronal populations and their connections underlying these responses have also been extensively investigated and documented. Therefore, combining the bottom-up (building computational understanding from components characterisation) and top-down (breaking down behavioural circuits via gain and loss-of-function experiments) in the study of the mouse instinctive defense circuit has the potential of bridging the gap between molecules and behaviour, providing new insights towards an algorithmic and computational level understanding of the behavioural neural circuit.

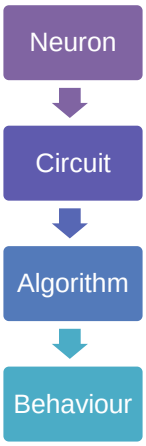

Figure 1. Levels of understanding neural circuits

1.2 Neural Circuits underlying Instinctive Defensive Behaviour

Defense against threats is a fundamental requirement of life (LeDoux 2012). Defensive mechanisms and behaviour are observed in all living things, from single cell organisms responding to noxious environmental stimuli, to animals escaping from predators. It is also one of the three classes of behaviour that ethologists classically consider instinctive (Tinbergen 1951).

There is a wide variety of defensive mechanisms that one can observe in nature: lizards changing their skin colour to match their environment, the defensive spines of hedgehogs, molluscs squirting ink to cloud their predator's vision. This diversity evolved because different predators, threats and living environments necessitated different defensive strategies. One can therefore imagine that while the objective of the defensive behaviour could be similar (e.g. fleeing from predator), some aspects of the actual response are species-specific. One also needs to acknowledge that domesticated, laboratory animals will behave differently to their wild counterparts in the fields. Hence, while we should use studies in rodents and other animals to understand general principles underlying defensive behaviour, in designing behavioural tests and paradigms to address our hypotheses, we need to consider specifically defensive responses in lab mice.

1.2.1 Innate defensive behaviours

Defensive behaviors are a group of responses or response patterns elicited by threat (D. Caroline Blanchard and Blanchard 2008). Threats are generally one of three categories: predators, aggressive conspecific, or from the environment (LeDoux 2012). Depending on the threat, animals obviously react differently, but the repertoire of their overt defensive behaviour is generally the same, consisting of namely flight, freezing, defensive attack and risk assessment (Blanchard et al. 1998; Blanchard and Blanchard 2008; Bolles 1970).

Flight is observed in mice (and also other rodents) when the predator is extremely close, or about to make contact. It is regarded as the classical "circa-strike" defense response, a vigorous attempt to flee (Fanselow and Lester 1988; Fanselow 1989). When faced with a predator in an oval runway, mice invariably run around the wall, avoiding eye contact with the predator (Blanchard, Griebel, and Blanchard 2003). Flights occur only when escape is a viable option, are oriented away from threat and towards safety, and is influenced by proximity to predator and the approaching speed of the predator (Cooper 2006; Blanchard and Blanchard 1971; Blanchard et al. 1981). Flights are accompanied by tachycardia, and closely followed by the

emission of 22 kHz ultrasonic vocalisation (USV), a widely acknowledged alarm call (Schenberg, Vasquez, and da Costa 1993; Blanchard et al. 1991). All these features of flight suggest that it is a goal-directed escape response.

Freezing is characterised by a complete absence of movement, except for that associated with respiration, and a tense body posture (M. S. Fanselow 1984). In rats, while bradycardia has been shown to consistently occur with freezing, tachycardia has also been detected during freezing to conditioned fear stimulus (Stiedl and Spiess 1997; Vianna and Carrive 2005). Both increases and decreases in USV have been observed with freezing, and these seemingly contradictory findings suggest while freezing is a general fear response, the underlying motivations can be diverse (Hagenaars, Oitzl, and Roelofs 2014; Blanchard and Blanchard 2008). Freezing occurs in response to a wide variety of threats, including but not limited to predators, conspecifics, looming stimulus, open fields and fear-conditioned tones (Hagenaars, Oitzl, and Roelofs 2014; Yilmaz and Meister 2013; Blanchard et al. 1998). In rats, when escape or concealment is not possible, or when flights are punished, freezing is the dominant response (Blanchard et al. 1981). Immobility is also frequently observed in mice and rats after flights (Blanchard, Griebel, and Blanchard 2003; Deng, Xiao, and Wang 2016; Fanselow 1991). Ethologically, the evolutionary advantages of freezing include avoiding predator detection, optimising perceptual and attentional processes, and preparation for rapid escape or defensive fighting (Hagenaars, Oitzl, and Roelofs 2014). All in all, freezing appears to be a general fear response that an animal engages in depending on the nature of the threat, the context and its internal state.

Defensive attack happens when the animal is in contact with the threat. When in forced contact with a hand-held rat, mice have been shown to attack by adopting an upright posture, biting, jump attacking and sonic vocalisation, presumably as a “last-resort” (Blanchard, Blanchard, and Griebel 2005). Whereas when faced with a conspecific threat, however, a mouse attacks its opponent by approaching (straight, laterally or via a circular path), biting (and sometimes maintaining this bite and chasing the opponent around), and standing over or on top of its opponent (Blanchard and O’Donnell 1979). Depending on the dynamics of the fight, attack is often mixed with defensive behaviour, such as boxing (standing on hind limbs and oriented towards the opponent) and freezing (Blanchard and O’Donnell 1979).

Risk assessment is considered a “pre-encounter” strategy, where animals forage beyond the known safe area (Fanselow 1991). In predatory risk assessment, after a period of no futher evidence of danger, the animal ventures into the danger zone to explore it, followed by rapid retreats; this represents a balance between risk avoidance and risk assessment (Blanchard and

Blanchard 1988). When danger appears to be absent, the duration of risk assessment and foraying grows longer. In mice and rats, risk assessment is manifested mainly in two modes: stretch-attend, where the animal orients towards the threat with fore- and hind-limbs far apart and body elongated with a low back; and stretch-approach, where the animal moves towards the threat with an elongated body and low back (Blanchard, Blanchard, and Griebel 2005; Pinel, Mana, and Ward 1989). Stretch-approach appears to be preferred when the threat is localised and discrete, possibly to allow for the animal to collect more visual, olfactory and tactile information regarding the threat, whereas when the threat is ambiguous and poorly localised, stretch-attend and freezing are dominant (Pinel, Mana, and Ward 1989). Lab mice have been shown to perform more risk assessment (and fewer flights) than wild mice (Blanchard, Griebel, and Blanchard 2001).

It is worth noting that in the presence of a threat to survival, all other survival behaviours, such as ingestion and reproduction, are suppressed (Fanselow 1994; Lima and Dill 1990; Blanchard et al. 1990; LeDoux 2012). All behaviours, including fleeing and risk assessment, require energy, and in the natural environment potential threats are always present; animals need to forage or hunt to gain energy. The prioritising of survival behaviours requires astute assessment of circumstances and internal states, which in turn necessitates interactions of the neural circuits underlying these behaviours, and the integration of sensory and other information into these circuits, to produce the most appropriate behavioural responses.

1.2.2 Subcortical circuits for instinctive defense

Through classical lesion, electrical/chemical stimulation and neural activity mapping studies, scientists have identified key subcortical structures involved in the regulation of innate defensive behaviours: the amygdala, the medial hypothalamus, and the periaqueductal grey (PAG). They receive input from sensory and cortical structures, connect with each other and output to downstream motor circuits.

1.2.2.1 Amygdala

The amygdala is the most studied brain structure in the context of emotions and fear. It is partitioned anatomically into a cortical division (comprised of the basolateral (BLA), basomedial (BMA) and lateral (LA) subdivisions) and a striatal division (comprised of the medial (MEA) and central (CeA) subnuclei) (Swanson and Petrovich 1998). Rats show a major increase in neural activity in the MEA (particularly to the posteroventral region, MEApv) specifically upon exposure to cat odour (but not control odour), whereas increased neural activity was found in MEA, BMA and LA on exposure to a living cat (Dielenberg, Hunt, and

McGregor 2001; Martinez et al. 2011). The LA has been shown to be essential for defensive responses to looming stimulus (Wei et al. 2015). Combined with the facts that the olfactory bulb projects to the MEA, and that the BMA and LA receive inputs from visual and auditory association areas, the MEA is likely to be involved mainly in processing olfactory cues from predators, while the BMA and LA in integrating visual and auditory cues (Gross and Canteras 2012; Scalia and Winans 1975; McDonald 1998; Swanson and Petrovich, 1998). Exposure to a conspecific also activates the MEA, but in a slightly different subregion (posterodorsal, MEApd), indicating threat differentiation already at the level of the amygdala (Kollack-Walker et al. 1999).

1.2.2.2 Medial Hypothalamus

The hypothalamus is composed of three distinct longitudinal zones (periventricular, medial, and lateral), divided into four rostro-caudal levels or regions (preoptic, anterior, tuberal, and mammillary). The medial hypothalamus comprises a number of nuclei arranged lateral to the paraventricular zone: medial preoptic nucleus (MPN), anterior hypothalamic nucleus (AHN), descending division of the paraventricular nucleus (PVN), ventromedial nucleus (VMH), dorsomedial nucleus (DMH) dorsal and ventral premammillary nuclei (PMD, PMV), and mammillary body (Swanson 2000).

The MEApv sends major projections to the VMH, particularly the dorsomedial subdivision (VMHdm) (Canteras, Simerly, and Swanson 1995). The VMHdm is the centre of the "predator defense behaviour control column" proposed by Swanson, which consists of VMHdm, AHN and PMD (Swanson 2000). VMHdm receives most sensory inputs from the MEApv and BMA, but also somatosenory information from the parabrachial nucleus (Canteras, Simerly, and Swanson 1995; Saper and Loewy 1980; Petrovich, Risold, and Swanson 1996). Optogenetic activation of VMHdm SF1+ neurons promotes immobility, running and jumping, while their pharmacogenetic inhibition reduces mice defensive behaviour against rats (Silva et al. 2013; Wang, Chen, and Lin 2015). Single unit recordings in the mouse VMHdm show that there are distinct populations of neurons activated during flights from and risk assessment towards a predator (Masferrer et al. 2018). There are extensive reciprocal connections between the VMH and AHN, and classical electrical stimulation of AHN triggers similar jumping and running responses to that of VMH Canteras, Simerly, and Swanson 1994; Lammers et al. 1988; Saper, Swanson, and Cowan 1978). Wang et al. found that VMH stimulation is highly effective in inducing C-fos expression in AHN (much weaker vice versa); they also optogenetically activated the VMHdm SF1+ projection to AHN, which elicited escape and avoidance, but not immobility, suggesting that the running/jumping signal is passed from VMHdm to AHN (Wang, Chen, and Lin 2015). Rat

exposure to a predator causes increase c-fos expression in especially the ventrolateral PMD (PMDvl), while lesion and pharmacogenetic inhibition of PMD reduce rodents' fear responses to predators (Cezario et al. 2008; Canteras et al. 1997; Motta et al. 2009).

Another well-studied medial hypothalamic behavioural control column regulates social fear and reproductive behaviour; this comprise the ventrolateral subregion of VMH (VMHvl), MPN and PMV (Swanson 2000; Canteras 2018; Gross and Canteras 2012). VMHvl has been shown to be important for social fear, aggression and reproduction in males and females (Lin et al. 2011; Falkner et al. 2014; Sakurai et al. 2016; Silva et al. 2013). Optogenetic activation of male VMHvl neurons can trigger attack towards conspecific males, females and inanimate objects (Lin et al. 2011). Specifically in the context of defense, it has been shown that pharmacogenetic inhibition of VMHvl, but not VMHdm, reduces defensive behaviour against aggressive conspecifics (Silva et al. 2013). More recently, in vivo neural activity recording using microendoscopic calcium imaging shows the existence of distinct neuronal ensembles that encodes for the gender of the conspecific (males vs females) which only emerges after sexual experience, suggesting experience-dependent plasticity (Remedios et al., 2017). Neural activity increases in the medial preoptic area (MPoA), dorsomedial PMD (PMDdm) and PMV in rats in response to a conspecific intruder (Motta et al. 2009). The PMV has also been shown to be involved in maternal aggression in lactating rats, suggesting that the MPN-VMHvl-PMV network could be important for all forms of social interaction (Motta et al. 2013; Canteras 2018).

The DMH is studied for its roles in regulating the circadian rhythm, and heart rate and blood pressure under stress (Chou et al. 2003; Stotz-Potter, Willis, and DiMicco 1996). It receives inputs from all hypothalamic nuclei and the PAG (Thompson and Swanson 1998). DMH neural activity is upregulated in response to both predator and intruder exposure (Motta et al. 2009).

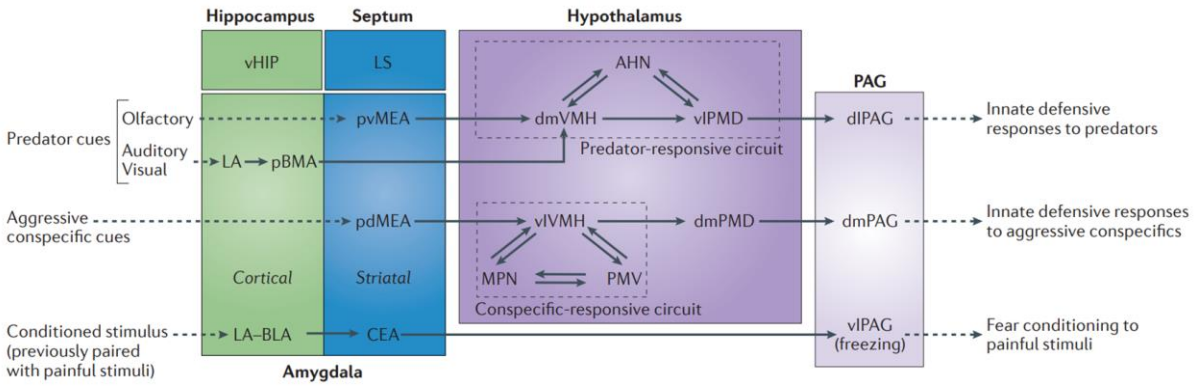

Figure 2. (Reproduced from Gross and Canteras, 2012) Separate pathways underlying different types of fear

1.3 The periaqueductal grey

The periaqueductal grey (PAG), also known as the central grey, is regarded as the final exit relay for survival behaviours, in particular for defense responses (Bandler, Carrive, and Depaulis 1991; LeDoux 2012; Vianna and Brandão 2003). It comprises neurons highly heterogeneous in their neurotransmitter profiles, connectivity and functions. In this section, I will review previous efforts to understand this complex structure that is the heart of this thesis, focusing in particular on its role in innate defensive behaviour.

1.3.1 Anatomy

Anatomically, the PAG refers specifically to the region of ventricular grey matter surrounding the midbrain aqueduct (Bandler, Carrive, and Depaulis 1991). Rostrally, as the third ventricle narrows and becomes the aqueduct, the PAG forms an oval cylindrical collection of neurons continuing from the paraventricular hypothalamus; caudally, the PAG ends as the aqueduct expands into the fourth ventricle (Keay and Bandler 2015). Other than these rostrocaudal boundaries, the boundaries of the PAG are formed by two fibre-streams: (1) the tectobulbospinal fibres originating from the intermediate and deep layers of the superior colliculus (SC), and (2) the mesencephalic trigeminal tract, which separates the PAG from the more dorsal deep layers of the SC, and the more lateral Cuneiform nucleus (CnF) (Holstege 1991). Hence, it is entirely possible that the PAG, as defined here, is a central portion of a large accumulation of neurons that form the caudal pole of the limbic system, and these "artificial boundaries" do not correspond with functional ones, and this is supported by further functional and connectivity studies on the areas around the PAG (see sections below; also (Holstege 1991)).

Early seemingly contradictory results from electrical stimulation and lesion studies have led scientists to hypothesise that there are subdivisions within the PAG (Hamilton 1973). However, there was little consensus as to how the PAG should be subdivided; in the 1970s, the two main prevailing models were based on cytoarchitectural and functional studies respectively (reviewed in (Bandler and Carrive 1988)). Through careful studies of the cytoarchitecture and neuronal morphologies, it was proposed that the PAG is subdivided into (1) a medial division closely surrounding the aqueduct, (2) a ventrolateral division, (3) a dorsolateral division, and (4) a dorsal division (Beitz 1982; Mantyh 1982). Bandler and Carrive, in attempting to demarcate a "defence region" within the PAG with microinjections of excitatory amino acids, were first to suggest a columnar organisation, stating in the discussion: "A more likely explanation of the difficulty in precisely localizing a specific part of the PAG from which a

defence reaction can be best elicited, is our finding that the 'defence region' of the PAG takes the form of a longitudinal column, which shifts its position, from dorsal to ventral, along the rostrocaudal extent of the pretentorial PAG and is not delimited by the boundaries of any PAG subnucleus." (Bandler and Carrive 1988). This is supported by the observation that afferents to and efferents from the PAG form longitudinal columns that extend at varying distances along its rostrocaudal axis (Meller and Dennis 1986; Marchand and Hagino 1983; Beitz 1982; Morrell, Greenberger, and Pfaff 1981).

In the current model, formalised by Bandler et al., the PAG is organised in 4 longitudinal columns: dorsomedial (dm), dorsolateral (dl), lateral (l) and ventrolateral (vl) (Richard Bandler, Carrive, and Depaulis 1991). Biochemically, the wedge-shaped dlPAG can be clearly marked by NADPH and cytochrome oxidase staining; dmPAG and lPAG are then defined as the NADPH-negative region medial to and below the dlPAG respectively (Conti, Barbaresi, and Fabri 1988; Carrive et al. 1997). The ventral border of the lPAG is rostrally defined by the Darkschewitsch nucleus, and caudally by the emergence of the NADPH-positive supraoculomotor cap (Carrive et al. 1997). The ventral border of vlPAG is demarcated by the NADPH-positive laterodorsal tegmental nucleus, which sits dorsolaterally to the dorsal raphe nucleus (Carrive et al. 1997).

There is little agreement as to whether the PAG should be further subdivided along the rostrocaudal axis. Indeed, there have been studies on the functions of "rostrolateral PAG" and "caudal ventrolateral PAG" in instinctive behaviours, but these areas have not been carefully defined in mice. In rats, a 6-level scheme of rostrocaudal division has been proposed (Ruiz-Torner et al. 2001). It is known that afferent terminal patterns differ within columns rostrocaudally (Beitz 1982).

1.3.2 Evolution and Development

The PAG is highly conserved evolutionarily across vertebrate species; its homologue is found in lamprey, zebrafish, reptiles, birds and mammals (Olson et al. 2017; Linnman et al. 2012; Watson, Paxinos, and Puelles 2012). The Griseum Centrale (GC), the PAG homologue in lamprey and zebrafish, receives input from the hypothalamus, pallium (cortex in mammals), pretectum, raphe and substantia nigra pars compacta (Olson et al. 2017). Reptiles GC have virtually no neurons (no 'grey' in this case), nonetheless the lizard GC seems to be a thick and complex neuropile full of varied peptidergic terminals (Wolters, ten Donkelaar, and Verhofstad 1986; Díaz et al. 2000).The rainbow trout GC is similarly rich in enkephalinergic fibres (Vecino et al.

1992). In birds, the corresponding periaqueductal midbrain stratum is poorly populated and thinner than in reptiles, but equally richly peptidergic (Puelles et al. 2007). The mammalian PAG is instead rich in both peptidergic terminals and neurons, suggesting that while the PAG's behaviour modulatory roles can have ancient origins, the neuronal bodies inside the mammalian PAG can give rise to new PAG functions not seen in lower animals (Watson, Paxinos, and Puelles 2012). The cytoarchitecture of the PAG is similar in mouse, rat, cat, macaque, and squirrel monkey, in line with the similarities observed in the PAG functional studies in these animals (Mantyh 1982; R. Bandler and Shipley 1994).

In mice, the midbrain is formed by two segments, known as mesomeres 1 and 2. Mesomere 1 encompasses the tectal grey (TG), the two colliculi (superior (SC) and inferior (IC)), and most of the PAG. Both mesomeres develop distinct domains along their dorso-ventral (D-V) axis (a common feature in the neural tube), from dorsal to ventral: roof, alar, basal and floor plates. At early embryonic stages the roof and floor plates act as the D-V axis organisers, giving the alar and basal plates their respective characteristics. The m1 alar plate has a much longer proliferative and neurogenetic program than the m1 basal plate, which gives rise to the expanse of the TG, SC, IC and dorsal PAG. Histogenetic studies in the amniote, avian and reptilian optic tectum have revealed that while cell type composition differs between the periventricular area and more superficial strata, most cell types are not confined to a single strata, and cell types which are typically periventricular in one species may be recognised as a more superficial type of neuron in another (Báez et al. 2003; Puelles and Bendala 1978). We should therefore be cautious when regarding the PAG as an isolated brain region distinct from the more dorsal colliculi (Altman and Bayer 1981)

1.3.3 Types of PAG neurons

1.3.3.1 Morphologies

Morphological studies of PAG neurons in rats, cats and monkeys with classical dyes like Nissl and Golgi have shown that they vary widely in their sizes, somatic shapes and dendritic arborisations; the degree of variation is much higher than that observed in surrounding areas like the SC (Mantyh 1982). PAG neurons can be divided into 4 morphological classes:

Class	Features	Somatic diameter	Location
Fusiform/ bipolar	Long elliptical soma with one or several dendritic processes at each end	small: 8-18μm; large 19-35μm	Most prominent in the central region around the aqueduct, also at the rostral end of the PAG
Multipolar/ Stellate	Large nucleus; extensive dendritic arbors that spread in the coronal plane	10-30μm	All areas of the PAG
Pyramidal/ triangular	Large triangular neurons with round nuclei. These have the most extensive arborisations of any cells in the PAG, with dendrites spreading to every region of the PAG and far into the SC, deep and intermediate tegmentum	15-35μm	All areas of the PAG, but more numerous and larger at the periphery than the center
Ependymal	elliptical cell body with the long axis lying at right angles to the aqueduct	15μm	Lining the aqueduct

Table 1. Morphologies of PAG neurons, summarised from (Mantyh 1982; Beitz 1985)

1.3.3.2 Electrophysiological profiles

In vitro and in vivo single unit experiments, carried out mainly in rats, have shed light on the various firing properties of PAG neurons. PAG neurons generally have variable but low baseline firing rates; dorsal and caudal PAG neurons appear to have lower spike rates than ventral and rostral ones (Sandner, Schmitt, and Karli 1986; Sandner and Di Scala 1991), although some studies did not report these regional differences (Ogawa et al. 1991). Whole-cell patch-clamp recordings from dPAG excitatory neurons reveal that excitatory neurons in dPAG have high input resistance and can fire action potentials at high frequency (Evans et al. 2018).

PAG neurons respond differently to a variety of neurotransmitters and neuromodulators, and electrical stimulation from input regions; for example, a large proportion of PAG neurons are inhibited by GABA both in vitro and in vivo (Behbehani et al. 1990; Ogawa et al. 1991). This will be further discussed in the following sections.

1.3.3.3 Neurochemical profiles

PAG neurons are mainly glutamatergic, although there are also a substantial population of GABAergic neurons (Watson, Paxinos, and Puelles 2012). All major glutamate receptor types, including AMPA, NMDA, kainate and metabotropic receptors, are present in the PAG, while the majority of neurons are inhibited by GABA (Ogawa et al. 1991; Albin et al. 1990). One of the most striking features of the PAG is the vast number of active neurotransmitter and neuromodulatory mechanisms; many neurons are shown to express genes involved in the production of neurotransmitters and/or their receptors (Lein et al. 2007). Studies done on some of these are summarised below (Table 2):

Family	**Members**	**PAG Regional specificity**	**Function in the PAG**	**Selected references**
Serotonin (5-HT)	5-HT, 5-HT receptors, serotonin transporter (SERT)	5-TH neurons mainly vlPAG, diffused in dmPAG and lPAG	5-HT generally reduces aversion and flights (except that $5HT_{2C}$ receptor activation seems to have opposite effects)	(Graeff 2004; Yin et al. 2014)
Noradrenaline (NA)	NA, NA receptors, Norepine-phrine Transporter (NET)	No NA neurons, only NA receptor + neurons	NA injected into dm/l PAG has no effect on dPAG triggered escape, but is anxiolytic; NA depolarises 54% of lPAG neurons, 85% of vlPAG neurons	(Estrada et al. 2016)
Enkephalins	Met/Leu-enkephalins, δ/κ/μ opioid receptors (OR)	lPAG has fewer μOR+ neurons; κOR+ neurons mostly in vlPAG; met-enkephalin highly enriched in dlPAG	Morphine (an OR agonist) injection in PAG is anti-nociceptive and triggers flights in dPAG and immobility in vlPAG; ORs interact with many other neurotransmitter systems and have potential roles in lordosis, micturition, etc.	(Ogawa et al. 1991; Morgan, Whitney, and Gold 1998; Matsumoto et al. 2004; Gutstein et al. 1998)
Oxytoxin	Oxytoxin, oxytoxin receptor (Oxtr)	Oxtr+ neurons concentrated in vlPAG	Oxytocin excites some PAG neurons; anxiolytic effects in mother rats; increases pain threshold	(Yang et al. 2011; Nasanbuyan et al. 2018; Ogawa et al. 1991)

Neurotensin (NT)	NT, NT receptors (Ntsr)	NT+ neurons in all regions, more dense in l/vlPAG	NT excites PAG neurons; analgesic	(Shipley, McLean, and Behbehani 1987; Feng et al. 2015; Yin et al. 2014)
Tachykinin	NKA, NKB, Substance P (SP), Tachykinin receptors (Nk1R, Nk2R, Nk3R)	NKB+ neurons are restricted to dmPAG, NK_3 is enriched in dm/lPAG	SP is anxiogenic and promotes aversion; Activation of NK_1 mechanisms is analgesic and anxiogenic and causes immobility, while that of NK_3 is hyperalgesic and enhances exploratory behaviour	(Mongeau et al. 1998; Bassi et al. 2009; De Araújo et al. 1999)
Endocannabinoids	AEA, 2-AG, cannabinoid receptors (CB1, CB2, TRPV1)	TRPV1 enriched in lPAG	TPRV1 activation causes decreased nociception at low dose, and opposite at high dose; CB1 and TRPV1 interact with NO to modulate anxio	(Corcoran, Roche, and Finn 2015; Lisboa and Guimarães 2012)
Cholecytokinin (CCK)	CCK, CCK receptor (CCK_2)	CCK-immunoreactive fibres are highly enriched in dlPAG	CCK injection in dPAG is anxiogenic and pro-nociceptive	(Liu et al. 1994; Netto and Guimarães 2004; Lovick 2008)
Nitric Oxide (NO)	NO synthase nNOS	*Nos1* mRNA is highly enriched in dlPAG	NO scavenging in dlPAG is anxiolytic, while injecting NO donor causes flights; dlPAG NO also regulates arterial blood pressure	(Hall and Behbehani 1997; Lisboa and Guimarães 2012)
Corticotropin -releasing hormone (CRH)	CRH, CRH receptors ($CRF_{1,2}$)	/	Activation of CRF_1 but not CRF_2 in dmPAG, but not in dl/lPAG is anxiogenic and anti-nociceptive	(Miguel and Nunes-de-Souza 2011; Litvin et al. 2007; Borelli and Brandão 2008)

Table 2. Main neurotransmitter and neuromodulation mechanisms active in the PAG

1.3.4 Inputs to the PAG

The PAG receives input from a large number of cortical and subcortical structures, as well as ascending inputs from the spinal cord, reflective of its role in integrating survival behaviours, autonomic and nociceptive responses (Bandler, Carrive, and Depaulis 1991).

1.3.4.1 Cortical inputs

The major cortical input to the PAG comes from the medial prefrontal cortex (mPFC). In humans, it was shown that as the imminence of a threat increases, brain activity shifts from the mPFC to the PAG (Mobbs et al. 2007). It is postulated that while the threat is further away, the mPFC assesses alternative defensive strategies ("pre-encounter" defense), whereas the activity increase in PAG when the threat is proximal represents "circa-strike" defensive reactions (Mobbs et al. 2007; Mobbs 2018).

The mPFC projection to the PAG has been shown to be topographically organised, and this feature is highly conserved from rodents to non-human primates, despite the fact that non-human primates have a much larger PFC. In macaques, the mPFC (Brodmann areas 10, 25 and 32) projects mainly to dlPAG, cingulate cortex mainly to dm/lPAG, and orbito-insular PFC to vlPAG (An et al. 1998; Keay and Bandler 2001). In rats, the mPFC rostral prelimbic cortex (PL) projects mainly to vlPAG, caudal PL to dlPAG, anterior cingulate cortex (Acc) to dlPAG, and infralimbic cortex (IL) mainly to l/vlPAG (Floyd et al. 2000; Vertes 2004). Similar projection patterns are observed in mice; moreover, dorsal Acc was shown to project preferentially to lPAG, and ventral Acc to dlPAG (Oh et al. 2014; Fillinger et al. 2018). Acc and PL are known to serve a direct role in limbic/cognitive functions, while IL modulates visceral/autonomic activity; these functional distinctions could shed light on the behaviours regulated by these connections and PAG columns (Vertes 2004).

Other cortical areas that project to the PAG include primary motor areas projecting exclusively to l/vlPAG, and primary auditory and secondary visual areas preferentially projecting to dlPAG (Vianna and Brandão 2003).

1.3.4.2. Subcortical inputs

The CEA is the only amygdala subnucleus that substantially projects to the PAG (Franklin et al. 2017; Vianna and Brandão 2003). This projection has been shown to be a disinhibitory pathway targeting glutamatergic neurons in vlPAG and drives immobility (Tovote et al. 2016).

In the hypothalamus, all the aforementioned "medial hypothalamic defensive" nuclei project to the PAG, though the columnar specificity varies: the PMD projects almost exclusively to dlPAG, PMV to dl/lPAG, DMH and VMH to dm/lPAG and MPN and AHN to mostly lPAG (with sparse terminals in dmPAG) (Canteras, Simerly, and Swanson 1992; Canteras and Swanson 1992; Thompson and Swanson 1998; Risold, Canteras, and Swanson 1994; Canteras, Simerly, and Swanson 1994; Simerly and Swanson 1988). More laterally, the lateral hypothalamic area (LHA)

sends a GABAergic projection to the l/vlPAG, and when optogenetically activated in mice, it drives predatory hunting towards crickets, supporting a strong role of PAG in predatory behaviour (Li et al. 2018). Dorsolateral to the LHA is the Zona Incerta (ZI), which also sends GABAergic projections to l/vlPAG (Chou et al. 2018). This projection inhibits excitatory neurons in the PAG and decreases freezing to conditioned fear stimulus (Chou et al. 2018).

In the superior colliculus, excitatory neurons synapse onto vglut2+ neurons in dPAG at a high rate, but the connection is weak and unreliable; it is hypothesized that the dPAG integrates visual threat information from recurrent excitatory networks in the deep medial SC (Evans et al. 2018). At the level of the oculomotor nucleus, the dorsal raphe projects to both the dlPAG and vlPAG; the dorsal raphe projection to dlPAG is inhibitory and serotonergic, and could potentially modulate dPAG-mediated defensive behaviours (Vianna and Brandão 2003; Lovick 1994).

1.3.4.3 Inputs from the spinal cord and brainstem

The spinal cord and laminar spinal trigeminal nucleus send topographically organised, predominantly crossed projections to the l/vlPAG in monkeys, cats and rats (Keay et al. 1997; Keay and Bandler 2001; Blomqvist and Craig 1991). PAG-projecting neurons are present in both superficial and deep dorsal horn, with ~50% coming from C1 to C3 segments (Keay et al. 1997). These afferents are somatotopically organised, with lumbar enlargement neurons afferenting to caudal PAG, and spinal trigeminal and cervical enlargement neurons afferenting progressively more rostrally (Keay and Bandler 2001). Interestingly, there is a substantial population of neurons in the intermediate and ventral grey matter of the sacral spinal cord that projects to l/vlPAG; this region is a major site of termination of both pelvic visceral (including nociceptive) afferents via pelvic nerves, and cutaneous perineal afferents via the pudendal nerve, and the function of this projection is yet to be addressed (Keay et al. 1997).

In the hindbrain, PAG-projecting areas include the lateral paragigantoreticular nucleus (part of the ventromedial medulla), medullary reticular nucleus and nucleus ambiguus (Oh et al. 2014; Klop, Mouton, and Holstege 2002).

1.3.5 Outputs of the PAG

1.3.5.1 Descending efferents

Retrograde tracing experiments showed that the cuneiform nucleus (CnF) receives inputs from the PAG, exclusively from the dorsolateral column (dlPAG), and the SC (Redgrave et al. 1988). The CnF is activated by predator odour and dPAG stimulation, and optogenetic excitation of the

CnF excitatory neurons can elicit high speed, synchronous-gait movement (Dielenberg, Hunt, and McGregor 2001; Sandner et al. 1992; Caggiano et al. 2018). The CnF is part of the mesencephalic locomotor region (MLR) together with the pedunculopontine nucleus (PPN), which also receives input from the PAG, and the excitatory neurons in these two regions control gait and locomotion (Caggiano et al. 2018).

PAG also project to the lateral parabrachial nucleus (LPB) with columnar specificity: dm/dlPAG projects to the superior region of LPB (LPBS), while l/vlPAG innervates the dorsal and central LPB as well as the surrounding crescent areas (Meller and Dennis 1991). The LPB has been shown to be important for cardiovascular responses and thermoregulation; inhibition of LPB neurons reduces dPAG evoked cardiovascular changes (Davern 2014; Hayward 2007).

More caudally, all columns of the PAG except dlPAG send direct projections to the caudal raphe nucleus and the rostroventral lateral medulla (Meller and Dennis 1991; Holstege 1991). These areas are known for their roles in pain modulation and the regulation of autonomic behaviours, such as heart rate and baroreflex (Mason 2005). Only vlPAG sends direct projections to the spinal cord (Vianna and Brandão 2003). dPAG also projects to locus coeruleus, Barrington's nucleus and nucleus retroambiguus (Luppi et al. 1995; Cameron et al. 1995; Holstege 1991). The locus coeruleus is a norepinephrinergic nucleus well-studied for its role in the sleep/wake cycle and stress response, the Barrington's nucleus is involved in micturition, and the nucleus retroambiguus in vocalisation; these projections can be responsible for the autonomic aspects of defensive behaviour (Sasaki 2005; Berridge and Waterhouse 2003; Holstege 1991).

1.3.5.2 Ascending projections.

The dPAG sends strong ascending projections to the defensive hypothalamic network, especially to the DMH and AHN, while vlPAG projects substantially instead to the LHA and ZI (Meller and Dennis 1991; Cameron et al. 1995). The PAG also efferents to the thalamus, with the dPAG to the centromedial thalamus, and vlPAG to the centrolateral subdivision (Cameron et al. 1995).

1.3.6 PAG and Defense

The PAG has long been recognised as an essential coordinator of fear and defensive responses (Fanselow 1991). In delineating the subcortical defensive circuit in cats, De Molina and Husperger noted that while PAG lesion abolishes defensive responses triggered by electrostimulation of the amygdala and hypothalamus, large scale amygdalar and hypothalamic lesions did not alter defense from PAG stimulation, positing the PAG as the final output structure for defensive responses (Fernandez de Molina and Hunsperger 1962, 1959). Electrical

stimulation of the PAG in humans elicits strong fear and pain (Amano et al. 1978; Nashold, Wilson, and Slaughter 1969). In one case reported by Amano et al., the patient reported "somebody is now chasing me, I am trying to escape from him", indicative of an imminent threat (Amano et al. 1978).

Finer lesion and stimulation experiments revealed functional distinctions between different PAG areas. One of the earliest and most well-established ideas is a dorsal-ventral separation, with the dPAG being responsible for "active defense", in contrast with the vPAG for "passive" defensive strategies (Keay and Bandler 2001). Electrical and neurochemical stimulation of dPAG (which comprise dm, dl and lPAG) elicits strong "activity bursts" and flight responses in rats and cats, while those of vlPAG cause immobility, hyporeactivity and freezing (Fanselow 1991; Bittencourt et al. 2004; Vargas, Marques, and Schenberg 2000; Behbehani 1995; Bandler and Carrive 1988). Lesioning experiments have produced very similar results (Fig. 3, Fanselow 1991). The flight responses from electrical/chemical stimulation of the dPAG are accompanied by autonomic changes that indicate an increase in fear and readiness to escape: an increase in heart rate and arterial blood pressure, vasodilation in skeletal muscles, an increase in rate and depth of respiration, piloerection, and pupil dilation (Lovick 1993; Sudré et al. 1993). Stimulating the vlPAG, on the other hand, causes hypotension and bradycardia (Lovick 1993; K. A. Keay and Bandler 2001).

More recent experiments have indicated that "active" vs "passive" defense may not be the most accurate description of this functional divide. Upon exposure to a cat or predator odour, rats showed a dramatic increase in C-fos expression in dPAG, in particular in dlPAG (Cezario et al. 2008; Sukikara et al. 2010). In contrast, freezing to foot shock, or a tone conditioned to foot shock, increases C-fos expression in the vlPAG (Herry and Johansen 2014). The dPAG receives major inputs from the medial hypothalamic defense network, while the vlPAG is innervated heavily by the CEA, another structure shown to be important for conditioned fear responses and expression of freezing, suggesting the existence of parallel pathways for instinctive and learnt defensive responses in the PAG (Tovote et al. 2016; Gross and Canteras 2012). More recent pharmacogenetic, optogenetic and electrophysiological studies lent support for this hypothesis. Single unit recording in the mouse dPAG found cells firing or inhibited in response to flights from and risk assessment of a rat (Deng, Xiao, and Wang 2016; Masferrer et al. 2018). Pharmacogenetic inhibition of mouse dPAG reduces fear responses towards predators and increases investigation towards aggressive conspecifics, but no difference was recorded in freezing to foot shock (Silva et al. 2013; Franklin et al. 2017). Optogenetic activation of dPAG CamKII+ neurons promotes flight and post-flight freezing, while that of vlPAG vGlut2+ neurons

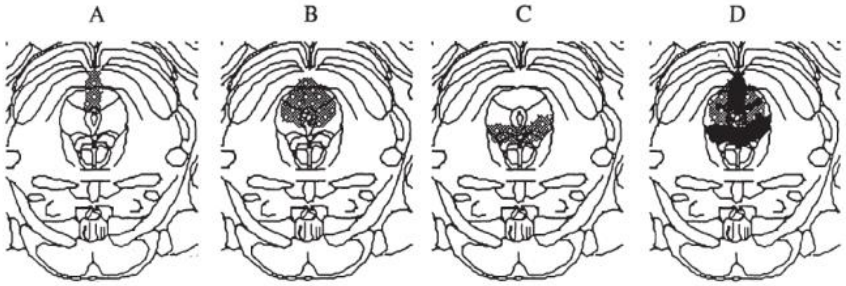

Figure 11. Examples of the electrolytic lesions of PAG examined by Kim, Gold and Fanselow. Panel A: the shaded portion indicates a lesion that affected neither freezing nor the activity burst. Panel B: The shaded portion indicates a lesion that completely eliminated the activity burst but had no effect on freezing. Panel C: The shaded portion represents a lesion that eliminated freezing but did not affect the activity burst. Panel D: The lesions which did not effect the activity burst (A and C) are superimposed in black on the lesion that eliminated the activity burst (B). It is suggested that the shaded portion on this section (D) corresponds to the areas of the PAG mediating circa-strike behavior. This region is referred to as l-PAG in this chapter.

Figure 3. (Reproduced from Fanselow 1991). Lesions of different regions of the PAG produced diverse behavioural effects, illustrating distinct functional roles of PAG columns.

causes immobility and analgesia; in contrast, optogenetic inhibition of vlPAG vglut2+ neurons abolishes freezing to tone in a conditioned cue fear paradigm (Tovote et al. 2016; Deng, Xiao, and Wang 2016). All together, the dPAG is clearly involved in instinctive, circa-strike fear responses against natural threats, and while there is a clear difference between the dPAG and vlPAG-triggered defensive responses, the role of the vlPAG in defense is more elusive. It has recently been proposed that the distinction lies in the proximity and discreteness of the threat: the most imminent threats (with very little "cognition time" allowed) are processed via the dPAG, while more distal and non-discrete threats (like a tone) activates the vPAG (Mobbs 2018).

The PAG's role in mediating defensive behaviours also comes in the context of coordinating defense with other survival behaviours, which as mentioned above, is crucial for maintaining energy balance and optimising survival strategies in response to changing external situations. The PAG has been shown to be important for maternal behaviour and predatory hunting in addition to defense (Sukikara et al. 2006; Li et al. 2018). In a series of studies, Sukikara et al., showed that activating lPAG neurons abolishes maternal behaviour in lactating female rats and induces predation, whereas in the presence of a predator, dlPAG is required to suppress maternal behaviours (Sukikara et al. 2006; Sukikara et al. 2010). Excitatory neurons in dlPAG have also been shown to synapse on GABAergic neurons in vlPAG, suggesting direct interaction between dPAG and vlPAG defensive pathways (Tovote et al. 2016). PAG local circuitry is likely to be responsible for this behavioural adaptation.

1.4 Aims of the study

In the last section, I reviewed our existing knowledge of the components (neurons and their connections) of the PAG neural circuit, and the known roles of PAG in instinctive defensive behaviour. The main knowledge gap in fully understanding the PAG defense circuit lies at the circuit and algorithmic level: how the threat signals (from afferents) are assessed, computed and transformed into the appropriate behavioural output.

The key obstacle towards understanding at this level, in line with Selverston's idea, is the lack of systematic characterisation of the PAG circuit components. While there are detailed descriptions of neuronal morphologies and connectivity mapping experiments, considering the molecular complexity of the PAG, these shed little light on the computational function of neurons and synapses at a circuit level. Hence, this study first adopts a bottom-up approach. I aim to systematically characterise PAG neurons at the molecular level using high-throughput single neuron transcriptome profiling.

At the same time, behavioural outputs of a circuit cannot be inferred by simply looking at molecular profiles or wiring diagrams: theories can be proposed, but they need to be tested. Here I propose, based on existing research, that molecularly distinct subpopulations of PAG neurons regulate different aspects of instinctive behaviour. We test this theory systematically using a top-down approach, by screening for behavioural changes evoked by cell type specific activation. We hope to demonstrate that a combination of these two approaches will lead to new insights towards a comprehensive understanding of the PAG neural circuit.

2 Methods

2.1 Animals

C57BL/6 and CD-1 mice were obtained from local EMBL or EMMA colonies, or from Charles River Laboratories. CD-1 intruders were selected as aggressors if they attacked during the first 3 min after placement in the home cage of a novel C57BL/6 mouse across 3 consecutive days, and non-aggressors if they do not show aggressive behaviours for 10 mins in a novel C57BL/6 mouse home cage.

Male C57B6/J wild-type mice, 8-10 weeks old, were used for single neuronal nuclei RNA-seq experiments. Male C57B6/N BAC-Vglut2::Cre (Borgius et al. 2010), PACAP-IRES-Cre (Krashes et al. 2014), and Tac2-Cre (Mar, Yang, and Ma 2012) were used for optogenetic manipulations. All behavioural experiments were performed on mice of at least 8 weeks old.

Mice were maintained in a temperature- and humidity-controlled facility on a 12-h light–dark cycle (lights on at 07:00) with food and water provided ad libitum. All behavioral testing occurred during the animals' light cycle. All mice were handled according to protocols approved by the Italian Ministry of Health (#137/2011-B, #231/2011-B and #541/2015-PR) and commensurate with NIH guidelines for the ethical treatment of animals.

2.2 Single neuronal nuclei RNA-seq

2.2.1 PAG cell/nuclei isolation and FACS sorting

The single cell isolation protocol is adapted from (Zeisel et al. 2015)). Mice were sacrificed by cervical dislocation and the brains are immediately harvested and placed in ice-cold oxygenated slicing solution (87 mM NaCl, 2.5 mM KCl, 1.25mM NaH_2PO_4, 26 mM $NaHCO_3$, 75 mM sucrose, 20 mM glucose, 1 mM $CaCl_2$, and 2 mM $MgSO_4$) Cortical tissue is manually dissected and quickly minsed with a scalpel before immediately being dropped into cold HBSS solution (Sigma). The dissected tissue is dissociated using the Papain Dissociation System according to manufacturer's instruction (Worthington Biochem). Cell density in the suspension is estimated with a haemocytometer and a brightfield microscope.

The PAG nuclei dissociation protocol is similar to that described in (Lacar et al. 2016) with some modifications. After brain extraction (detailed above), a coronal mouse brain matrix (Harvard Apparatus) was used to cut 1mm sections that contain the PAG (3-4 sections), and the PAG was punched using a circular punch 1.25mm in diameter (WPI) from the sections. Punches are immediately placed into ice-cold nuclei isolation medium (sucrose 0.25 M, KCl 25 mM, MgCl2 5 mM, Tris-Cl 10 mM, dithiothreitol, 0.1 % Triton, 0.4U/ul RNAse Inhibitor (NEB cat #M0314L)). Tissue was Dounce homogenized, 10 strokes with the loose pestle followed by 10-12 strokes with the tight. Samples were then 35um filtered, spun down (600rcf at 4°C) and resuspended in nuclei storage buffer (sucrose, MgCl2 10 mM, EDTA, Tris 10 mM and 0.2U/ul RNAse inhibitor) containing anti-NeuN-AF488 antibody (Merck #MAB377X, 1:2000). After 15 minutes of staining, the nuclei are spun down and resuspended in fresh nuclei storage buffer with DAPI (1ng/ml, Sigma).

Single nuclei were sorted using a BD FACSAria III (BD Biosciences). DAPI positive nuclei were gated first, followed by exclusion of debris using forward and side scatter pulse area parameters (FSC-A and SSC-A), exclusion of aggregates using pulse width (FSC-W and SSC-W). Neuronal nuclei were gated based on NEUN fluorescence, and 3000 NeuN+ events were sorted directly into each of the 8 source wells on a 384-well plate (TakaraBio), each well already containing the dispense solution (DAPI 0.3ng/ml, ERCC 1:1mil, 0.4U/ul RNAse inhibitor, 1x secondary diluent in nuclei storage buffer). Nuclei were sorted with a 100-um nozzle at 22.5 PSI sheath pressure. The number of NeuN+ events sorted has been optimised to maximise the number of single nucleus wells on the chip (see below).

2.2.2 Nanogrid single nucleus system

The single nuclei suspension in the 384-well plate is dispensed by a multisample nanodispenser (Takara Bio ICELL8™ system) that uses microsolenoid-control to precisely dispense 50nL volumes into the nanowells, onto a nanogrid chip. The nanogrid chip is has a 5184 wells (150nL each) in a square layout, each preprinted with barcoded primers (UMIs) with poly(dT) ends during manufacturing. The dispense takes approximately 15 minutes, with 3 pauses where the single nuclei suspension is manually mixed by gentle pipetting to ensure even nuclei density within the source wells. The chip is centrifuged at 300g for 3 min to collect cells in a single imaging plane before being transferred to the automated imaging system, which composed of an Olympus BX43 microscope fitted with a 4x objective, a robotic stage, and a CCD camera that is programmed to take images of all wells using a customized version of μManager open source software. The imaging process takes ~10 minutes, immediately after which the chip is sealed, put on dry ice and transferred to the -80°C freezer until reverse transcription (RT).

After adjusting the contrast of images, wells containing single round DAPI stained objects were manually identified and selected using the CellSelect™ software. The software generates a map that instructs the nanodispenser to deposit RT reagents only into the selected wells.

2.2.3 Library construction and RNA-seq

Frozen chips were thawed on ice, and 50 nL of RT solution (88 μL 5 × RT buffer, 44 μL 10 mM RT dNTPs, 4.4 μL 100 μM RT-E5OLIGO, 57.2 μL D-RNase-free water, 0.2% Triton, and 26.4 μL 200 U/μL RT enzyme) was deposited into each selected well using the nanodepositing system. After RT, cDNA products from selected wells were pooled together, purified (with DNA Clean & Concentrator, Zymo Research), and underwent exonuclease I treatment (2 μL 10× exonuclease buffer, 1 μL 20 U/μL exonuclease I, NEB) to remove unannealed primers. The pooled barcoded cDNA libraries then underwent PCR amplification (5 μL 10× amplification buffer, 1 μL 50× amplification dNTPs, 1 μL amplification primer, 1 μL amplification enzyme, 22 μL D-RNAse free water) for 18 cycles. The PCR products were purified with 0.6× AMPure XP beads and eluted in 12 μL D-RNase free water. The concentration of the full-length cDNA library was quantified using the Qubit dsDNA HS fluorometric assay, and the library was diluted to 0.2ng/ul to construct Nextera XT (Illumina) DNA libraries with i7 index primers following the manufacturer's instructions. The size distribution of the final library was QCed using Agilent's High Sensitivity DNA chip on the Bioanalyzer system.

The sequencing of the library was carried out by GeneCore at EMBL Heidelberg on the NextSeq2500 system (Illumina). It was sequenced paired-end asymmetrically, 21/26 cycles from the barcoded end (read1) and 71/66 cycles (read2) from the other. Data were processed using the CASAVA 1.8.1 pipeline (Illumina Inc.), and sequence reads were converted to a master FASTQ files.

2.2.4 Data processing

Read qualities are first checked with FASTQC. The master FASTQ files containing total reads was demultiplexed into individual fastq files with each representing one single nucleus using a Perl script and the list of barcodes from selected wells. Maximum 2 mismatches to barcodes are tolerated. The reads are then trimmed from adapters, polyA and polyG using cutadapt (Martin 2011); reads <15bp post-trimming are discarded. Reads are then mapped to the annotated genome and ERCCs using STAR (Dobin et al. 2013), and mapped features are counted with FeatureCounts (Liao, Smyth, and Shi 2014). Finally, UMI-tools are used for deduplicate reads that came from the same transcript based on UMI-gene assignment pairing (Smith, Heger, and Sudbery 2017); the tools was ran with “directional” error correction. This results in a table, with the number of transcripts for each gene in each nucleus (well barcode), for downstream analysis.

2.2.5 Data analysis

The data is first read into an annotated data frame with the R package Scater (McCarthy et al. 2017). First, all nuclei with <700 transcripts, more than 2% counts assigned to mitochondrial genes and 5% attributed to ERCCs are discarded. Also, only genes that has are detected across all three chips, have mean expression >0.001 per chip and are expressed in at least 3 nuclei per chip are retained. This leaves 3581 nuclei and 18654 genes. Next, the filtered data is loaded into Seurat (Satija et al. 2015), which is used for log normalization (scale factor=10,000); the chip and number of UMI are regressed out. Qualitative parameter scanning was used to optimise the highly variable gene (HVG) expression (Supplementary figure 3). The final chosen parameters are: mean expression lower bound: 0.05, mean expression upper bound: 2, dispersion lower bound: 1; resulting in 2146 HVG chosen for principal component analysis (PCA). The principal components (PCs) were chosen based on results from Seurat’s Jackstraw implementation and manual screening and exclusion of PCs that are highly differentially expressed between the chips. These were used for clustering and t-distributed stochastic neighbour embedding (t-SNE) visualisation Clustering was performed using Seurat’s implementation of the SNN-CLiP algorithm, using the default distance calculation (Louvain) algorithm. Unsupervised clustering

was performed with default parameters k=30 and resolution=0.8. Cluster marker identification was performed using the Wilcoxon Rank Sum test for differential expression in Seurat, with the threshold of percentage expression set at 0.10, threshold for average log fold change at 0.25 and adjusted p-value <0.05. This revealed 2 subclusters that are highly enriched in ribosomal genes, so these are removed from downstream analyses (194 neurons removed).

For supervised clustering using neuron function related candidate genes, PCA on the expression of these genes were first performed, followed by Jackstraw analysis of the significance of the PCs; 4 PCs were chosen for clustering. The clustering parameter space sampled was resolution =0.6, 0.8, 1.0, 1.2 (recommended range for ~3000 cells) and k=20, 25, 30, 35, 40 (the default was 30). This resulted in 6 to 16 clusters (Supplementary Figure 4). A dissimilarity score was calculated between each pair of nuclei based on how many times they were in the same cluster (using the R function Daisy for computing euclidean distances between nominal variables). Hierarchical clustering on the matrix of dissimilarity scores was performed, and the dendrogram was cut at a distance of 0.8, resulting in 28 clusters. Clusters of fewer than 30 (less than 1% of sample size) were eliminated, as these are unlikely to be real, leaving 17 clusters. Differential gene expression analysis was performed as described above. For the extended analyses into non-candidate differentially expressed genes, only positive markers are returned for the ease of interpretation.

2.3 Optogenetic manipulation of neural activity

2.3.1 Surgeries for optogenetic activation

Isoflurane (induction 3%, maintenance 1.5%; Provet) in oxygen-enriched air was used to anaesthetize mice fixed in a stereotactic frame (Kopf Instruments). The skull surface was exposed and cleaned with 0.3% hydrogen peroxide.

For cell-type specific dPAG activation, vGlut2:cre, PACAP-IRES-Cre and Tac2:Cre animals were infused bilaterally with 60-120nl of AAV5-EF1a-DIO-hChR2(E123T/T159C)- EYFP or AAV5-EF1a-DIO-EYFP control (UNC Vector Core) using a glass capillary filled with 0.4ul of the virus. The capillary was first lowered into one side of the dPAG (AP: -4.40, L:+/-0.30, DV:-2.45 from Bregma) then the other, with a 5 min pause after each infusion before retraction of the capillary. Mice were then implanted with custom-built fibre connectors (fibre: 0.66 numerical aperture, 200µm diameter; ceramic ferrule: 230µm internal diameter, 1.25mm outer diameter; Prizmatix). For unilateral optic fibre implantation, the tip of the fibre were unilaterally lowered to dPAG, just above the viral infection sites (AP: -4.40, L:0.90, DV:-2.15 from Bregma at an angle of 26°).

For dPAG projection activation, male wild type C57B6/J mice were infused bilaterally with AAV-hSyn-hChR2(H134R)-EYFP (UNC Vector Core) in the dPAG (120nl each side). For optic fibre implantation over the CnF, fibres were implanted at an anteroposterior angle of 20° to avoid damage of the PAG in the process (AP: -5.7, L: +/-1.20, DV: -2.9 from Bregma with an AP angle of 20°).

For retrograde efferent activation, male wild type C57B6/J were injected bilaterally at CnF (AP: -4.75, L: +/- 1.30, DV: -3.80 from Bregma) with 180nl of AAV-CMV-Hi.eGFP-Cre (Penn Vector Core) mixed with AAV-hSyn-iRFP670 (to mark the site of injection) at a ratio of 2:1. Animals were then injected with a mix of AAV5-EF1a-DIO-hChR2(E123T/T159C)- EYFP and AAV5-hSyn-tdtTomato (ratio 5:1) bilaterally at the dPAG at 2 levels, 120nl at each, dorsoventrally to ensure maximum coverage of the structure (AP: -4.30, L: +/- 0.32, DV: -2.40, -2.60 from Bregma). Then custom-built fibres were implanted bilaterally over the dPAG (AP: -4.40, L:+/-1.35, DV: -2.15 from Bregma at an angle of 26°).

The implants were fixed to the skull with skull screws, superglue (Loctite Attak) and dental cement (Duralay). All fibre connectors were tested for effective light transduction before

Implantation. All animals are injected with 1 mL saline I.P. post-surgery, remained on a heat pad overnight and were given paracetamol (0.8mg/mL, Tachipirina) in their drinking water for 3 days.

For optical stimulation of ChR2, LED light (Plexon PlexBright) was applied. Light intensity was adjusted with an optical power meter (Thorlabs) to reach 5–10mW at the end of the implanted fibre stub, unless otherwise specified.

2.3.2 Optogenetically-optimised defensive behaviour test battery

All stimulation trains were generated with Radiant V2.2 (Plexon). The light is delivered from the LED lights attach to a rotary joint to the implanted fibre stub via high performance patch cables (Plexon Plexbright high performance, LC Ferrule tip). The power of the patch cables were checked at the beginning of every behavioural session. All behavioural videos were recorded with a top view camera and Biobserve Viewer, at ambient lighting.

2.3.2.1 Overt behaviour test

Animals were handled for at least 2 days before the start of any behavioural assay. For assaying overt behaviour in response to optogenetic stimulation, mice are attached to optical patch cables and placed in a novel transparent plexiglass chamber (24cm x 24cm x 24cm). They are free to explore and habituate for 5 minutes. Stimulation lasts 1 second at intended intensity and frequency, followed by 60s inter-stimulation interval (ISI). Each stimulation condition is repeated for 5 times.

2.3.2.2 Real time place preference

Animals are placed in two chambers (each 24cm x 24cm x 24cm) connected by a small door (10 cm in width) and are free to access both chambers for 10 minutes. Then, the initial preferred chamber is selected as the stimulation chamber, and for the next 10 minutes, the animal is stimulated at 10mW, 20Hz whenever it is in the stimulation chamber. If it stays in the stimulation chamber for more than 90s, stimulation is turned off for 30s before proceeding with another 90s of stimulation should the animal remain in the stimulation chamber.

2.3.2.3 Goal-directed escape assay

Animals are placed in a transparent plexiglass chamber (24 x 24 x 24 cm) with a shelter (18 x 7 x 13 cm) placed in a corner. The shelter's floor is lined with the animal's home cage bedding. Animals are free to explore and habituate for 5 minutes, or until it displays no aversion towards

the shelter, after which whenever the animal is outside of and faraway from the shelter, it is stimulated (10mW, 20Hz) until it returns to the shelter. This is repeated 3-5 times.

2.3.2.4 Anaesthetised heart rate measurement

Heart rate is measured with a pulse oximeter (Kent Scientific, kindly lent by H. Asari) with an accompanying paw clip. Animals are anaesthetised with isoflurane in a chamber before being moved to a mask supplying maintenance level isoflurane (1.5-2%). Optic fibre patch cable(s) and the paw clip are attached, then the animal is left untouched for at least 7 mins or until the heart rate is stabilised (<30 bpm fluctuation in the minute before the start of stimulation). The animal is then stimulated at a low power (5mW, 20Hz, 15ms pulse width) for 5s, followed by 115s ISI, then 5s stimulation at high power (10mW), then another 115s ISI. This is then repeated. During the whole period of anaesthetisation, the animal's body temperature is maintained with an electric heat pad (Kent Scientific) to avoid hypothermia, and any isoflurane-induced tachycardia is closely observed.

2.3.2.5 Stimulus-response paradigm

A transparent chamber-corridor-chamber apparatus (similar to the one in Silva et al., 2013, also see Fig. 13) was used to assess animal's defensive behaviour towards a predator or an aggressive conspecific in this 5/6-day paradigm). Animals are first allowed to explore the 3 chambers freely for 2 days, 15 mins each day, to habituate to the novel environment and the patch cables. On day 3, after 5 minutes for free exploration, the animal is trapped in one of the chambers (the 'stimulus' chamber) for 5 minutes. After, the animal is released from the stimulus chamber, the optical patch cables are attached, and a behavioural baselining period with no stimulation takes place for 3 minutes, followed by 3 repeats of 2 mins stimulation (10mW, 20-40 Hz), each preceded by 2 mins inter-stimulation interval. Day 4 is similar to day 3, except that when the animal is trapped in the stimulus chamber, an aggressive CD1 male (that has previously been screened for aggression) is placed in the same chamber. When the subject animal has been attacked 3 times, it is released, patch cables are attached and the behavioural baselining and stimulation follows. The CD1 remains trapped in the stimulus chamber, and the subject animal is allowed to investigate through a small mesh-covered hole (2 x 3 cm) at the bottom of the dividing barrier. On day 5, the subject animal is exposed to a rat instead of an aggressive CD1. To prevent the rat from killing the subject animal, the rat is held by the tail and perched on the edge of the box. To gather more data, a 6th day, which is a repeat of the predator test on day 5, is sometimes added.

2.4 Afferents Mapping with Cholera toxin subunit-B (CTB)

Vglut2::Cre or Gad2-IRES-Cre adult animals are first injected bilaterally in the dPAG with AAV-hSyn-DIO-mCherry (150nl each side). After one week, animals are injected with 0.5% CTB-Alexa Fluor 488 (Thermo Fisher #C34775) and 0.5% CTB-Alexa Fluor 647 (Thermo Fisher #C34778), 60nl unilaterally at CnF (AP: -4.75, L: 1.30, DV: -3.80 from Bregma), PPN (AP: -4.60, L: 1.15, DV: -5.00) or DMH (AP: -1.00, L: -0.80, DV: -5.00). The capillary is left in place for at least 10 mins to avoid CTB spread along the injection tract. Animals are perfused one week after the CTB injection.

2.5 General histological procedures

Animals are transcardially perfused, first with PBS, followed by 4% PFA in 0.1M PB. The brain is left to postfix overnight in 4% PFA at 4°C. Brains are either sectioned in PBS with the vibratome (Leica VT1000s) or cryosectioned. For cryosectioning, brains are first briefly rinsed in PBS after post-fixation, then left in 30% sucrose (in PBS) for 2 days, or until they sink the the bottom of the 15 ml Falcon tube, before flash freezing in pre-chilled isopentane. Frozen brains are stored at -80°C before they are ready to be sectioned on the cryostat (Leica CM3050s). Sections of 50/70um are taken from the area(s) of interest.

Sections are stored in PBS (and in case of long-term storage, in PBS with 0.01% sodium azide (Sigma)) before manual mounting on Superfrost Plus slides (Thermo Scientific). Sections are left to dry briefly before the addition of the mounting medium (MOWIOL) and coverslip. In experiments with no other stainings, DAPI (5mg/ml) is added directly to the mounting medium. Slides are left to dry overnight before storage at 4°C.

Widefield images are acquired with Leica LMD5, while confocal images with Leica SP5 with resonant scanning. For optogenetics experiments, placement of optic fibres and injection sites are checked and animals are eliminated from data analysis if either are out of position.

2.6. Data Analysis

2.6.1 Behavioural data analysis

Velocity and real time place preference data are obtained from automatic tracking information from the recording software. All other behaviours are manually scored using Solomon Coder (http://solomoncoder.com/) and Bonsai (http://bonsai-rx.org/), with the following criteria: flights as a sudden burst in velocity, immobility as total absence of visible movement for at least 1 second, and stretch as an elongated body shape towards the stimulus.

For heart rate changes, the baseline is taken as the average beat per minute (bpm) of the 30s before stimulation, and 60-90s after the start of stimulation; the response bpm is calculated as an average over the 30s after the beginning of the stimulation.

2.6.2 Statistics

All statistical analysis were carried out using Prism 7 (GraphPad) using recommended options. All p-values are adjusted and error bars are mean +/- s.e.m. unless otherwise noted. Group differences were determined using multiple t-test with Holm-Sidak post hoc tests, Mann-Whitney unpaired t-test, or two-way ANOVA with Tukey's post hoc tests.

3 High throughput profiling of PAG neuronal transcriptomes reveals diverse neuron types

3.1 Establishment of a pipeline for single neuronal nuclei profiling

In the 1990s, microarray hybridisation assays enabled the first comparative transcriptome analyses, despite being prone to technical biases, batch effects, etc. The advancement in next generation sequencing technologies made it possible to sequence complete mRNA libraries with increasing depth, faster turnover and lower cost. The only remaining hurdle towards obtaining single cell transcriptomes was to develop a method that can reliably construct a cDNA library from an extremely small amount of starting material (e.g. 0.1-10pg RNA from a small eukaryotic cell) (Ramsköld et al. 2012). Early single cell microarray techniques overcame this problem by making use of a combination of exponential and linear amplification (Kurimoto et al. 2006). Exponential amplification is needed for efficient amplification to generate enough cDNA, but is extremely susceptible to amplification biases. From these methods stemmed the first single cell RNA-seq library preparation protocols, and with the introduction of template-switching oligos and specialised reverse transcriptases, the sensitivity and coverage of single cell cDNA libraries improved significantly, and the cost was lowered (Tang et al. 2009; Ramsköld et al. 2012; Picelli et al. 2014). Single cell RNA-seq became routinely used to catalogue cell subpopulations, identify new genetic markers, trace developmental lineages, etc. (Deng et al. 2014; Treutlein et al. 2014; Jaitin et al. 2014)

The brain is known to be a highly heterogeneous structure, hence the maturation of single cell RNA-seq techniques offers a great opportunity for neuroscientists to explore and characterise this heterogeneity. By knowing the expression profile of neurotransmitter, neuromodulator, ion channel and plasticity related genes in each neuron, one could make sound hypotheses regarding their function and computation in vivo (Kodama et al. 2012). Identifying key genetic markers for subpopulations of neurons in one's area of interest in the mouse brain also then allows one to generate transgenic mouse lines to selectively target these subpopulations in one's manipulation.

The first large-scale high throughput single brain cell transcriptome project profiled >3000 cells in young mouse somatosensory cortex and hippocampus (Zeisel et al. 2015). Making use of the Fluidigm C1 platform and the Smart-seq2 library construction protocol, 47 molecularly distinct subclasses were identified. These include non-neuronal cells such as astrocytes,

oligodendrocytes and microglia, and neurons that correspond molecularly to known neuronal subtypes in cortex and hippocampus, such as CA1 glutamatergic neurons, pvalb+ and sst+ interneurons, thus validating the experimental workflow.

I used the work of Zeisel et al. as a starting point for setting up the pipeline to profile PAG neuronal transcriptomes. The TakaraBio iCELL8™ system presents a few advantages over the Fluidigm C1 and Smart-seq2 approach: (1) It offers the capacity to process up to 1800 samples in parallel, as opposed to 384 (which was the biggest Fluidigm C1 chip at that time), (2) it allows pooling of samples after reverse transcription, whereas the Smart-seq2 requires each sample to be processed individually in a separate reaction vessel. The iCELL8 system thus lowers the cost per sample and reduces the technical noise introduced, while retaining the ability to image samples prior to library construction (which the Fluidigm C1 also has).

I also opted to profile nuclear transcriptomes instead of whole-cell (cytoplasmic) transcriptomes. Lacar et al. showed that the long cell dissociation protocol with heating and protease digestion can induce aberrant transcription and expression of intermediate early genes (IEGs) (Lacar et al. 2016). The rapid nuclei dissociation protocol reduces spurious gene expression, as mature ribosomes are localised to the cytoplasm. The resulting single nucleus suspension is also much cleaner, with easily identifiable round, DAPI+ nuclei, in comparison to single cell suspension from primary brain tissue, which is often full of debris of various sizes, almost impossible to distinguish from neurons. Without cell membranes, nuclei suspensions could also be stained for various markers using antibodies (while membranes of living cells are impermeable to antibodies), which can be useful for enrichment of specific populations and for validation.

In the first proof-of-concept experiment, I aimed to show that with the iCELL8 system, one can identify the same brain cell subpopulations as those found in (Zeisel et al. 2015) from single nucleus transcriptomes. Cells and nuclei were dissociated from the same brain (from a P21 male mouse, same as those used by Zeisel et al.) and processed with the iCELL8 system. 147 wells with single cells and 200 cells with single nuclei were selected after the dispense for library construction. When processing the NGS data, reads from nuclei showed a much lower mapping rate than reads from cells, due to nuclei transcriptomes containing many intronic reads (close to 50%, (Habib et al. 2016) and the default mapping settings of mapping reads to exons. Upon mapping to the entire gene bodies, the mapping rate of nuclei reads rose to similar levels to those from cells (Table 3).

Assigning to	Cells (% reads)	Nuclei (% reads)
Exons	79.7%	37.4%
Genes	84.8%	81.3%

Table 3. Assigning reads to genes instead of exons drastically increases mappability of nuclei reads

With unbiased hierarchical clustering, two main clusters were immediately revealed: one composed mainly of cells and the other of nuclei (Fig. 4). However, further clustering within each of the clusters revealed no expected brain cells subpopulations, while looking at expression levels of known cell type markers across cells and nuclei suggested that these genes are mostly not well detected in this experiment, indicating a sensitivity issue. The genes that were driving the main clusters (beyond cells vs nuclei) were mostly highly expressed genes whose expression level in a cell varies linearly with the total number of reads for that cell, hinting that the normalisation strategy might be suboptimal.

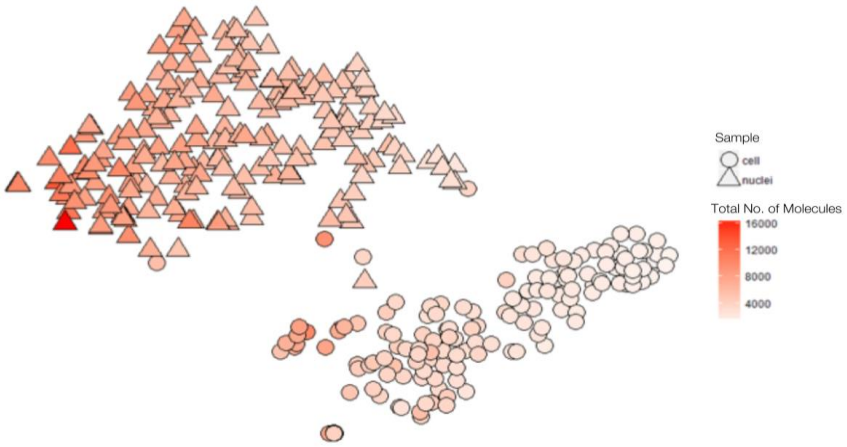

Figure 4. t-SNE shows clear separation between single cells (n=147) and single nuclei (n=200) wells. Colour bar shows total number of counts per well.

I then sought to benchmark the performance of the iCELL8 platform and my data processing pipeline with existing single cell pipelines, in the hope to address and uncover the cause of some of the issues in the initial experiment. Adding External RNA Controls Consortium (ERCC) RNA spike-ins into the nuclei suspension prior to dispense to enable cross-platform comparisons (Svensson et al. 2016; Jiang et al. 2011). To increase sensitivity, the sequencing depth of the library was increased, and more nuclei were selected for downstream processing as higher sample sizes allow for more robust normalisation and clustering, but not too many nuclei such that the read depth per nucleus would be compromised.

Cortical brain cells were again isolated, and 428 wells with single nuclei were selected for reverse transcription. Hierarchical clustering revealed subpopulations of brain cells marked by known markers (Fig. 6A-F). Further clustering the samples within the putative neuronal cluster (n=144), excitatory and inhibitory neurons were separated (Fig. 6G, H). However, further neuronal subpopulations are difficult to discern due to the insufficient number of samples.

To compare the sensitivity and accuracy of our set-up with other existing single cell RNA-Seq platforms, the ERCC data from this experiment was analysed using the methods employed by Svensson et al., which gives a sensitivity (lowest number of counts to be detected with a 50% probability) and an accuracy (Pearson coefficient between detected and expected number of counts) measurement for each sample ((Svensson et al. 2016)). The results show that our pipeline is as sensitive and as accurate as other existing pipelines (Fig. 5).

Having validated the performance of our pipeline, I sought to enrich for neurons in the PAG single nuclei transcriptome experiment, as only around half of the PAG brain cells are neurons, which are my primary cell type of interest. To be able to dispense only neurons onto the nanochip will help maximise the number of neurons per experiment, thus reducing the number of experiments needed and cost. To achieve this, single nuclei are first immunostained with an anti-NeuN antibody, then fluorescence-activated cell sorting (FACS) is used to sort NeuN+ nuclei directly onto the source plate for dispense (Supplementary Figure 1).

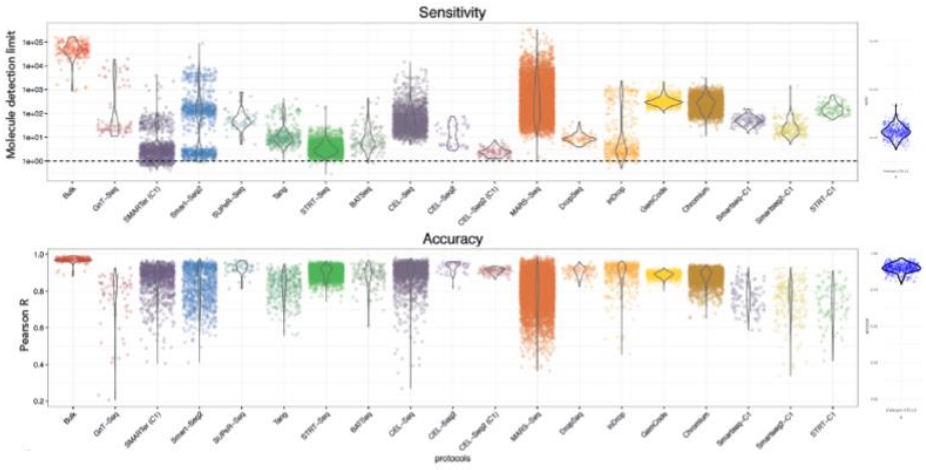

Figure 5 (adapted from Svensson et al., 2016). **The iCELL8 system's sensitivity and accuracy measurements in comparison with other platforms**. The iCELL8's performance, shown in the blue violin plots at the far right of each graph, is comparable with the other existing protocols. Each open circle represents an individual well/sample.

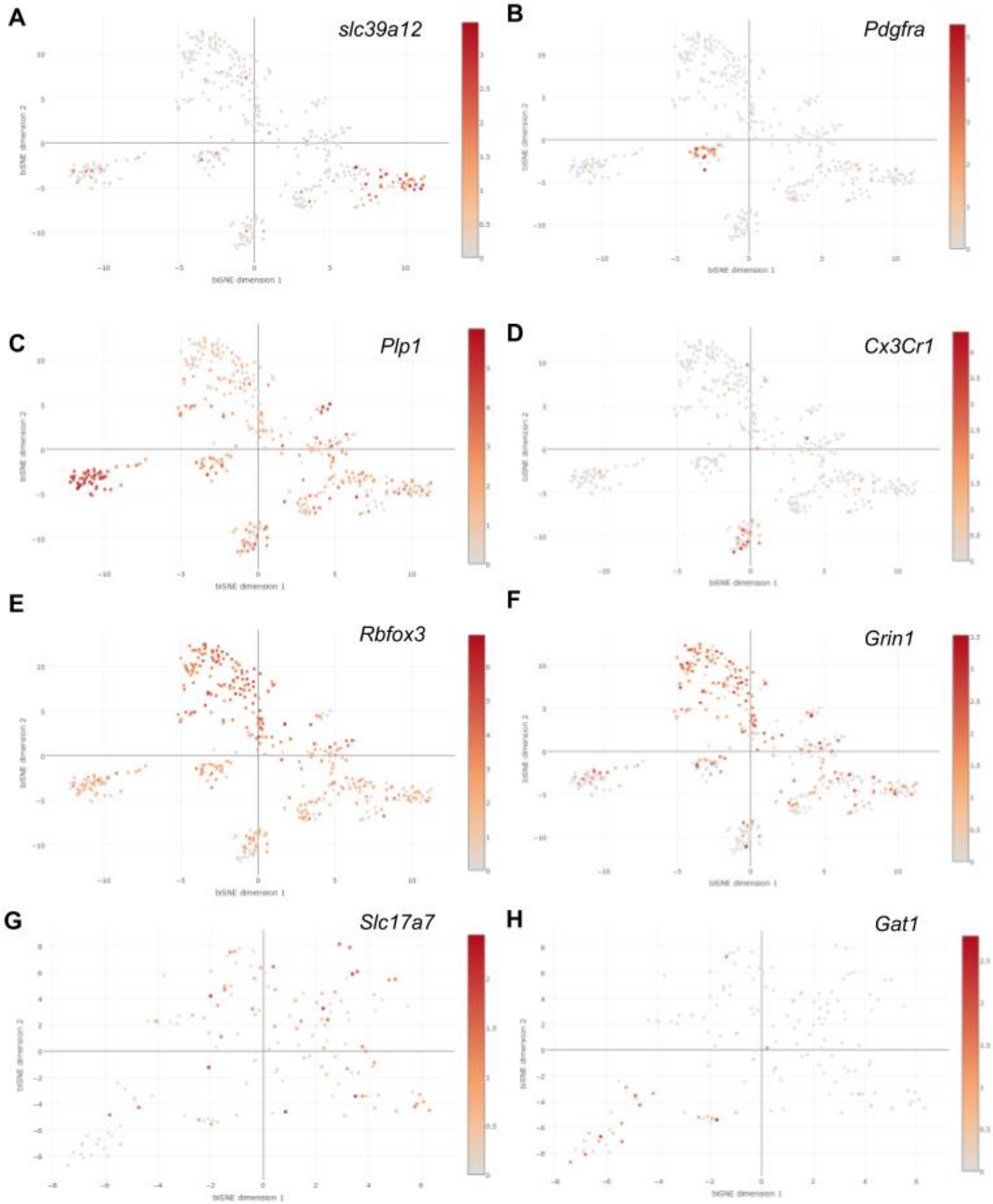

Figure 6. Hierarchical clustering reveals distinct subpopulations of brain cells. (A-F) t-SNE on all wells (n=428) shows clear separation between the different subpopulations of brain cells which express well known marker genes (marker gene name at top-right of each plot): (A) astrocytes, (B) oligodendrocyte precursors, (C) oligodendrocytes, (D) microglia, (E-F) neurons. (G-H) t-SNE on putative neurons (n=144) shows (G) excitatory neurons marked by Slc17a7 (vglut1), and (H) inhibitory neurons marked by Gat1. Colour bars indicate normalised expression level of each gene.

3.2 Transcriptome cataloguing of PAG neuron subtypes

The final PAG neuron dataset was produced using 14 mice and 3 nanochips: 4 mice for the first nanochip (ID: 94610) and 10 mice across the second and third (ID: 100283, 100339; the library construction for these nanochips was done separately). This resulted in a final 3,012 PAG neuronal nuclei selected for sequencing. I also processed some cortical neurons and unsorted cortical neurons as a control (see supplementary table 1 for details).

FACS seems to have slightly decreased the quality of the library produced, and the number of transcripts detected in PAG neurons is on average slightly lower than that in cortical neuronal nuclei (could be due to the fact that PAG neurons are on average smaller than cortical neurons), but it is still more than what was used in a recently published single nuclei RNA-Seq study for neuronal subtypes (supplementary figure 1). The two main challenges in the analysis pipeline come from normalising the batch effects across experiments, and choosing variable genes for clustering. Prior to normalisation, we can see that the batch effect produces most of the variability between nuclei; in particular, there is a larger separation between the nuclei from nanochip #94610 and the 2 other nanochips (Fig. 7); it shows that a different sample preparation (with the same protocol, but on a different day with different mice) produces extra technical variability. To this end, we applied careful gene and sample filtering, regression and selection of high variability genes to minimise the effects of batch on downstream analysis.

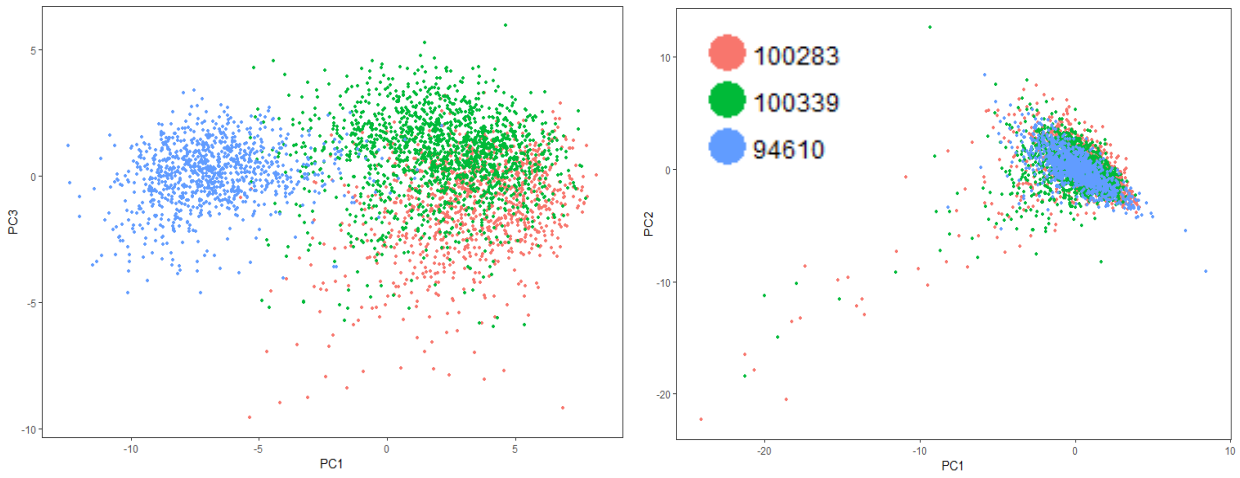

Figure 7. Normalisation and regression strategy corrected experimental batch effects. PCA plots showing (A) clear batch effects before regression, and (B) neurons no longer separate by experiments after batch correction.

Unbiased clustering revealed 8 clusters of nuclei (Fig. 8). Each cluster contains nuclei from all 3 chips, and the t-SNE visualisation showed cortical neurons separating away from PAG neurons, lending support to the validity of the normalisation and feature selection approaches (Fig. 8B-C). Most cortical neurons are in one cluster (cluster '5'), and positively enriched genes of this cluster correspond to genes known to be enriched in the cortex in comparison to the PAG, and vice-versa for genes of negative differential expression (Fig. 8C-D). There are also 2 small clusters of neurons marked by high expression of ribosomal genes, indicating that these samples were not neurons (Fig. 8E). These were removed from subsequent analysis.

However, there are very few statistically significant differentially expressed genes for the remaining clusters (Supplementary Table 2); furthermore, it is difficult to correlate the enrichment of these genes to neuronal functions. I therefore adopted a semi-supervised approach based on the method used by Wu et al., by compiling a list of 352 genes that were directly related to neuronal function and using these to cluster the neurons, of which 299 are detected in our dataset (Supplementary Table 3) (Wu et al. 2017).

Clustering results vary hugely based on the parameters used for the cluster algorithm. For the graph-based community clustering method that is adopted here, the two main variables are (1) the number of neighbours chosen for nearest-neighbour calculations, and (2) the resolution, which controls the compactness of subgraphs (Xu and Su 2015). There is very little agreement in the field on how best to determine the optimal number of clusters. For this I employed the approach adopted by Kiselev et al., where the parameter space comprising the range of recommended values for each parameter is evaluated to obtain a set of clusterings, and a consensus is obtained by combining the results and looking at how often two nuclei are in the same cluster (Kiselev et al. 2017) (Supplementary Figure 4).

17 clusters were found after this procedure and further quality filtering, of which 11 were marked by enriched expression of neuronal function-related genes (Fig 9A-C, Supplementary Table 4). Similar to results from the previous unsupervised clustering, here cortical neurons form a cluster, marked by enrichment of Slc17a7 (vGlut1) and Slc1a2 (EAAT2) (cluster '12', Fig. 9C,D); both genes are known to be highly expressed in cortical excitatory neurons. Another cluster, marked by Slc18a2 and Slc6a4 enrichment, corresponds to neurons from the dorsal raphe (DR, present due to tissue dissection imprecision) (Fig. 9E). The remaining 9 clusters are marked by expression of ion channels, as well as important neurotransmitter and neuromodulator genes

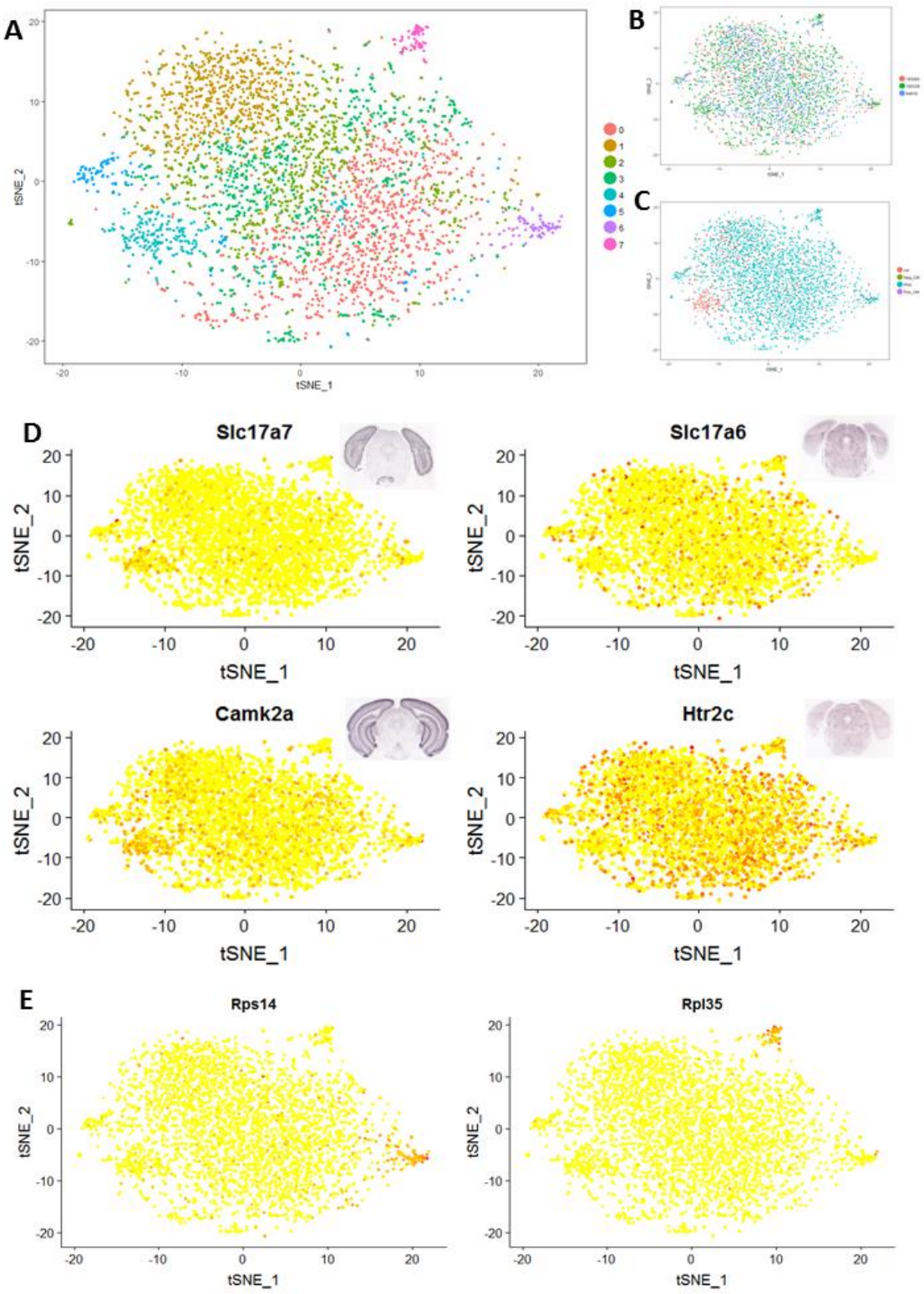

Figure 8. Unsupervised clustering reveals 8 distinct subpopulations (n=3581). t-SNE Plots overlaid with colours indicating (A) cluster identity, (B) experiment of origin, and (C) sample type (cortical neurons in red). (D-E) t-SNE plots overlaid with scaled gene expression levels of each indicated gene: yellow for low expression, red for high expression. (D) Cortically enriched genes Slc17a7 (vGlut1) and Camk2a are highly detected in neurons in cluster '4', while subcortical Slc17a6 (vGlut2) and Htr2c are comparatively enriched in all clusters other than '4'; insets are *in situ* hybridisation images against each gene (snapshot at the PAG level), taken from the Allen Brain Atlas. (E) clusters '6' and '7' show increased expression of ribosomal genes

known to be expressed in the PAG, e.g. Nos1, Tacr1 and Adcyap1r1. The remaining 6 clusters are marked by the relative absence of certain genes (negative markers), or without statistically significant neuronal markers; these are possibly positively marked by genes that are not on the current list of candidate genes used. This is confirmed by performing marker gene identification on the entire set of detected genes; additional markers for the clusters (not from the candidate list) are found (Supplementary Table 5)

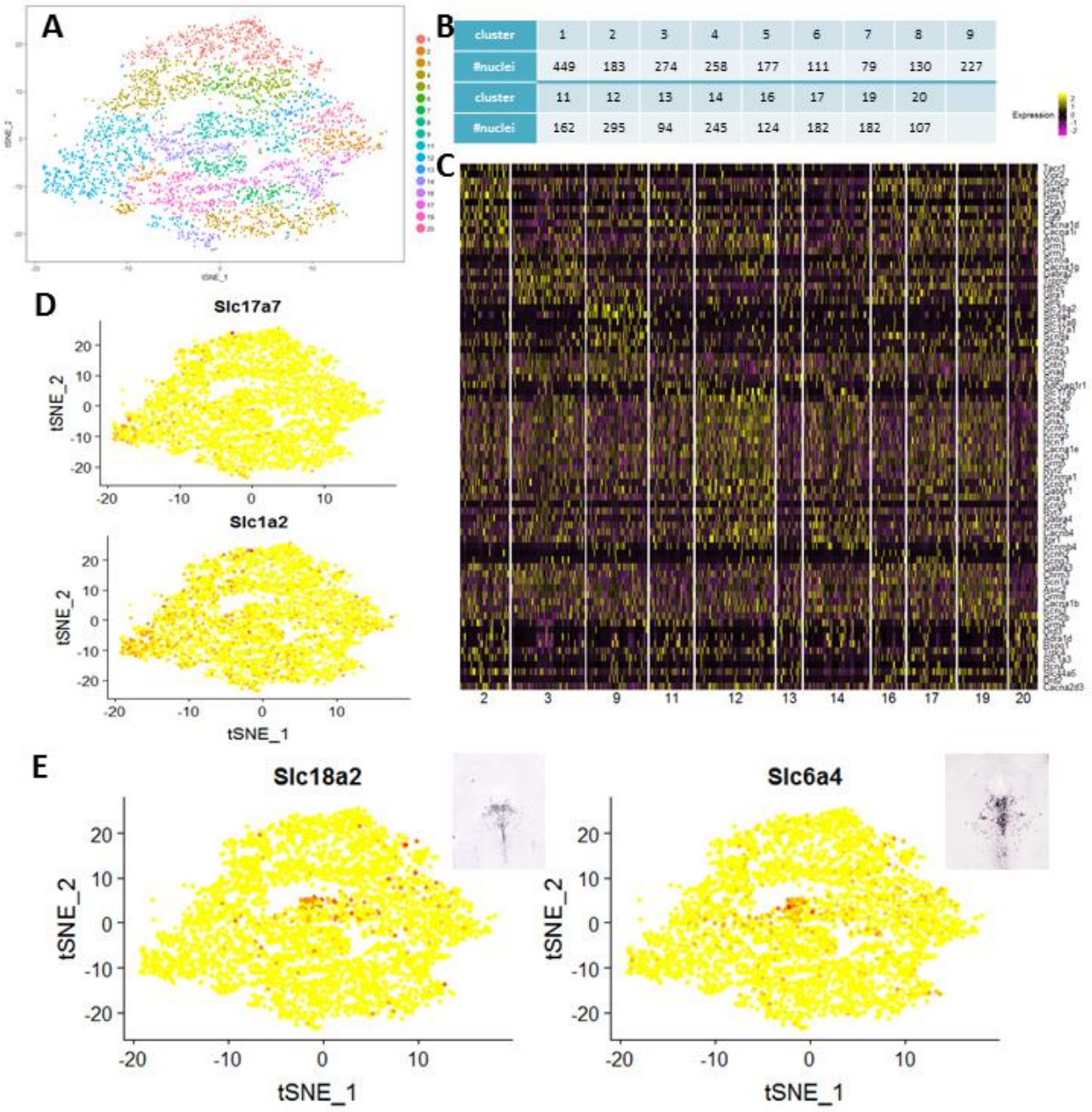

Figure 9. Supervised clustering reveals 17 distinct clusters of neurons (n=3279). (A) t-SNE plot depicting clusters. (B) Table detailing number of neurons in each cluster. (C) Heatmap showing the expression of the top markers for each positive-marked cluster; colour shows scaled expression level. (D-E) t-SNE plot showing enrichment of (D) cortical neuronal genes in cluster '12', and (E) dorsal raphe markers enrichment in cluster '9'; insets in (E) show *in situ* hybridisation against the gene of interest in the dorsal raphe and PAG, taken from the Allen Brain Atlas.

4 Functional mapping of PAG cell types identifies innate defense circuit

4.1 dPAG excitatory neurons trigger overt defensive behaviour

Having described PAG neuron types, we sought to identify their functional roles within the instinctive defense circuit. Previous studies aiming at finding PAG circuit components regulating defense have mostly involved pharmacological manipulations, via microinjections of agonists/antagonists of neurotransmitter/neuromodulatory receptors into different PAG subregions (see introduction). While these experiments have been informative, results could vary widely depending on the specificity of the drug used, the concentrations and the extent of drug diffusion, often producing contradictory results. The combined use of optogenetic/pharmacogenetic tools and transgenic animals offer temporal and spatial specificity to the manipulation, and together with well-designed behavioural assays, have proven to be superior in robustness and reliability. This enables the mapping of finer aspects of behaviour to smaller groups of neurons, which is crucial to the understanding of circuit dynamics at an algorithmic level.

Previous studies have shown that optogenetic activations of dPAG CAMKII+ and vGlut2+ neurons trigger flight and post-flight freezing, in line with results from similar electrical and chemical stimulation experiments; the speed of flight is proportional to the stimulation intensity (Deng, Xiao, and Wang 2016; Evans et al. 2018; Tovote et al. 2016). Optogenetic inhibition of dPAG vGlut2+ neurons, on the other hand, abolishes escape responses to a looming stimulus; instead, the animal freezes with fast reaction times (Evans et al. 2018). These results suggest that vGlut2+ neurons are sufficient and necessary for the locomotive aspect of the “circa-strike” behaviour. Single unit recordings in the mouse dPAG revealed that around 20% of the neurons fire during flight away from a rat (Deng, Xiao, and Wang 2016; Masferrer et al. 2018). Given that around 50% of dPAG neurons are excitatory, it is likely that only a subpopulation of dPAG are necessary for flights (Watson, Paxinos, and Puelles 2012). These neurons could be in a particular subregion of the dPAG (e.g. dlPAG), marked by a specific genetic marker in addition to vGlut2+, and/or connected to a specific structure. Also, defensive behaviours have been shown to be accompanied by autonomic responses, and whether these are triggered by the same subpopulation of vGlut2+ neurons eliciting escape locomotion, or whether vGlut2+ neurons mediate these autonomic changes at all, remains a mystery. Finally, it is not known whether dPAG vGlut2+ neurons encode any part of the motivational aspect of defence. Silva et al. showed

that the dPAG is important for the expression of fear, but not fear memory (Silva et al., 2016); it is possible that dPAG neurons only output motor commands for escape-like lomotion.

First, we confirmed that optogenetic stimulation of vGlut2+ neurons in dPAG induces flights, and the probability of flights increases with increasing stimulation frequency (Fig. 10C-D). We then carried out a real-time place preference test and found that, similar to that of CamKII+ neurons, optogenetic activation of vGlut2+ neurons is aversive; animals flee out of the stimulation chamber (Fig. 11 A-B). We sought to find out if vGlut2+ neurons control the autonomic aspects of the escape-like behaviour. Heart rate measurements were carried out with a pulse oximeter with the animal anesthetised, as a flight might indirectly cause an increase in heart rate. We found that vGlut2+ neuron stimulation repeatedly caused tachycardia; this was often accompanied slight movements of the animal (of the paw or head). This indicates that dPAG vGlut2+ neurons also coordinate heart rate in defensive responses.

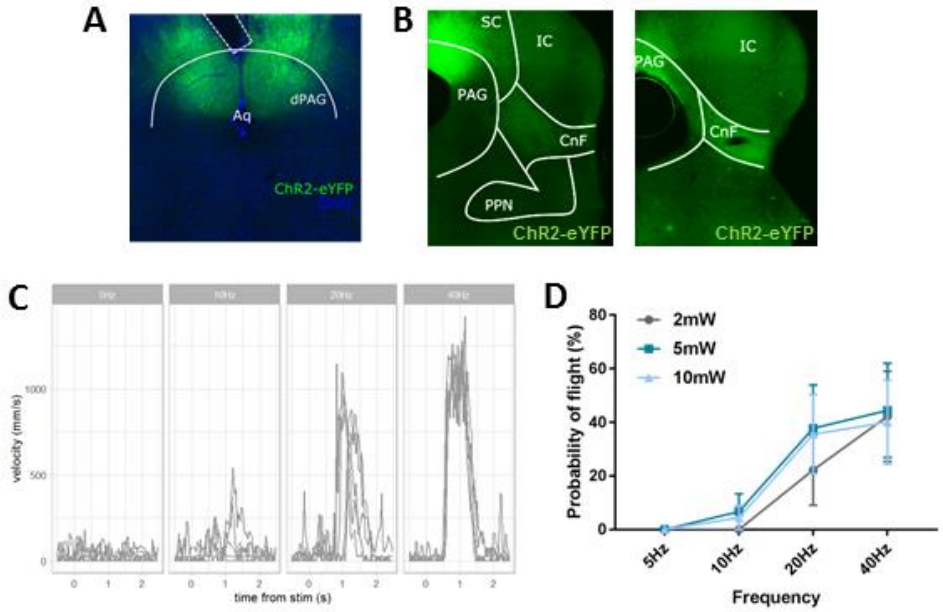

Figure 10. Optogenetic stimulation of dPAG vGlut2+ neurons triggers flights. (A) Widefield microscopic image of dPAG area showing site of injection, distribution of ChR2+ expressing cells, and placement of optic fibre (dashed line); Aq: aqueduct. (B) dPAG vGlut2+ neurons appear to project to the cuneiform nucleus (CnF), but not to the pedunculopotine nucleus (PPN): SC: superior colliculus, IC: inferior colliculus. (C) Velocity bursts from an exemplar animal for different frequencies of stimulation (power=5mW, pulse width=15ms). (D) Mean probability of flight for increases with increasing frequency (n=9). Statistical significance is analysed with 2-way ANOVA with Tukey post-hoc; all p-values reported here are adjusted p-values. At 2mW: 5Hz vs 20Hz p=0.0059, 5Hz vs 40Hz p<0.0001, 10Hz vs 20Hz p=0.0059, 10Hz vs 40Hz p<0.0001, 20Hz vs 40Hz p=0.0155; at 5mW: 5Hz vs 20Hz p<0.0001, 5Hz vs 40Hz p<0.0001, 10Hz vs 20Hz p<0.0001, 10Hz vs 40Hz p<0.0001; at 10mW: 5Hz vs 20Hz p<0.0001, 5Hz vs 40Hz p<0.0001, 10Hz vs 20Hz p<0.0001, 10Hz vs 40Hz p<0.0001. Error bars show mean +/- s.e.m.

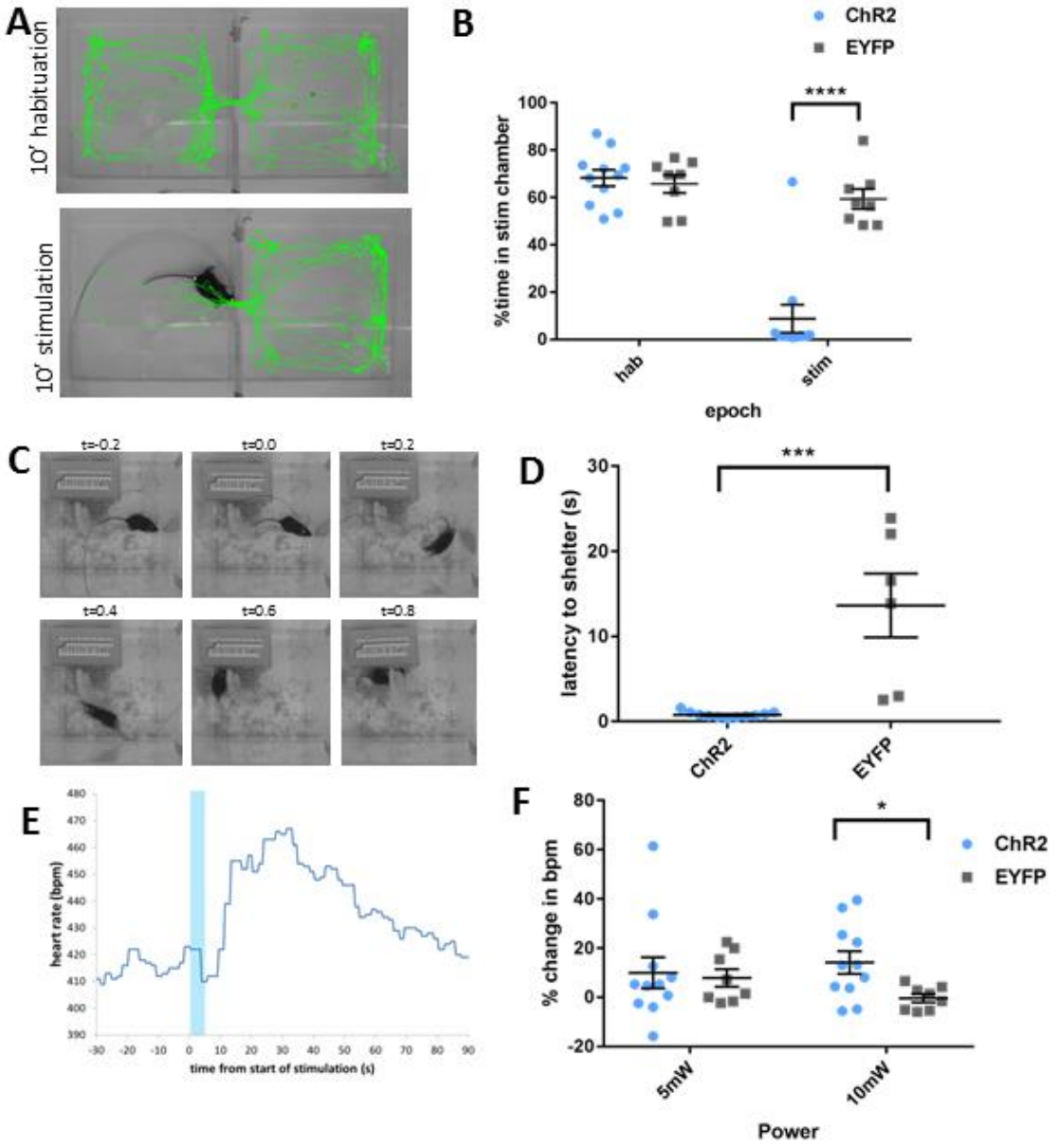

Figure 11. Optogenetic stimulation of dPAG vGlut2+ neurons elicits escape. (A) Path of an exemplar ChR2 animal during the (top) habituation epoch and (bottom) stimulation epoch in the real time place preference test; stimulation chamber is on the left. (B) ChR2 animals avoid the stimulation chamber in comparison to EYFP controls specifically during the stimulation epoch (ChR2 n=11; EYFP n=8); multiple t-test with Holm-Sidak post-hoc, t=6.435, adj. p<0.0001. (C) Example escape to shelter upon stimulation in a ChR2 animal, t=0 indicates beginning of stimulation. (D) ChR2 animals escape with shorter latency to home (ChR2 n=11, EYFP n=6); Mann Whitney unpaired t-test, p=0.0002. (E) Example tachycardiac response of a ChR2 animal to stimulation; blue shading indicates the light on period. (F) Tachycardia is observed in ChR2 animals but not EYFP controls at 10mW (ChR2 n=11, EYFP n=8), multiple t-test with Holm-Sidak post-hoc, t=2.585, p=0.038. All error bars are mean +/- s.e.m

To check whether these flights are actually escapes, instead of just fast running, we designed a test to see if these flights qwew aimed towards safety. As mice are known to prefer dark corners to open spaces, we placed a shelter in a corner of the apparatus, which is also filled with the animal's home bedding. Optogenetic stimulation of dPAG vGlut2+ stimulation repeatedly triggers flight towards the shelter in the ChR2-expressing animals, but not in EYFP only controls (Fig. 11C-D). The ChR2-expressing animals also remained in the shelter for long periods of time after stimulation, whereas control animals exit and re-enter the shelter much more frequently.

Next, we targeted pituitary adenylate cyclase-activating polypeptide (PACAP)-expressing neurons in the dPAG. PACAP (whose official name is ADCYAP1) is a 38-amino acid peptide encoded by the Adcyap1 gene; it is part of the family of neuropeptides that includes also vasoactive intestinal peptide (VIP), secretin and glucagon (Vaudry et al. 2009). It is expressed in various brain regions implicated in defensive behaviour, e.g. MeA, VMH, LC and LPB (Vaudry et al. 2009). In particular, PACAP mRNA has been shown to colocalise with that of SF1 in the VMH, and PACAP-expressing neurons in the VMH project to dPAG (Hawke et al. 2009; Maekawa et al. 2006). PACAP has been implicated in the regulation of survival behaviour, such as eating, drinking and reproduction, and autonomic responses, such as blood pressure and thermoregulation (Krashes et al. 2014; Ross et al. 2018; Farnham et al. 2012; Morley et al. 1992; Banki et al. 2014; Tan et al. 2016). In humans, single nucleotide polymorphisms (SNPs) in the PACAP receptor gene Adcyap1r1 are associated with post-traumatic stress disorder (PTSD) in female subjects; PACAP has been associated with aberrant stress responses in mice that underwent chronic social defeat (Ressler et al. 2011; Lehmann et al. 2013). In the dPAG, PACAP mRNA is enriched in dm/lPAG, which receives inputs in particular from the VMH (Lein et al. 2007). All these observations led us to hypothesise that PACAP+ neurons in the dPAG are important for instinctive defensive behaviour.

Optogenetic stimulation of dPAG PACAP+ neurons triggers flight, in a very similar manner to that from dPAG vGlut2+ stimulation (Fig. 12C,D). The stimulation is aversive and escape-oriented (Fig. 12E,F). Distinct from vGlut2+ activation, PACAP neurons do not seem to significantly regulate heart rate (Fig. 12G), although I cannot rule out that this is due to unreliability in the method of measurement, as one animal did show tachycardia upon stimulation.

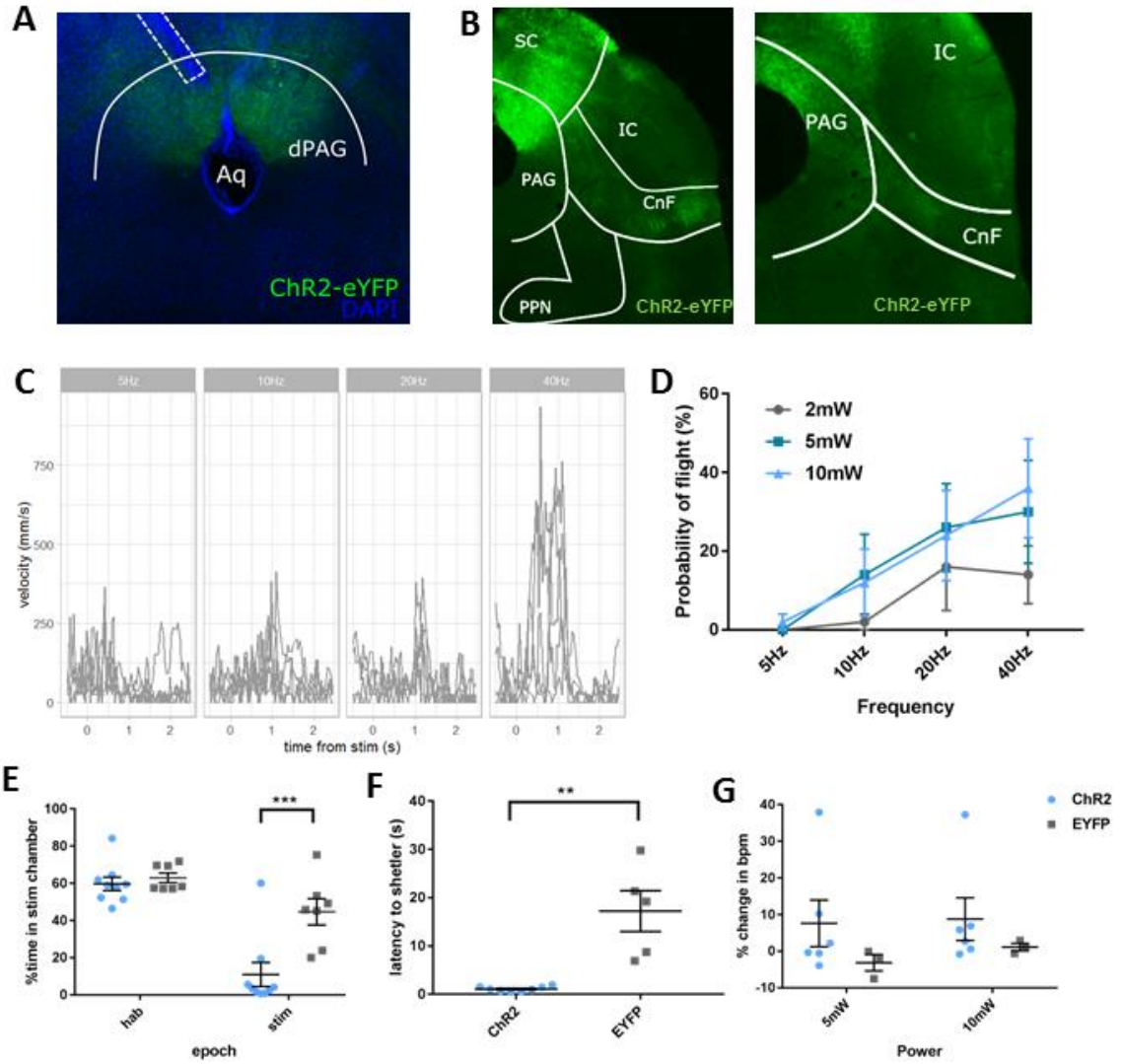

Figure 12. Optogenetic stimulation of dPAG PACAP+ neurons elicits escape.(A) Widefield microscopic image of dPAG area showing site of injection, distribution of ChR2+ expressing cells, and placement of optic fibre (dashed line); Aq: aqueduct. (B) PACAP+ neurons appear to project to the CnF, but not the PPN in the MLR. (C) Velocity bursts from an exemplar animal for different frequencies of stimulation (power=10mW, pulse width=15ms). (D) Mean probability of flight increases with increasing frequency at 5mW and 10mW (ChR2 n=10). Statistical significance is analysed with 2-way ANOVA with Tukey post-hoc; all p-values reported here are adjusted p-values.At 5mW: 5Hz vs 20Hz p=0.0066, 5Hz vs 40Hz p=0.0013; at 10mW: 5Hz vs 20Hz p=0.0278, 5Hz vs 40Hz p=0.0002, 10Hz vs 40Hz p=0.0138. (E) ChR2 animals avoid the stimulation chamber in comparison to EYFP controls specifically during the stimulation epoch (ChR2 n=9; EYFP n=7); multiple t-test with Holm-Sidak post-hoc, t=3.518, adj. p=0.0068. (F) ChR2 animals escape with shorter latency to shelter (ChR2 n=8, EYFP n=5); Mann Whitney unpaired t-test, p=0.0016.(G) No significant heart rate response is observed in ChR2 or EYFP animals with stimulation (ChR2 n=6; EYFP n=3). All error bars show mean +/- s.e.m

4.2 dPAG Tac2+ neurons regulate defensive responses towards predator and conspecific threats

Tac2 encodes the neuropeptide Neurokinin B (NKB), which is a member of the tachykinin family along with Neurokinin A (NKA) and substance P (SP) (Severini et al. 2002). Tac2 is expressed in very specific areas of the adult mouse brain: the antero-dorsal bed nucleus of the stria terminalis, medial habenula, CeA, DMH, arcuate nucleus, LHA, and dmPAG (Lein et al. 2007; Zelikowsky et al. 2018). Tachykinins have been implicated in pain, anxiety, stress and aggression in rodents (Severini et al. 2002). In the mouse amydala, Tac2 and its receptor NK3R affect the consolidation of fear memory (Andero, Dias, and Ressler 2014). Recently, Zelikowsky et al. found that chronic isolation stress causes a brain-wide upregulation of Tac2 expression, and this change is necessary and sufficient for the behavioural influence of chronic isolation stress (Zelikowsky et al. 2018). In the rat dPAG, injection of an NK3R (neurokinin receptor which preferentially binds NKB) agonist causes an increase in exploratory behaviour in an elevated-plus maze, hyperalgesia and an increase in 22kHz USV (Bassi et al. 2009).

Optogenetic stimulation of the dmPAG Tac2+ neurons does not produce any overt behaviours (i.e. flight/freezing). Further testing with real time place preference showed neither preference nor aversion (Fig. 13E). Given that Tac2 was shown to play modulatory roles, we hypothesised that its activation would cause a change in defensive behaviour in the presence of a stimulus, i.e. a predator or a conspecific. To test this, we adopted a modified version of the classic three-chamber test (adopted from Silva et al., 2013; see Fig. 13C,D and methods section 2.3.2.5). Animals first interact with the threat in the 'stimulus' chamber, and after are allowed to escape through the connected corridor and 'far' chamber. Its behaviour towards the threat is then recorded and quantified during repeated sessions of optogenetic activation.

Using this paradigm, we showed that optogenetic stimulation of dmPAG Tac2+ increases immobility of mice in the presence of both an aggressive conspecific and a rat. There are no significant changes in other defense-related behaviours such as stretching (Fig. 13C,D). We also tested for heart rate changes, and no heart rate responses were observed during stimulation (Fig. 13F). This suggests that dmPAG Tac2+ neurons are responsible for modulating a very specific aspect of the mouse instinctive defensive behaviour.

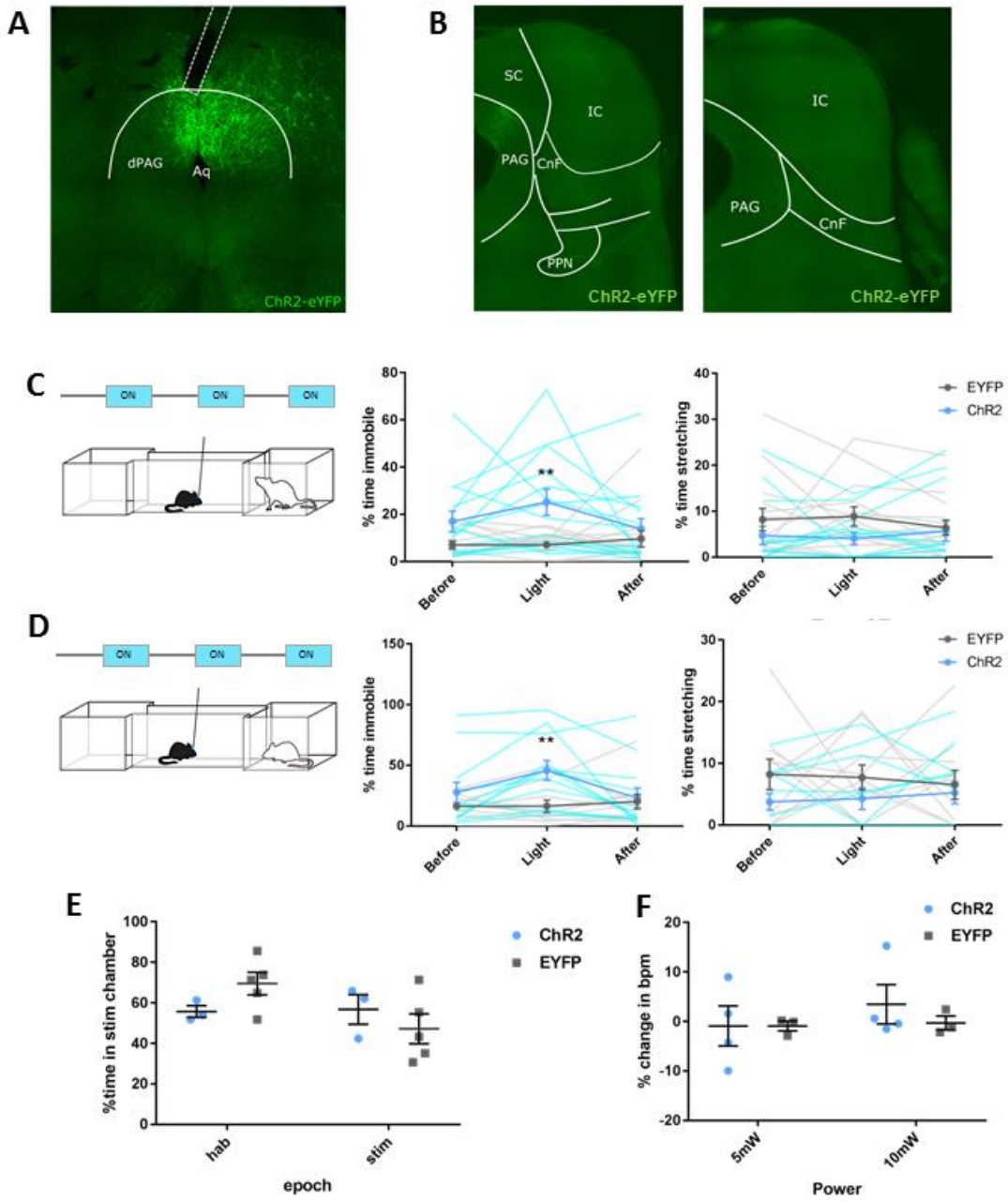

Figure 13. Optogenetic stimulation of dmPAG Tac2+ neurons induces immobility against predator and conspecific threats. (A) Widefield microscopic image of dPAG area showing site of injection, distribution of ChR2+ expressing cells, and placement of optic fibre (dashed line); Aq: Aqueduct. (B) Tac2+ neurons do not appear to project to the MLR. (C) Tac2+ activation enhances immobility towards predator. (left) Diagram showing experimental set-up and stimulation pattern: 3 stimulation periods of 2 mins are each interleaved by 2 mins inter-stimulus interval (ISI); (middle) immobility is increased in ChR2 animals but not EYFP controls during stimulation; (right) stretching is not affected (no. of stimulations: ChR2=14, EYFP=14; no. of animals: ChR2=6, EYFP=5); multiple t-test, Holm-Sidak post-hoc, t=3.337, adj. P=0.00389; light blue and grey lines show individual trials. (D) Tac2+ activation enhances immobility towards an aggressive conspecific. (left) Diagram showing experimental set-up and stimulation pattern; (middle) immobility is increased in ChR2 animals but not EYFP controls during stimulation; (right) stretching is not affected (no. of stimulations: ChR2=12, EYFP=10; no. of animals: ChR2=6, EYFP=5); multiple t-test, Holm-Sidak post hoc, t=2.938, adj. P=0.0140; light blue and grey lines show individual trials. (E) Preference for stimulation chamber during stimulation epoch in RTPP does not differ between groups of animals (ChR2 n=3, EYFP n=5). (F) No observable heart rate responses are evoked by Tac2+ stimulation (ChR2 n=4, EYFP n=3). All error bars indicate mean +/- s.e.m; all data shown in this figure has been produced jointly with Isabelle Prankerd.

5 Identification of PAG output pathways mediating defensive responses

5.1. dPAG-CnF projection regulates flight

We hypothesise that functionally distinct dPAG neuron types project to different downstream areas, and hence are able to regulate different aspects of defensive behaviour. A major target of dPAG projections is the midbrain locomotor region (MLR), which in mice comprises the cuneiform nucleus (CnF) and the pedunculopontine nucleus (PPN) (Caggiano et al. 2018). The MLR controls gait selection and speed of movement; while excitatory neurons in both nuclei contribute to slower, alternating-gait locomotion, optogenetic activation experiments demonstrated that only CnF neurons are capable of triggering high speed, escape-like locomotion (Caggiano et al. 2018).

We first targeted the dPAG neurons projecting to CnF using retrograde delivery of Cre-recombinase. AAV serotype 5 (AAV5) had been shown to transduce retrogradely along the axon (Aschauer, Kreuz, and Rumpel 2013); injecting an AAV5 encoding Cre in the CnF, and an AAV expressing ChR2 Cre-dependently in the dPAG allows us to optogenetically manipulate specifically the CnF-projecting dPAG neurons (Fig. 14A). Optogenetic stimulation of these neurons triggers flight (Fig. 14B), and similar to the flights resulted from the optogenetic stimulation of dPAG excitatory neurons, these flights are escape-oriented (Fig. 14C). However, no changes in heart rate were observed with the optogenetic activation, indicating that this output pathway may control only the locomotive aspect of escape behaviour, although a larger number of animals are needed to confirm this.

To show that escape is regulated specifically by this projection (and not by these neurons' projections to other downstream areas), we also optogenetically activated the axonal terminals of the projection, by expressing ChR2 in dPAG neurons and delivering light to the CnF, which resulted similarly in flights (Fig. 14D-F).

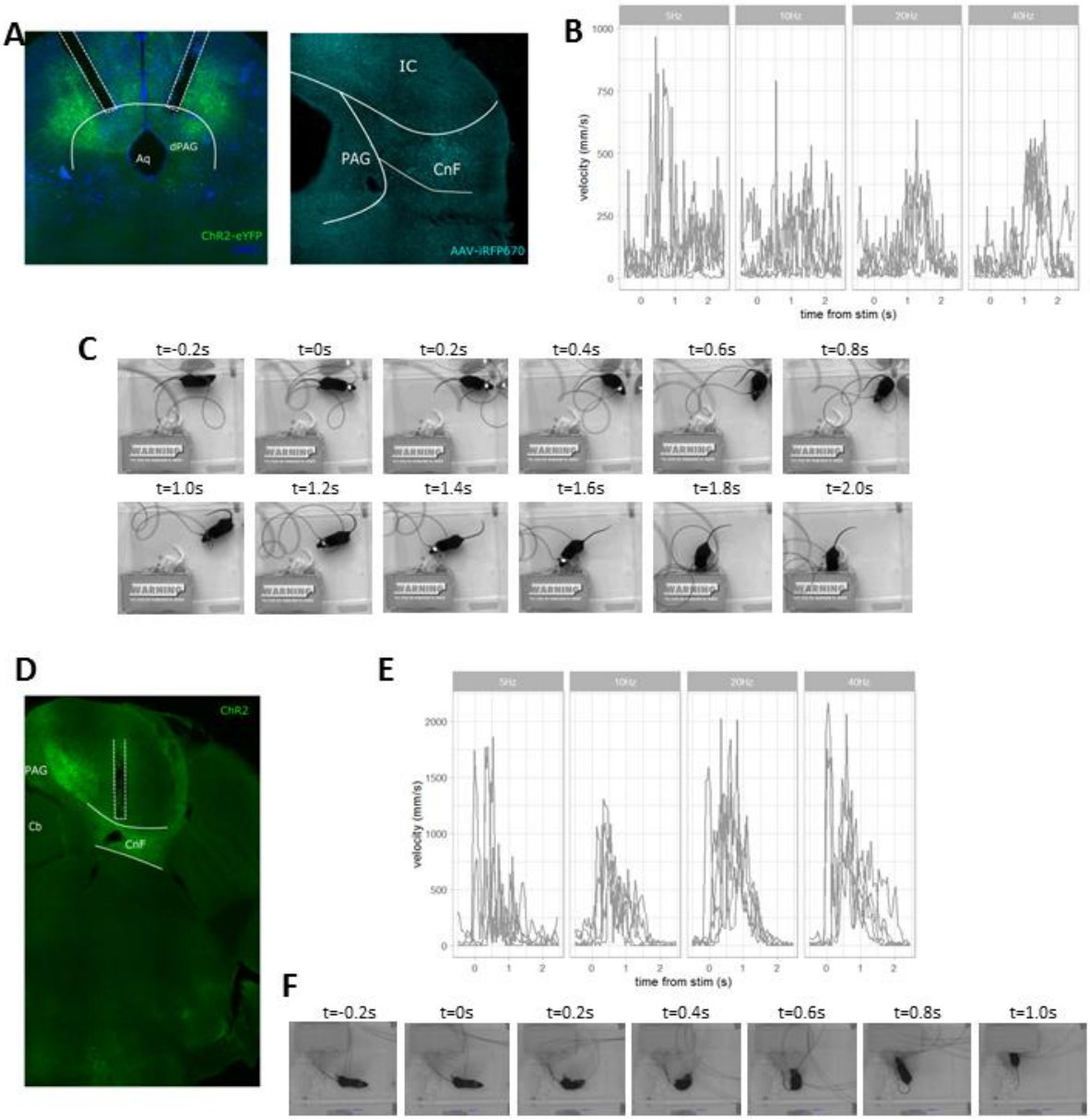

Figure 14. Optogenetic stimulations of both the soma and axonal terminal of CnF-projecting neurons in the dPAG elicit escape. (A) widefield micrograph showing (left) retrograde-cre dependent ChR2 expression in the dPAG; optic fibre placements are indicated by dashed lines; (right) expression of iRFP670 used to mark site of injection of retrograde-Cre virus at the CnF. (B) and (C) show results from somatic activation of CnF-projecting neurons (n=2). (B) Velocity bursts of an exemplar animal during optogenetic stimulation across varying frequencies (power= 2mW, pulse width=15ms). (C) An example of a light-evoked escape to home, t=0 is when stimulation began. (D) Widefield micrograph showing expression of ChR2 in dPAG neurons and its transport down to axonal terminals at the CnF; dashed line indicate placement of optic fibre over the CnF. (E) and (F) show results from axonal projection activation at the CnF of dPAG CnF-projecting neurons (n=2). (E) Velocity bursts of an exemplar animal during optogenetic stimulation across varying frequencies (power = 5mW, pulse width=15ms), (F) An example of a light-evoked escape to home, t=0 is when stimulation began.

5.2 Diverse dPAG output pathways to the MLR

To investigate the nature of dPAG output neurons to the MLR, we made use of Cholera toxin subunit B (CTB) retrograde tracing. We labelled dPAG vGlut2+ neurons using vGlut2::Cre animals and an AAV expressing mCherry in a Cre-dependent manner, and delivered CTB conjugated to fluorescent proteins of two different colours to CnF and PPN. While CnF-projecting PAG neurons are located specifically in the dorsolateral column as previously described (see Introduction section 1.3.5.1), PPN projecting neurons are sparse but evenly distributed across dPAG columns (Fig 15B). Most CnF-projecting neurons are vGlut2+, but PPN neurons appear to have less of an overlap with the vGlut2+ signal (Fig 15C). That being said, because this method of labelling vGlut2+ neurons is non-exhaustive, an alternative is needed to confirm this potential finding.

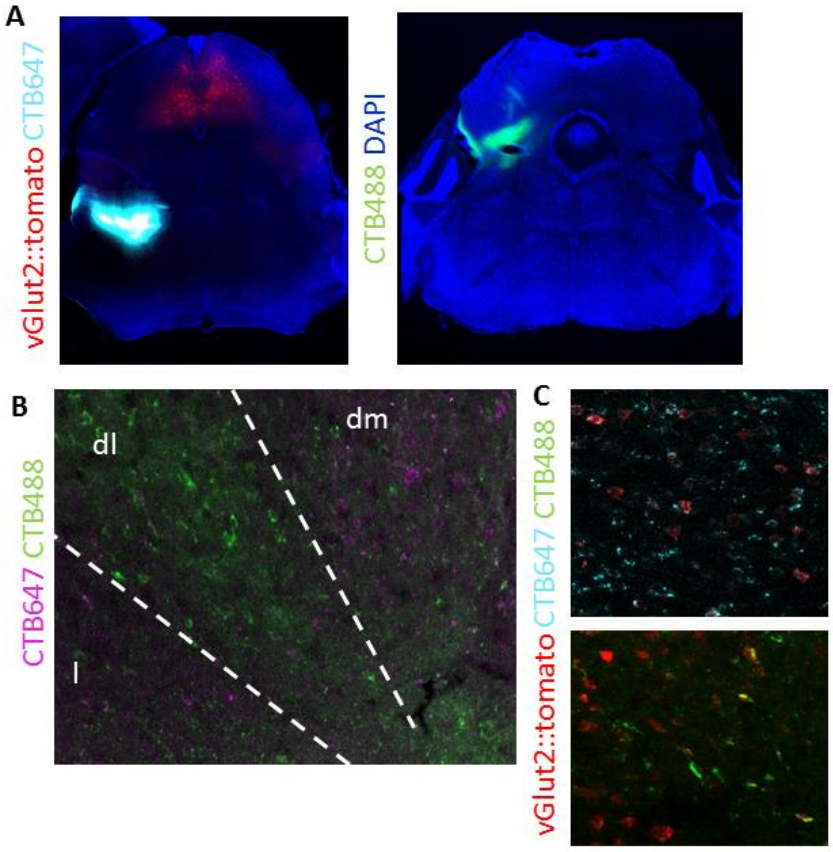

Figure 15. CTB retrograde tracing from CnF and PPN (n=4) shows divergent output pathways from dPAG to MLR. (A) Widefield micrographs showing sites of injections of (left) CTB-647 at PPN and labelling of dPAG vGlut2+ neurons with injection of an AAV expressing cre-dependent tomato, and (right) CTB-488 at CnF. (B) Confocal image showing enrichment of CnF-projecting neurons in dlPAG (dl), while PPN-projecting neurons are found also in the lateral (l) and dorsomedial (dm) PAG columns. (C) Confocal image in the dPAG with vGlut2+ neurons labelled with tomato expression, showing that (bottom) CnF-projecting neurons are largely glutamatergic, but (top) not PPN projecting neurons.

6 Discussion

The PAG has been regarded as the final controller of defensive behaviours, integrating sensory, cognitive and internal state information to produce the most appropriate response to threats. In this study, we first investigated the PAG neural circuit using a bottom-up approach, by cataloguing its components. We showed that a large array of neurotransmitter and neuromodulator genes are expressed in PAG neurons, and different combinations mark at least 9 distinct types of neurons. Using optogenetics stimulation, We mapped selected classes of neurons to their roles in defense, demonstrating that there are transcriptomically diverse subclasses of PAG neurons responsible for different aspects of defensive behaviours.

In this final section, I will discuss our findings and reflect on the approach in the context of instinctive behaviour neural circuit research.

6.1 Transcriptomic dissection of PAG neurons reveals distinct subpopulations

Previous research has demonstrated the involvement of a large number of neurotransmitter and neuromodulatory systems in the regulation of PAG neuronal activity and related behaviour (summarised in section 1.3.3.3). While efforts have been made to resolve the interaction between these systems (mainly by using various antagonists and agonists together), this has not been done systematically, leaving many potential interactions unexplored. We present the first attempt to transcriptomically catalogue PAG neurons, with the aim of generating a more comprehensive and quantitative description, and of advancing the understanding of the PAG instinctive behavioural circuit on a molecular level.

Using supervised clustering, we first identified 9 clusters of PAG neurons marked by enriched expression of neuronal function related genes. Many of these encode for proteins with well documented roles in the PAG, e.g. Tacr1 (marking cluster ‘2’) encodes the neurokinin receptor NK_1 that preferentially binds to Substance P and mediates pain and anxiety responses (see section 1.3.3.3). Cluster ‘2’ neurons also show enrichment of Nos1, encoding nitric oxide synthase (nNOS). A previous pharmacological study demonstrated that NOS inhibition removes the anxiogenic effect caused in intracerebroventricular injection of Substance P (Baretta, Assreuy, and De Lima 2001); building on that, our data suggests that there are PAG GABAergic neurons (Gad2 is also a marker of this cluster) that are activated by Substance P and synthesise nitric oxide (NO) in response, and these are potentially important for the modulation of anxiety.

Nitric oxide has been shown to have diverse roles in synaptic modulation in the PAG (Fogaca et al., 2011). Using slice electrophysiological recording, NO has been shown to suppress dlPAG neuronal activity through potentiating the synaptic release of GABA and presynaptically inhibiting glutamate release in a GABA(A) receptor-dependent manner (Xing et al., 2008). Taken together, GABA(A) receptor expressing excitatory neurons in the dlPAG could be the downstream target of the Tacr1+ Nos1+ inhibitory neurons in cluster '2'; these cluster '2' neurons could have the capacity to modulate the array of defensive behaviours regulated by dlPAG vGlut2+ neurons (shown by the optogenetic experiments in Section 4.1); this represents a potential mechanism for integrating pain and anxiety information into the computation of a defensive strategy.

Interestingly, in the dPAG, nNOS expression is highly localized to the dorsolateral column, and local injection of NO donors in the dPAG induces flight and a decrease in mean arterial pressure, implicating dlPAG nNOS+ neurons in "circa-strike" defense (Braga et al., 2009, Hall and Behbehani, 1998). Electrophysiological recordings from a dPAG slice revealed that NO could induce excitatory postsynaptic potentials (EPSPs), but these are dependent on ionotropic glutamatergic receptors (Hall and Behbehani, 1998). NO here seems to play an opposite role to the aforementioned inhibitory one, suggesting that there is more than one NO population within the PAG. Indeed, this is reflected in our single neuron trascriptome data, as Nos1 is also enriched in cluster '20'. In addition to Nos1+, this cluster also differentially expresses Slc1a3 (encoding the excitatory amino acid transporter EAAT1), indicating that these are excitatory neurons. Cluster '20' neurons also shows increased expression of Grm1, which encodes the Class I post-synaptic metabotropic glutamatergic receptor mGluR1. Slice recordings in the PAG found that mGluR1 agonists inhibit evoked inhibitory post-synaptic currents (iPSCs) (Drew and Vaughan, 2004). Assuming that these cluster '20' Nos1+ Slc1a3+ neurons are the 'flight' neurons of the PAG ('flight' neurons are also found electrophysiologically by Deng et al., 2016 and Masferrer et al., 2018), excitatory inputs from other areas (e.g. SC, VMH) could inhibit the GABAergic inputs to these neurons via the activation of mGluR1. This post-synaptic inhibition mechanism could be part of the molecular substrate underlying the integration of threat signals and other circumstantial/internal variables in deciding whether or not to escape at the PAG level.

Htr2c positive expression is detected in 3 of the 9 clusters. This gene encodes the serotonin receptor subtype 5HT-2C, which in the PAG has been shown to mediate both anxiety and antinociception (Baptista, Nunes-de-Souza, and Canto-de-Souza 2012; Yamashita, de Bortoli, and Zangrossi 2011). In particular, 5HT-2C receptor activation in the PAG, in contrast to that of

5HT-2A, has been shown to facilitate medial hypothalamus triggered defensive responses ('hissing') in a scalable manner in cats (Shaikh, De Lanerolle, and Siegel 1997). Serotoninergic projections to the PAG originate from the raphe nuclei in the medulla and midbrain (Lovick 1994). Specifically, stimulation of the dorsal raphe (DR) serotoninergic projection to the PAG (but not the one from the median raphe nucleus) evokes both excitatory and inhibitory responses in the dPAG (Lovick 1994); this could potentially be explained by our discovery of multiple subtypes of 5HT-2C expressing neurons in the PAG (only around 25% of the dPAG neurons recorded showed both inhibitory and excitatory responses to DR stimulation). Deep brain stimulation of DR inhibits avoidance and escape (Wscieklica et al., 2017); this could potentially be explained by the release of serotonin activating 5HT-2C expressing Gad2+ neurons (cluster '16') in the PAG, which then inhibits the flight neurons. This is supported by the finding that activating the PAG-projecting neurons in the DR causes an increase in blood pressure, opposite to the decrease triggered by the activation of dPAG flight neurons (Lovick 1994, Hall and Behbehani, 1998). The potential interplay between 5HT-2C and other neurotransmitter mechanisms, such as with glycine receptor genes in cluster '3' (see below), could be crucial to the modulation and integration of afferent signals in defensive behaviour.

Glycine receptor (GlyR) genes (Glra1, Glra2, Glra3, and Glrb) are upregulated in 5 PAG neuron clusters. GlyR is an ionotropic receptor that is selectively permeable to chloride ions; its activation causes hyperpolarisation. Glycine has been shown to inhibit PAG neurons, and glycine level in PAG is implicated in nociception (Maione et al. 2000; Shin et al. 2003; Min et al. 1996). Glycinergic neurons are found in abundance in the ventromedial medulla and the spinal cord, and given that both structures project to the PAG and their functions in pain, these projections could be the source of intra-PAG glycine (Marchand and Hagino 1983). Furthermore, the inhibitory effects of these inputs could be modulated by 5HT-2C, as they are both enriched in cluster '3', postulating a synaptic mechanism for serotonergic modulation of pain in the PAG.

Transcriptome profiling of ion channel genes allows hypotheses to be made regarding the electrophysiological properties of the neurons, since ion channel composition of a neuron determines its firing pattern. Here we show that different ion channel subunit genes are expressed in distinct PAG neuron clusters. For example, cluster '2' shows significantly increased expression of Kcnc2, which encodes $K_v3.2$, a potassium voltage-gated channel subfamily C member 2. $K_v3.2$ is prominently expressed in neurons that fire at high frequency; $K_v3.1/3.2$ conductance is necessary and kinetically optimized for high-frequency action potential generation (Lien and Jonas 2003; Rudy and McBain 2001). This cluster (that is also Gad2+) thus

potentially contains the fast spiking GABAergic interneurons in the PAG that have been described (Park et al. 2010).

Another ion channel gene, Cacna1d, is enriched in cluster '11', which is also marked by Adcyap1r1 (PACAP receptor) expression. Cacna1d encodes $Ca_v1.3$, a voltage-dependent non-inactivating calcium channel. $Ca_v1.3$ mediates persistent inward currents and serves to amplify neuronal input signals (Sukiasyan, Hultborn, and Zhang 2009). In comparison with other L-type voltage-gated Ca2+ channels, $Ca_v1.3$ has faster kinetics and lower activation thresholds; $Ca_v1.3$ L-type channels will activate in response to physiological stimuli that do not open $Ca_v1.2$ L-type channels (Lipscombe, Helton, and Xu 2004). $Ca_v1.3$ immunoreactivity neurons are widely distributed in rat spinal cord, brainstem and midbrain, including the PAG (Sukiasyan, Hultborn, and Zhang 2009). Neurons expressing Cacna1d hence have the potential to be activated in response to fast, subthreshold depolarisations. Taking into account that PACAP facilitates and potentiates excitatory responses (see section 6.2), this cluster of PAG neurons potentially serves to amplify input signals. PACAP+ neurons from the VMH project to the PAG, and hence these cluster '11' neurons could be the downstream target of this VMH PACAP+ projection (Maekawa et al., 2006). The expression of PACAP in the VMH is regulated according to energy levels (low energy, e.g. during fasting, reduces PACAP mRNA levels) (Hawke et al., 2009); furthermore, these neurons are inhibited by subparaventricular zone neurons signaling circadian rhythm (Todd et al., 2018). PACAP largely co-expresses with SF-1 in the VMH, and the VMH SF1+ neurons have been shown to encode contextual memory of fear (Hawke et al., 2009; Silva et la., 2016). The VMH and PAG have both been well-implicated in defense, but interestingly, optogenetic stimulation of the projection (stimulating the axonal terminals in the PAG) had produced mixed behavioural results (Silva et al., 2013, Wang et al., 2015). This could possibly be explained by varying levels of PACAP (potentially indicative of the internal state of the animal) amplifying this excitatory signal to the dPAG to varying degrees. A defensive strategy has to be optimised in accordance with the internal state of the animal, and the PACAP signaling from the VMH to PAG, together with the enhanced machinery ($Ca_v1.3$) to receive this signal, could be behaviourally crucial for generating a fast, optimized defensive response to sudden incoming threat.

In addition, our transcriptome profiling also implicated novel neuromodulatory mechanisms in the dPAG. Scg2, which marks cluster '13', encodes Secretogranin II, a protein involved in the packaging and sorting of peptide hormones and neuropeptides into secretory vesicles (Huttner, Gerdes, and Rosa 1991; Ozawa et al. 2017). To my knowledge, its role in the PAG (or any other brain structure) has not been looked into.

Expanding the search from candidate genes to all genes revealed 6 more clusters of PAG neurons, and also additional non-neuronal function related markers for previously identified clusters. While the interpretation of the circuit functions of these new clusters of neurons is more challenging, a thorough inspection of the enriched genes could yield new hypotheses regarding properties and functions of PAG neurons. For example, Mrap, a positive marker for cluster '4', encodes melanocortin-2 receptor accessory protein, which is responsible for transporting the melanocortin-2 receptor to the cell surface. Brain-wide Mrap2 (mammalian paralogue of Mrap) has been shown to lead to obesity in mice (Asai et al. 2013). Given its enriched expression in hypothalamus and brainstem, Mrap+ PAG neurons can be participating in the regulation of hyperphagia.

On the whole, our findings from this high-throughput transcriptome profiling experiment have fulfilled the aim of systematically describing and cataloguing PAG neuron subpopulations. The data offers molecular and circuit level explanations of known interactions between types of neurotransmitter in the PAG, and brings into view potential modulatory mechanisms underlying the PAG's regulation of behaviours that await further experimental exploration and verification.

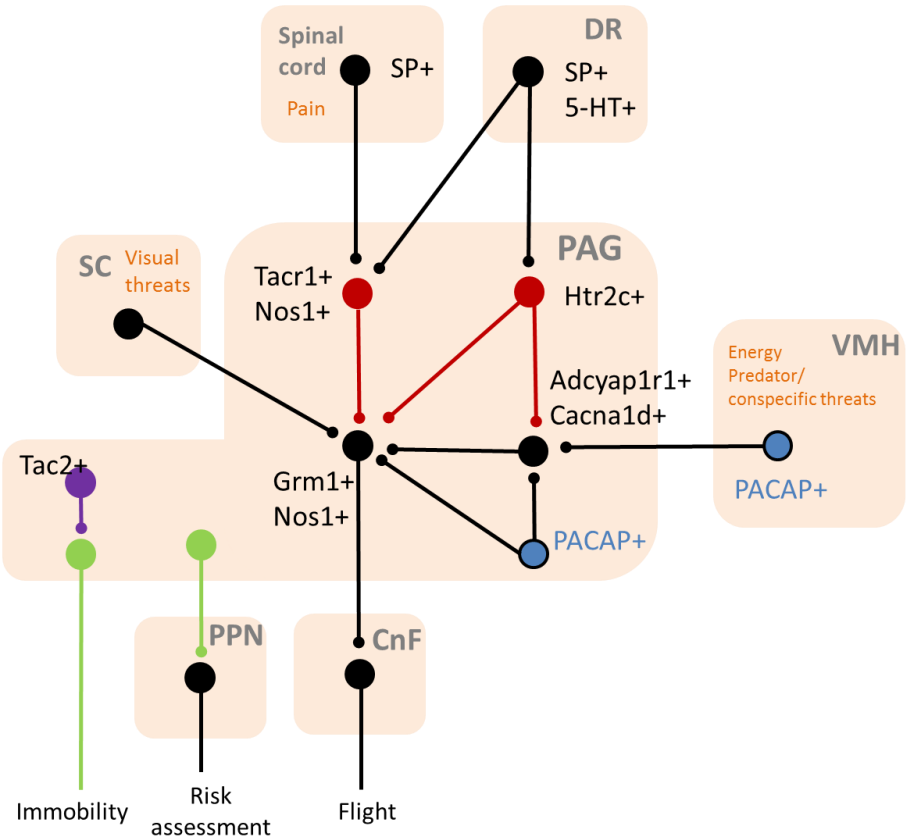

Figure 16. A model for a molecularly-defined PAG defense circuit. Black: excitatory neurons; red: inhibitory neurons; blue: PACAP+ neurons (which are also excitatory); purple: Tac2+ neurons; green: neurons of unknown identity

6.2 The dPAG escape pathway

It is well-established that dPAG stimulation triggers flights, which are accompanied by fear-related autonomic responses such as tachycardia and ultrasonic vocalisation (R. Bandler and Shipley 1994). However, it was not previously known whether the same dPAG neurons trigger both the locomotive and autonomic aspects of the fear behaviour. With optogenetic stimulation and a defensive behavioural test battery, we identified at least two classes of neurons responsible for escape behaviour in mice. Our data from optogenetic stimulation of dPAG vGlut2+ neurons agree with recently published results that described an increase in flight speed with increasing intensity and frequency of stimulation. We further showed that these flights are not simply locomotive, but are safety-oriented escapes accompanied by tachycardia.

Our experiments on PACAP (officially named Adcyap1) expressing neurons are, to my knowledge, the first attempt to functionally map dPAG neuron types beyond excitatory versus inhibitory. We showed that the activation of PACAP+ neurons, like that of vGlut2+ neurons, are sufficient for triggering escape. It is likely the PACAP+ neurons are a subset of vGlut2+ neurons; PACAP+ neurons have been demonstrated to be glutamatergic in the PVN, PMV and suprachiasmatic nucleus (SCN), for example (Krashes et al. 2014; Ross et al. 2018; Michel et al. 2006). Furthermore, in the SCN, it was found that PACAP release itself causes very little effect on postsynaptic Ca2+ transients, but potentiates AMPA-evoked currents and enhances AMPA and NMDA evoked Ca2+ transients, through PAC1 receptor binding and the adenylyl cyclase signalling cascade, suggesting a role as an amplifier at excitatory synapses (Michel et al. 2006). Whether or not PACAP the neuromodulator itself modulates escape is not clear from this experiment: it is not clear what causes its synaptic release. That being said, PACAP mRNA enrichment has been identified as a marker for specific behaviour. For example, using activity-dependent ribosomal profiling, Tan et al. identified PACAP as a marker for warm-sensitive neurons in the ventral MPO (Tan et al. 2016). PACAP+ neurons have also been shown to be involved in local circuits: in the VMH, PACAP+ neurons are enriched in the central zone (VMHc) (T. C. Chou et al. 2003; Todd et al. 2018). VMHc PACAP+ neurons activate VMHvl neurons, and pharmacogenetic activation of VMHc PACAP+ neurons, like that of VMHvl Esr1+ neurons, drives aggression in mice (Todd et al. 2018; Lin et al. 2011). Given that PACAP+ neurons are enriched in dm/lPAG, while the dPAG output pathway for flights are from the dlPAG, it is possible that dm/lPAG PACAP+ neurons project to dlPAG vGlut2+ neurons in driving escape. The PACAP neurons in the dPAG could also project the distinct population of Adcyap1r1+ neurons revealed by our single neuron transcriptome study (see the last section for a discussion of their potential role), adding another layer of control on defensive behaviour at the PAG level. The

transciriptome profiling and optogenetic activation data together provided entirely novel insights into a PACAP-mediated subcortical defense circuit.

We further identified the dlPAG-CnF pathway as an output pathway for escape. CnF vGlut2+ neurons have been shown to drive high-speed escape-like locomotion (Caggiano et al. 2018). The CnF is a central structure within the Midbrain Locomotor Region (MLR), an area that, when activated, initiates locomotor activity in all vertebrates (Robertson et al. 2014). The MLR represents a convenient locomotor control interface between the brain and the spinal cord: the higher its activation, the stronger the activity in the downstream spinal networks and the higher the resulting motor activity level. We showed that the optogenetic activation of both the soma and axonal terminal of the dPAG-CnF projection neurons drive safety-oriented escape, which is surprising considering the exclusively locomotor role of the CnF. This could be explained potentially by feedback from the spinal cord to the PAG and/or CnF.

PPN is another structure within the MLR, and it has been implicated in regulating slow, exploratory locomotion; like the CnF, it receives projections from the PAG (Caggiano et al. 2018). We showed that different PAG neuronal subpopulations project to the PPN and CnF using CTB retrograde tracing, in line with our observation that vGlut2+ and PACAP+ neurons send a dense projection to the CnF but not the PPN. While it is well-established that the PAG sends a variety of ascending and descending projections to different areas, this bissection in projection neurons, which could be critical for the PAG's role as the coordinator of different aspects of defensive behaviour, have not been previously explored. Previous single unit recording experiments in mice have identified a subpopulation of dPAG neurons that fires during risk assessment towards a predator (right before a flight from the predator), and is distinct from flight neurons (H. Deng, Xiao, and Wang 2016; Masferrer et al. 2018). These neurons could potentially project to the PPN to drive cautious exploration. They can be receiving separate inputs from output neurons to the CnF (given that they do not seem to be confined to a specific PAG column), and/or local interneurons could be mediating the level of activity between the two subpopulations to adjust defensive strategies in response to different threats.

6.3 Immobility is regulated by a separate pathway in dPAG

We identified a separate subpopulation of dPAG neurons, marked by Tac2 enrichment, that modulates immobility in response to a threat. This represents the first optogenetic study on dmPAG neurons; the role of this column has been relatively elusive. The behavioural function of Tac2 in the PAG has only been studied in the context of Nk3R function: Nk3R preferentially binds Tac2 (instead of Tac1 or substance P), and pharmacological activation of of Nk3R causes hyperalgesia and increase in exploratory locomotion. The physiological source of Tac2 causing this effect does not necessarily come from PAG Tac2+ neurons; Tac2+ neurons in the CeA projects to the PAG (Raul Andero, personal communications). Recently, Tac2 has been implicated in social isolation stress. Zelikowsky et al. reported an upregulation of Tac2 expression in the brains of mice that had been socially isolated for 2-4 weeks, in comparison with group-housed control (Zelikowsky et al. 2018). Using an Nk3R antagonist and pharmacogenetic activation of Tac2 neurons (with additional viral-delivered Tac2 mRNA), they showed that Tac2 is necessary and sufficient for the behavioural effects of social isolation stress.

We showed that dmPAG Tac2+ neurons specifically modulate immobility, but not other aspects of defensive behaviours, such as stretch, nor heart rate changes. The modulation effect size is statistically significant but small; this could potentially be explained by the fact that due to experimental needs, animals are singly housed for at least 2 weeks prior to behavioural testing. This would presumably cause an increase in Tac2 and freezing already prior to the start of our behavioural test, limiting the range of possible responses. It would be interesting to check if other aspects of defensive behaviours would be modulated by Tac2+ activation if the animals were not subjected to social isolation before behavioural testing.

We do not observe descending projections of dmPAG Tac2+ neurons to anywhere other than to the deep layers of the SC, unlike vGlut2+ or PACAP+ neurons. While this should be confirmed with another tract tracing approach (such as using an AAV expressing fluorescent- tagged synaptophysin in a Cre-dependent manner, as ChR2-eGFP might not strongly label all axonal terminals), it suggests that these are not output neurons, but interneurons modulating the activity of immobility neurons in the PAG. vlPAG vGlut2+ and Gad2+ neurons drive and inhibit freezing respectively, and vlPAG Gad2+ neurons receive projections from dlPAG vGlut2+ neurons (Tovote et al. 2016). It is possible that Tac2+ neurons interact with this pathway to modulate immobility towards conspecific and predator threats. Confirming the identity of the dmPAG Tac2+ neurons (we were unable to reliably detect Tac2 expression in the single neuron study) would aid in elucidating its role in the immobility circuit.

6.4 Top-down vs Bottom-up: a concluding remark

Neurons are complex machines. The same input to two neurons can result in completely different responses, depending on the ion channels in the neurons, the receptors on their dendritic terminals, the neurotransmitters they use, etc. Neurons can be described by their location, morphology, connectivity, electrophysiologically profiled firing properties, or c-fos mapped behavioural roles. A transcriptomic description is advantageous mainly for two reasons: the gene expression profile of a neuron correlates tightly with its molecular and hence functional capabilities, and it provides a genetic handle for their manipulation.

Over the past few years, there has been a boom in large-scale single brain cell transcriptome profiling studies, cataloguing millions of neurons in different areas of the mouse, primate and human brains (Zeisel et al. 2015, 2018; Hochgerner et al. 2018; La Manno et al. 2016; Habib et al. 2016; Lacar et al. 2016; Zhong et al. 2018; Fan et al. 2018; Chen et al. 2017; Wu et al. 2017; Habib et al. 2017). These have identified genetically marked neuronal subpopulations, and the potential hierarchical relationships between them. Yet to integrate this molecular information into circuit level understanding has proven to be extremely challenging. Without prior knowledge the functions of most of these genes in the context of a neural circuit, it is difficult to make hypotheses regarding the functional consequences of distinct transcriptome profiles. As shown here, to interpret the results from our single neuron transcriptome dataset, we relied heavily on existing knowledge of neurotransmitter and neuropeptide genes.

The obvious question that extends from this line of thought (and the elephant in the room for the field) is the relevant level of brain organisation in behaviour (Krakauer et al. 2017). While our optogenetic manipulation results showed neatly that different transcriptomically-defined subpopulations of neurons regulate distinct aspects of defense, we cannot conclude that the *molecular difference* is the reason for this divergence. Our optogenetic tools activate these neurons but do not specifically trigger the release of the molecule of question. Molecular definitions of neurons are convenient, but the functional and behavioural relevance of the molecule(s) in question is unfortunately left under-appreciated due to this technological limitation. At least within a molecularly complex circuit like the PAG, the development of tools to trigger specific neuromodulator release with high temporal and regional specificity will be key to the advancement of circuit level understanding of how behavioural output is computed and fine tuned.

Ironically, I argue that perhaps a complete description of every single neuron, even if achievable, is meaningless in understanding behavioural circuits. The challenges faced in the

data analysis process to disentangle true biological variation from technical noise illustrate why an unbiased profiling of single cell transcriptome is impossible. We investigated *single neurons* with the motivation to find *populations*; bigger clusters with highly expressed genes are much more robust than small clusters and genes with low expression. Expression of known genes in previously described populations gives power to the methods, and understanding potential functional roles of subpopulations relies on prior knowledge from hypothesis-driven experiments. It is possible that every difference in gene expression could mean a different behavioural role for a neuron, but this is at least currently beyond our capabilities to detect and interpret at a circuit level, let alone in mouse behaviour. Studies into the dynamics between *ensembles* of neurons, defined by connectivity and/or transcriptome, is likely to be the most productive in terms of understanding the neural substrate underlying behaviour.

6.5 Experimental outlook

The results of this study created many new hypotheses and questions regarding the PAG neural circuit. In particular, the single neuron transcriptome data opens up opportunities to probe functional roles of specific elements of this circuit. In this final section, I will outline the most pressing questions that I feel need to be addressed.

The role of dPAG inhibitory neurons in defense

Gad2 emerged as a marker for two dPAG neuronal subpopulations from the single neuron transcriptome profiling experiment. While vGlut2+ and Gad2+ neurons in the vlPAG have opposing roles in behaviour, this does not seem to be the case in dPAG (Tamara Franklin and Bianca Silva, unpublished data). Identifying the functions of dPAG Gad2+ neurons in defense using optogenetic and/or pharmacogenetic manipulations and their connections both within the PAG and beyond will be crucial for a comprehensive understanding of the role of the PAG in innate defensive behaviour.

Identifying the PAG risk assessment pathway

There exists a subpopulation of neurons that regulates risk assessment in the dPAG, separate from the flight and immobility neurons described in this study. Risk assessment is a key aspect of mouse defensive strategy, especially when the threat is not discrete and its imminence is unclear. One approach for their identification and manipulation will be to retrogradely label them from the PPN, then perform transcriptome analysis on labelled neurons in the PAG to map them molecularly, and use an optogenetic stimulation approach similar to the one used in Chapter 5 to confirm their role in risk assessment. This, of course, is all based on the assumption that the dPAG risk assessment neurons project to the PPN.

In vivo Calcium imaging of PAG neurons during defense

Another approach to functionally dissect the PAG neural circuit underlying defensive responses is to make use of in vivo calcium imaging, where single neuronal activity can be repeatedly recorded across multiple behavioural sessions spanning weeks. GCaMP expression could be restricted to one of the cell types identified in Chapter 3 using Cre driver lines. In vivo calcium imaging in the midbrain has delineated a SC-PAG synaptic mechanism involved in the computation of escape decision (Evans et al. 2018); to employ the same technique in our

behavioural paradigms would bring an added level of understanding to our current molecular knowledge of the circuit.

Understanding the integration of inputs in the PAG

Central to the PAG's regulation of defense is the array of inputs it receives, yet it remains unclear how the information is integrated in the PAG. Our results suggest both neuromodulation at the synaptic level and local interneurons could be involved. Inputs from the mPFC are of particular interest, as they represent a high level control over a primary behavioural structure. It has been demonstrated that the mPFC-dPAG projection is involved in social avoidance in mice, and this connection appears to encode the imminence of threat in humans. Knowledge of the molecular underpinnings of cortical regulation of PAG activity will provide an entry point for understanding how the PAG computes defensive and other instinctive behaviours.

Bibliography

Albin, R. L., R. L. Makowiec, Z. Hollingsworth, L. S. Dure 4th, J. B. Penney, and A. B. Young. 1990. "Excitatory Amino Acid Binding Sites in the Periaqueductal Gray of the Rat." *Neuroscience Letters* 118 (1): 112–15.

Altman, J., and S. A. Bayer. 1981. "Development of the Brain Stem in the Rat. V. Thymidine-Radiographic Study of the Time of Origin of Neurons in the Midbrain Tegmentum." *The Journal of Comparative Neurology* 198 (4): 677–716.

Amano, K., T. Tanikawa, H. Iseki, H. Kawabatake, M. Notani, H. Kawamura, and K. Kitamura. 1978. "Single Neuron Analysis of the Human Midbrain Tegmentum." *Stereotactic and Functional Neurosurgery* 41 (1-4): 66–78.

Andero, Raül, Brian G. Dias, and Kerry J. Ressler. 2014. "A Role for Tac2, NkB, and Nk3 Receptor in Normal and Dysregulated Fear Memory Consolidation." *Neuron* 83 (2): 444–54.

An, X., R. Bandler, D. Ongür, and J. L. Price. 1998. "Prefrontal Cortical Projections to Longitudinal Columns in the Midbrain Periaqueductal Gray in Macaque Monkeys." *The Journal of Comparative Neurology* 401 (4): 455–79.

Asai, Masato, Shwetha Ramachandrappa, Maria Joachim, Yuan Shen, Rong Zhang, Nikhil Nuthalapati, Visali Ramanathan, et al. 2013. "Loss of Function of the Melanocortin 2 Receptor Accessory Protein 2 Is Associated with Mammalian Obesity." *Science* 341 (6143): 275–78.

Aschauer, Dominik F., Sebastian Kreuz, and Simon Rumpel. 2013. "Analysis of Transduction Efficiency, Tropism and Axonal Transport of AAV Serotypes 1, 2, 5, 6, 8 and 9 in the Mouse Brain." *PloS One* 8 (9): e76310.

Báez, Jesús, Maximina Monzón-Mayor, Carmen Yanes, Maria del Mar Romero-Alemán, Juan Francisco Arbelo-Galván, and Luis Puelles. 2003. "Neuronal Differentiation Patterns in the Optic Tectum of the Lizard Gallotia Galloti." *Brain Research* 975 (1-2): 48–65.

Bandler, R., and P. Carrive. 1988. "Integrated Defence Reaction Elicited by Excitatory Amino Acid Microinjection in the Midbrain Periaqueductal Grey Region of the Unrestrained Cat." *Brain Research* 439 (1-2): 95–106.

Bandler, Richard, Pascal Carrive, and Antoine Depaulis. 1991. "Emerging Principles of Organization of the Midbrain Periaqueductal Gray Matter." In *The Midbrain Periaqueductal Gray Matter: Functional, Anatomical, and Neurochemical Organization*, edited by Antoine Depaulis and Richard Bandler, 1–8. Boston, MA: Springer US.

Bandler, R., and M. T. Shipley. 1994. "Columnar Organization in the Midbrain Periaqueductal Gray: Modules for Emotional Expression?" *Trends in Neurosciences* 17 (9): 379–89.

Banki, Eszter, Eszter Pakai, Balazs Gaszner, Csaba Zsiboras, Andras Czett, Paras Rahul Parkash Bhuddi, Hitoshi Hashimoto, et al. 2014. "Characterization of the Thermoregulatory Response to Pituitary Adenylate Cyclase-Activating Polypeptide in Rodents." *Journal of Molecular Neuroscience: MN* 54 (3): 543–54.

Baptista, Daniela, Ricardo Luiz Nunes-de-Souza, and Azair Canto-de-Souza. 2012. "Activation of 5-HT(2C) Receptors in the Dorsal Periaqueductal Gray Increases Antinociception in Mice Exposed to the Elevated plus-Maze." *Behavioural Brain Research* 235 (1): 42–47.

Baretta, I. P., J. Assreuy, and T. C. De Lima. 2001. "Nitric Oxide Involvement in the Anxiogenic-like Effect of Substance P." *Behavioural Brain Research* 121 (1-2): 199–205.

Bassi, Gabriel S., Ana C. Broiz, Margarete Z. Gomes, and Marcus L. Brandão. 2009. "Evidence for Mediation of Nociception by Injection of the NK-3 Receptor Agonist, Senktide, into the Dorsal Periaqueductal Gray of Rats." *Psychopharmacology* 204 (1): 13–24.

Behbehani, M. M. 1995. "Functional Characteristics of the Midbrain Periaqueductal Gray." *Progress in Neurobiology* 46 (6): 575–605.

Behbehani, M. M., M. R. Jiang, S. D. Chandler, and M. Ennis. 1990. "The Effect of GABA and Its Antagonists on Midbrain Periaqueductal Gray Neurons in the Rat." *Pain* 40 (2): 195–204.

Beitz, A. J. 1982. "The Organization of Afferent Projections to the Midbrain Periaqueductal Gray of the Rat." *Neuroscience* 7 (1): 133–59.

———. 1985. “The Midbrain Periaqueductal Gray in the Rat. I. Nuclear Volume, Cell Number, Density, Orientation, and Regional Subdivisions.” *The Journal of Comparative Neurology* 237 (4): 445–59.
Berridge, Craig W., and Barry D. Waterhouse. 2003. “The Locus Coeruleus-Noradrenergic System: Modulation of Behavioral State and State-Dependent Cognitive Processes.” *Brain Research. Brain Research Reviews* 42 (1): 33–84.
Bittencourt, A. S., A. P. Carobrez, L. P. Zamprogno, S. Tufik, and L. C. Schenberg. 2004. “Organization of Single Components of Defensive Behaviors within Distinct Columns of Periaqueductal Gray Matter of the Rat: Role of N-METHYL-D-Aspartic Acid Glutamate Receptors.” *Neuroscience* 125 (1): 71–89.
Blanchard, D. Caroline, and Robert J. Blanchard. 2008. “Chapter 2.4 Defensive Behaviors, Fear, and Anxiety.” In *Handbook of Behavioral Neuroscience*, edited by Robert J. Blanchard, D. Caroline Blanchard, Guy Griebel, and David Nutt, 17:63–79. Elsevier.
Blanchard, D. Caroline, Robert J. Blanchard, and Guy Griebel. 2005. “Defensive Responses to Predator Threat in the Rat and Mouse.” *Current Protocols in Neuroscience / Editorial Board, Jacqueline N. Crawley ... [et Al.]* Chapter 8 (February): Unit 8.19.
Blanchard, D. Caroline, Guy Griebel, and Robert J. Blanchard. 2003. “The Mouse Defense Test Battery: Pharmacological and Behavioral Assays for Anxiety and Panic.” *European Journal of Pharmacology* 463 (1-3): 97–116.
Blanchard, D. C., and R. J. Blanchard. 1988. “Ethoexperimental Approaches to the Biology of Emotion.” *Annual Review of Psychology* 39: 43–68.
Blanchard, D. C., R. J. Blanchard, P. Tom, and R. J. Rodgers. 1990. “Diazepam Changes Risk Assessment in an Anxiety/defense Test Battery.” *Psychopharmacology* 101 (4): 511–18.
Blanchard, D. C., G. Griebel, and R. J. Blanchard. 2001. “Mouse Defensive Behaviors: Pharmacological and Behavioral Assays for Anxiety and Panic.” *Neuroscience and Biobehavioral Reviews* 25 (3): 205–18.
Blanchard, D. C., G. Williams, E. M. C. Lee, and R. J. Blanchard. 1981. “Taming of Wild Rattus Norvegicus by Lesions of the Mesencephalic Central Gray.” *Psychobiology* 9 (2): 157–63.
Blanchard, R. J., D. C. Blanchard, R. Agullana, and S. M. Weiss. 1991. “Twenty-Two kHz Alarm Cries to Presentation of a Predator, by Laboratory Rats Living in Visible Burrow Systems.” *Physiology & Behavior* 50 (5): 967–72.
Blanchard, R. J., M. A. Hebert, P. F. Ferrari, P. Ferrari, P. Palanza, R. Figueira, D. C. Blanchard, and S. Parmigiani. 1998. “Defensive Behaviors in Wild and Laboratory (Swiss) Mice: The Mouse Defense Test Battery.” *Physiology & Behavior* 65 (2): 201–9.
Blanchard, R. J., and V. O’Donnell. 1979. “Attack and Defensive Behaviors in the Albino Mouse.” *Behavior*. https://onlinelibrary.wiley.com/doi/abs/10.1002/1098-2337(1979)5:4%3C341::AID-AB2480050403%3E3.0.CO;2-H.
Blanchard, Robert J., and D. Caroline Blanchard. 1971. “Defensive Reactions in the Albino Rat.” *Learning and Motivation* 2 (4): 351–62.
Blomqvist, A., and A. D. Craig. 1991. “Organization of Spinal and Trigeminal Input to the PAG.” In *The Midbrain Periaqueductal Gray Matter: Functional, Anatomical, and Neurochemical Organization*, edited by Antoine Depaulis and Richard Bandler, 345–63. Boston, MA: Springer US.
Bolles, R. C. 1970. “Species-Specific Defense Reactions and Avoidance Learning.” *Psychological Review*. http://psycnet.apa.org/journals/rev/77/1/32/.
Borelli, Karina G., and Marcus L. Brandão. 2008. “Effects of Ovine CRF Injections into the Dorsomedial, Dorsolateral and Lateral Columns of the Periaqueductal Gray: A Functional Role for the Dorsomedial Column.” *Hormones and Behavior* 53 (1): 40–50.
Braga, Andréa Arantes, Daniele Cristina Aguiar, and Francisco Silveira Guimarães. 2009. “NOC-9, a Selective Nitric Oxide Donor, Induces Flight Reactions in the Dorsolateral Periaqueductal Gray of Rats by Activating Soluble Guanylate Cyclase.” Neuroscience Letters 459 (2): 79–83.
Borgius, Lotta, C. Ernesto Restrepo, Richardson N. Leao, Noor Saleh, and Ole Kiehn. 2010. “A Transgenic Mouse Line for Molecular Genetic Analysis of Excitatory Glutamatergic Neurons.” *Molecular and Cellular Neurosciences* 45 (3): 245–57.

Bullitt, E. 1990. “Expression of c-Fos-like Protein as a Marker for Neuronal Activity Following Noxious Stimulation in the Rat.” *The Journal of Comparative Neurology* 296 (4): 517–30.

Caggiano, V., R. Leiras, H. Goñi-Erro, D. Masini, C. Bellardita, J. Bouvier, V. Caldeira, G. Fisone, and O. Kiehn. 2018. “Midbrain Circuits That Set Locomotor Speed and Gait Selection.” *Nature* 553 (7689): 455–60.

Cameron, A. A., I. A. Khan, K. N. Westlund, and W. D. Willis. 1995. “The Efferent Projections of the Periaqueductal Gray in the Rat: A Phaseolus Vulgaris-Leucoagglutinin Study. II. Descending Projections.” *The Journal of Comparative Neurology* 351 (4): 585–601.

Cameron, Adrian A., Iqbal A. Khan, Karin N. Westlund, Kenneth D. Cliffer, and William D. Willis. 1995. “The Efferent Projections of the Periaqueductal Gray in the Rat: A Phaseolus Vulgaris-Leucoagglutinin Study. I. Ascending Projections.” *The Journal of Comparative Neurology* 351 (4): 568–84.

Canteras, Newton Sabino. 2018. “Hypothalamic Survival Circuits Related to Social and Predatory Defenses and Their Interactions with Metabolic Control, Reproductive Behaviors and Memory Systems.” *Current Opinion in Behavioral Sciences* 24 (December): 7–13.

Canteras, N. S., S. Chiavegatto, L. E. Ribeiro do Valle, and L. W. Swanson. 1997. “Severe Reduction of Rat Defensive Behavior to a Predator by Discrete Hypothalamic Chemical Lesions.” *Brain Research Bulletin* 44 (3): 297–305.

Canteras, N. S., R. B. Simerly, and L. W. Swanson. 1992. “Projections of the Ventral Premammillary Nucleus.” *The Journal of Comparative Neurology* 324 (2): 195–212.

———. 1994. “Organization of Projections from the Ventromedial Nucleus of the Hypothalamus: A Phaseolus Vulgaris-Leucoagglutinin Study in the Rat.” *The Journal of Comparative Neurology* 348 (1): 41–79.

———. 1995. “Organization of Projections from the Medial Nucleus of the Amygdala: A PHAL Study in the Rat.” *The Journal of Comparative Neurology* 360 (2): 213–45.

Canteras, N. S., and L. W. Swanson. 1992. “The Dorsal Premammillary Nucleus: An Unusual Component of the Mammillary Body.” *Proceedings of the National Academy of Sciences of the United States of America* 89 (21): 10089–93.

Carrive, P., P. Leung, J. Harris, and G. Paxinos. 1997. “Conditioned Fear to Context Is Associated with Increased Fos Expression in the Caudal Ventrolateral Region of the Midbrain Periaqueductal Gray.” *Neuroscience* 78 (1): 165–77.

Cezario, A. F., E. R. Ribeiro-Barbosa, M. V. C. Baldo, and N. S. Canteras. 2008. “Hypothalamic Sites Responding to Predator Threats--the Role of the Dorsal Premammillary Nucleus in Unconditioned and Conditioned Antipredatory Defensive Behavior.” *The European Journal of Neuroscience* 28 (5): 1003–15.

Chen, Renchao, Xiaoji Wu, Lan Jiang, and Yi Zhang. 2017. “Single-Cell RNA-Seq Reveals Hypothalamic Cell Diversity.” *Cell Reports* 18 (13): 3227–41.

Chou, Thomas C., Thomas E. Scammell, Joshua J. Gooley, Stephanie E. Gaus, Clifford B. Saper, and Jun Lu. 2003. “Critical Role of Dorsomedial Hypothalamic Nucleus in a Wide Range of Behavioral Circadian Rhythms.” *The Journal of Neuroscience: The Official Journal of the Society for Neuroscience* 23 (33): 10691–702.

Chou, Xiao-Lin, Xiyue Wang, Zheng-Gang Zhang, Li Shen, Brian Zingg, Junxiang Huang, Wen Zhong, Lukas Mesik, Li I. Zhang, and Huizhong Whit Tao. 2018. “Inhibitory Gain Modulation of Defense Behaviors by Zona Incerta.” *Nature Communications* 9 (1): 1151.

Conti, F., P. Barbaresi, and M. Fabri. 1988. “Cytochrome Oxidase Histochemistry Reveals Regional Subdivisions in the Rat Periaqueductal Gray Matter.” *Neuroscience* 24 (2): 629–33.

Cooper, William E. 2006. “Dynamic Risk Assessment: Prey Rapidly Adjust Flight Initiation Distance to Changes in Predator Approach Speed.” *Ethology: Formerly Zeitschrift Fur Tierpsychologie* 112 (9): 858–64.

Corcoran, Louise, Michelle Roche, and David P. Finn. 2015. “The Role of the Brain’s Endocannabinoid System in Pain and Its Modulation by Stress.” *International Review of Neurobiology* 125 (November): 203–55.

Dale, N., S. Schacher, and E. R. Kandel. 1988. “Long-Term Facilitation in Aplysia Involves Increase in Transmitter Release.” *Science* 239 (4837): 282–85.

Davern, Pamela J. 2014. “A Role for the Lateral Parabrachial Nucleus in Cardiovascular Function and Fluid Homeostasis.” *Frontiers in Physiology* 5 (November): 436.

De Araújo, J. E., R. C. Silva, J. P. Huston, and M. L. Brandão. 1999. “Anxiogenic Effects of Substance P and Its 7-11 C Terminal, but Not the 1-7 N Terminal, Injected into the Dorsal Periaqueductal Gray.” *Peptides* 20 (12): 1437–43.

Deng, Hanfei, Xiong Xiao, and Zuoren Wang. 2016. “Periaqueductal Gray Neuronal Activities Underlie Different Aspects of Defensive Behaviors.” *The Journal of Neuroscience: The Official Journal of the Society for Neuroscience* 36 (29): 7580–88.

Deng, Qiaolin, Daniel Ramsköld, Björn Reinius, and Rickard Sandberg. 2014. “Single-Cell RNA-Seq Reveals Dynamic, Random Monoallelic Gene Expression in Mammalian Cells.” *Science* 343 (6167): 193–96.

Díaz, C., C. Yanes, C. M. Trujillo, and L. Puelles. 2000. “Cytoarchitectonic Subdivisions in the Subtectal Midbrain of the Lizard Gallotia Galloti.” *Journal of Neurocytology* 29 (8): 569–93.

Dicks, D., R. E. Myers, and A. Kling. 1968. “Uncus and Amygdala Lesions: Effects on Social Behavior in the Free-Ranging Rhesus Monkey.” *Science* 165 (3888): 69–71.

Dielenberg, R. A., G. E. Hunt, and I. S. McGregor. 2001. “‘When a Rat Smells a Cat’: The Distribution of Fos Immunoreactivity in Rat Brain Following Exposure to a Predatory Odor.” *Neuroscience* 104 (4): 1085–97.

Dobin, Alexander, Carrie A. Davis, Felix Schlesinger, Jorg Drenkow, Chris Zaleski, Sonali Jha, Philippe Batut, Mark Chaisson, and Thomas R. Gingeras. 2013. “STAR: Ultrafast Universal RNA-Seq Aligner.” *Bioinformatics* 29 (1): 15–21.

Drew, Geoffrey M., and Christopher W. Vaughan. 2004. “Multiple Metabotropic Glutamate Receptor Subtypes Modulate GABAergic Neurotransmission in Rat Periaqueductal Grey Neurons in Vitro.” Neuropharmacology 46 (7): 927–34.

Estrada, Viviane Batista, Natália Kimie Matsubara, Marcus Vinicius Gomes, Fernando Morgan Aguiar Corrêa, and Gislaine Garcia Pelosi. 2016. “Noradrenaline Microinjected into the Dorsal Periaqueductal Gray Matter Causes Anxiolytic-like Effects in Rats Tested in the Elevated T-Maze.” *Life Sciences* 152 (May): 94–98.

Evans, Dominic A., A. Vanessa Stempel, Ruben Vale, Sabine Ruehle, Yaara Lefler, and Tiago Branco. 2018. “A Synaptic Threshold Mechanism for Computing Escape Decisions.” *Nature* 558 (7711): 590–94.

Falkner, Annegret L., Piotr Dollar, Pietro Perona, David J. Anderson, and Dayu Lin. 2014. “Decoding Ventromedial Hypothalamic Neural Activity during Male Mouse Aggression.” *The Journal of Neuroscience: The Official Journal of the Society for Neuroscience* 34 (17): 5971–84.

Fanselow, Michael S. 1991. “The Midbrain Periaqueductal Gray as a Coordinator of Action in Response to Fear and Anxiety.” In *The Midbrain Periaqueductal Gray Matter: Functional, Anatomical, and Neurochemical Organization*, edited by Antoine Depaulis and Richard Bandler, 151–73. Boston, MA: Springer US.

Fanselow, M. S. 1984. “Shock-Induced Analgesia on the Formalin Test: Effects of Shock Severity, Naloxone, Hypophysectomy, and Associative Variables.” *Behavioral Neuroscience* 98 (1): 79–95.

———. 1989. “The Adaptive Function of Conditioned Defensive Behavior: An Ecological Approach to Pavlovian Stimulus-Substitution Theory.” In *Ethoexperimental Approaches to the Study of Behavior*, edited by R. J. Blanchard, P. F. Brain, D. C. Blanchard, and S. Parmigiani, 48:151–66. NATO Advanced Science Institutes Series. Series D: Behavioural and Social Sciences. New York, NY, US: Kluwer Academic/Plenum Publishers.

———. 1994. “Neural Organization of the Defensive Behavior System Responsible for Fear.” *Psychonomic Bulletin & Review* 1 (4): 429–38.

Fanselow, M. S., and L. S. Lester. 1988. “A Functional Behavioristic Approach to Aversively Motivated Behavior: Predatory Imminence as a Determinant of the Topography of Defensive Behavior.” In *Evolution and Learning*, edited by R. C. Bolles and M. D. Beecher, 185–212. Lawrence Erlbaum Associates, Inc.

Fan, Xiaoying, Ji Dong, Suijuan Zhong, Yuan Wei, Qian Wu, Liying Yan, Jun Yong, et al. 2018.

"Spatial Transcriptomic Survey of Human Embryonic Cerebral Cortex by Single-Cell RNA-Seq Analysis." *Cell Research*, June. https://doi.org/10.1038/s41422-018-0053-3.

Farnham, M. M. J., M. S. Y. Lung, V. J. Tallapragada, and P. M. Pilowsky. 2012. "PACAP Causes PAC1/VPAC2 Receptor Mediated Hypertension and Sympathoexcitation in Normal and Hypertensive Rats." *American Journal of Physiology. Heart and Circulatory Physiology* 303 (7): H910–17.

Feng, Yu-Peng, Jian Wang, Yu-Lin Dong, Ya-Yun Wang, and Yun-Qing Li. 2015. "The Roles of Neurotensin and Its Analogues in Pain." *Current Pharmaceutical Design* 21 (7): 840–48.

Fernandez de Molina, A., and R. W. Hunsperger. 1959. "Central Representation of Affective Reactions in Forebrain and Brain Stem: Electrical Stimulation of Amygdala, Stria Terminalis, and Adjacent Structures." *The Journal of Physiology* 145 (2): 251–65.

———. 1962. "Organization of the Subcortical System Governing Defence and Flight Reactions in the Cat." *The Journal of Physiology* 160 (February): 200–213.

Fogaça, M. V., S. F. Lisboa, D. C. Aguiar, F. A. Moreira, F. V. Gomes, P. C. Casarotto, and F. S. Guimarães. 2012. "Fine-Tuning of Defensive Behaviors in the Dorsal Periaqueductal Gray by Atypical Neurotransmitters." Brazilian Journal of Medical and Biological Research = Revista Brasileira de Pesquisas Medicas E Biologicas / Sociedade Brasileira de Biofisica ... [et Al.] 45 (4): 357–65.

Fillinger, Clémentine, Ipek Yalcin, Michel Barrot, and Pierre Veinante. 2018. "Efferents of Anterior Cingulate Areas 24a and 24b and Midcingulate Areas 24a' and 24b' in the Mouse." *Brain Structure & Function* 223 (4): 1747–78.

Floyd, N. S., J. L. Price, A. T. Ferry, K. A. Keay, and R. Bandler. 2000. "Orbitomedial Prefrontal Cortical Projections to Distinct Longitudinal Columns of the Periaqueductal Gray in the Rat." *The Journal of Comparative Neurology* 422 (4): 556–78.

Franklin, Tamara B., Bianca A. Silva, Zinaida Perova, Livia Marrone, Maria E. Masferrer, Yang Zhan, Angie Kaplan, et al. 2017. "Prefrontal Cortical Control of a Brainstem Social Behavior Circuit." *Nature Neuroscience* 20 (2): 260–70.

Fremeau, Robert T., Jr, Susan Voglmaier, Rebecca P. Seal, and Robert H. Edwards. 2004. "VGLUTs Define Subsets of Excitatory Neurons and Suggest Novel Roles for Glutamate." Trends in Neurosciences 27 (2): 98–103.

Getting, P. A. 1989. "Emerging Principles Governing the Operation of Neural Networks." *Annual Review of Neuroscience* 12: 185–204.

Graeff, Frederico G. 2004. "Serotonin, the Periaqueductal Gray and Panic." *Neuroscience and Biobehavioral Reviews* 28 (3): 239–59.

Grillner, S., and T. Matsushima. 1991. "The Neural Network Underlying Locomotion in Lamprey--Synaptic and Cellular Mechanisms." *Neuron* 7 (1): 1–15.

Gross, Cornelius T., and Newton Sabino Canteras. 2012. "The Many Paths to Fear." *Nature Reviews. Neuroscience* 13 (9): 651–58.

Gutstein, H. B., A. Mansour, S. J. Watson, H. Akil, and H. L. Fields. 1998. "Mu and Kappa Opioid Receptors in Periaqueductal Gray and Rostral Ventromedial Medulla." *Neuroreport* 9 (8): 1777–81.

Habib, Naomi, Inbal Avraham-Davidi, Anindita Basu, Tyler Burks, Karthik Shekhar, Matan Hofree, Sourav R. Choudhury, et al. 2017. "Massively Parallel Single-Nucleus RNA-Seq with DroNc-Seq." *Nature Methods* 14 (10): 955–58.

Habib, Naomi, Yinqing Li, Matthias Heidenreich, Lukasz Swiech, Inbal Avraham-Davidi, John J. Trombetta, Cynthia Hession, Feng Zhang, and Aviv Regev. 2016. "Div-Seq: Single-Nucleus RNA-Seq Reveals Dynamics of Rare Adult Newborn Neurons." *Science* 353 (6302): 925–28.

Hagenaars, Muriel A., Melly Oitzl, and Karin Roelofs. 2014. "Updating Freeze: Aligning Animal and Human Research." *Neuroscience and Biobehavioral Reviews* 47 (November): 165–76.

Hall, C. W., and M. M. Behbehani. 1997. "The Medial Preoptic Nucleus of the Hypothalamus Modulates Activity of Nitric Oxide Sensitive Neurons in the Midbrain Periaqueductal Gray." *Brain Research* 765 (2): 208–17.

Hall, C. W., and M. M. Behbehani. 1998. "Synaptic Effects of Nitric Oxide on Enkephalinergic, GABAergic, and Glutamatergic Networks of the Rat Periaqueductal Gray." Brain Research

805 (1-2): 69–87.
Hamilton, B. L. 1973. “Cytoarchitectural Subdivisions of the Periaqueductal Gray Matter in the Cat.” *The Journal of Comparative Neurology* 149 (1): 1–27.
Harris-Warrick, R. M., and E. Marder. 1991. “Modulation of Neural Networks for Behavior.” *Annual Review of Neuroscience* 14: 39–57.
Hawke, Zoe, Tina R. Ivanov, David A. Bechtold, Harveen Dhillon, Brad B. Lowell, and Simon M. Luckman. 2009. “PACAP Neurons in the Hypothalamic Ventromedial Nucleus Are Targets of Central Leptin Signaling.” *The Journal of Neuroscience: The Official Journal of the Society for Neuroscience* 29 (47): 14828–35.
Hayward, Linda F. 2007. “Midbrain Modulation of the Cardiac Baroreflex Involves Excitation of Lateral Parabrachial Neurons in the Rat.” *Brain Research* 1145 (May): 117–27.
Herry, Cyril, and Joshua P. Johansen. 2014. “Encoding of Fear Learning and Memory in Distributed Neuronal Circuits.” *Nature Neuroscience* 17 (12): 1644–54.
Hochgerner, Hannah, Amit Zeisel, Peter Lönnerberg, and Sten Linnarsson. 2018. “Conserved Properties of Dentate Gyrus Neurogenesis across Postnatal Development Revealed by Single-Cell RNA Sequencing.” *Nature Neuroscience* 21 (2): 290–99.
Holstege, Gert. 1991. “Descending Pathways from the Periaqueductal Gray and Adjacent Areas.” In *The Midbrain Periaqueductal Gray Matter: Functional, Anatomical, and Neurochemical Organization*, edited by Antoine Depaulis and Richard Bandler, 239–65. Boston, MA: Springer US.
Huttner, W. B., H. H. Gerdes, and P. Rosa. 1991. “The Granin (chromogranin/secretogranin) Family.” *Trends in Biochemical Sciences* 16 (1): 27–30.
Jaitin, Diego Adhemar, Ephraim Kenigsberg, Hadas Keren-Shaul, Naama Elefant, Franziska Paul, Irina Zaretsky, Alexander Mildner, et al. 2014. “Massively Parallel Single-Cell RNA-Seq for Marker-Free Decomposition of Tissues into Cell Types.” *Science* 343 (6172): 776–79.
Jiang, Lichun, Felix Schlesinger, Carrie A. Davis, Yu Zhang, Renhua Li, Marc Salit, Thomas R. Gingeras, and Brian Oliver. 2011. “Synthetic Spike-in Standards for RNA-Seq Experiments.” *Genome Research* 21 (9): 1543–51.
Keay, K. A., and R. Bandler. 2001. “Parallel Circuits Mediating Distinct Emotional Coping Reactions to Different Types of Stress.” *Neuroscience and Biobehavioral Reviews* 25 (7-8): 669–78.
Keay, K. A., K. Feil, B. D. Gordon, H. Herbert, and R. Bandler. 1997. “Spinal Afferents to Functionally Distinct Periaqueductal Gray Columns in the Rat: An Anterograde and Retrograde Tracing Study.” *The Journal of Comparative Neurology* 385 (2): 207–29.
Keay, Kevin A., and Richard Bandler. 2015. “Chapter 10 - Periaqueductal Gray.” In *The Rat Nervous System (Fourth Edition)*, edited by George Paxinos, 207–21. San Diego: Academic Press.
Kiselev, Vladimir Yu, Kristina Kirschner, Michael T. Schaub, Tallulah Andrews, Andrew Yiu, Tamir Chandra, Kedar N. Natarajan, et al. 2017. “SC3: Consensus Clustering of Single-Cell RNA-Seq Data.” *Nature Methods* 14 (5): 483–86.
Klop, Esther-Marije, Leonora J. Mouton, and Gert Holstege. 2002. “Nucleus Retroambiguus Projections to the Periaqueductal Gray in the Cat.” *The Journal of Comparative Neurology*, The physiolog, 445 (1): 47–58.
Kodama, Takashi, Shiloh Guerrero, Minyoung Shin, Seti Moghadam, Michael Faulstich, and Sascha du Lac. 2012. “Neuronal Classification and Marker Gene Identification via Single-Cell Expression Profiling of Brainstem Vestibular Neurons Subserving Cerebellar Learning.” *The Journal of Neuroscience: The Official Journal of the Society for Neuroscience* 32 (23): 7819–31.
Kollack-Walker, S., C. Don, S. J. Watson, and H. Akil. 1999. “Differential Expression of c-Fos mRNA within Neurocircuits of Male Hamsters Exposed to Acute or Chronic Defeat.” *Journal of Neuroendocrinology* 11 (7): 547–59.
Krakauer, John W., Asif A. Ghazanfar, Alex Gomez-Marin, Malcolm A. MacIver, and David Poeppel. 2017. “Neuroscience Needs Behavior: Correcting a Reductionist Bias.” *Neuron* 93 (3): 480–90.

Krashes, Michael J., Bhavik P. Shah, Joseph C. Madara, David P. Olson, David E. Strochlic, Alastair S. Garfield, Linh Vong, et al. 2014. “An Excitatory Paraventricular Nucleus to AgRP Neuron Circuit That Drives Hunger.” *Nature* 507 (7491): 238–42.

Kurimoto, Kazuki, Yukihiro Yabuta, Yasuhide Ohinata, Yukiko Ono, Kenichiro D. Uno, Rikuhiro G. Yamada, Hiroki R. Ueda, and Mitinori Saitou. 2006. “An Improved Single-Cell cDNA Amplification Method for Efficient High-Density Oligonucleotide Microarray Analysis.” *Nucleic Acids Research* 34 (5): e42.

Lacar, Benjamin, Sara B. Linker, Baptiste N. Jaeger, Suguna Krishnaswami, Jerika Barron, Martijn Kelder, Sarah Parylak, et al. 2016. “Nuclear RNA-Seq of Single Neurons Reveals Molecular Signatures of Activation.” *Nature Communications* 7 (April): 11022.

La Manno, Gioele, Daniel Gyllborg, Simone Codeluppi, Kaneyasu Nishimura, Carmen Salto, Amit Zeisel, Lars E. Borm, et al. 2016. “Molecular Diversity of Midbrain Development in Mouse, Human, and Stem Cells.” *Cell* 167 (2): 566–80.e19.

Lammers, J. H., M. R. Kruk, W. Meelis, and A. M. van der Poel. 1988. “Hypothalamic Substrates for Brain Stimulation-Induced Patterns of Locomotion and Escape Jumps in the Rat.” *Brain Research* 449 (1-2): 294–310.

LeDoux, Joseph. 2012. “Rethinking the Emotional Brain.” *Neuron* 73 (4): 653–76.

Lehmann, Michael L., Tomris Mustafa, Adrian M. Eiden, Miles Herkenham, and Lee E. Eiden. 2013. “PACAP-Deficient Mice Show Attenuated Corticosterone Secretion and Fail to Develop Depressive Behavior during Chronic Social Defeat Stress.” *Psychoneuroendocrinology* 38 (5): 702–15.

Lein, Ed S., Michael J. Hawrylycz, Nancy Ao, Mikael Ayres, Amy Bensinger, Amy Bernard, Andrew F. Boe, et al. 2007. “Genome-Wide Atlas of Gene Expression in the Adult Mouse Brain.” *Nature* 445 (7124): 168–76.

Liao, Yang, Gordon K. Smyth, and Wei Shi. 2014. “featureCounts: An Efficient General Purpose Program for Assigning Sequence Reads to Genomic Features.” *Bioinformatics* 30 (7): 923–30.

Lien, Cheng-Chang, and Peter Jonas. 2003. “Kv3 Potassium Conductance Is Necessary and Kinetically Optimized for High-Frequency Action Potential Generation in Hippocampal Interneurons.” *The Journal of Neuroscience: The Official Journal of the Society for Neuroscience* 23 (6): 2058–68.

Lima, Steven L., and Lawrence M. Dill. 1990. “Behavioral Decisions Made under the Risk of Predation: A Review and Prospectus.” *Canadian Journal of Zoology* 68 (4): 619–40.

Lin, Dayu, Maureen P. Boyle, Piotr Dollar, Hyosang Lee, E. S. Lein, Pietro Perona, and David J. Anderson. 2011. “Functional Identification of an Aggression Locus in the Mouse Hypothalamus.” *Nature* 470 (7333): 221–26.

Linnman, Clas, Eric A. Moulton, Gabi Barmettler, Lino Becerra, and David Borsook. 2012. “Neuroimaging of the Periaqueductal Gray: State of the Field.” *NeuroImage* 60 (1): 505–22.

Lipscombe, Diane, Thomas D. Helton, and Weifeng Xu. 2004. “L-Type Calcium Channels: The Low down.” *Journal of Neurophysiology* 92 (5): 2633–41.

Lisboa, S. F., and F. S. Guimarães. 2012. “Differential Role of CB1 and TRPV1 Receptors on Anandamide Modulation of Defensive Responses Induced by Nitric Oxide in the Dorsolateral Periaqueductal Gray.” *Neuropharmacology* 62 (8): 2455–62.

Litvin, Yoav, Nathan S. Pentkowski, D. Caroline Blanchard, and Robert J. Blanchard. 2007. “CRF Type 1 Receptors in the Dorsal Periaqueductal Gray Modulate Anxiety-Induced Defensive Behaviors.” *Hormones and Behavior* 52 (2): 244–51.

Liu, H., S. Chandler, A. J. Beitz, M. T. Shipley, and M. M. Behbehani. 1994. “Characterization of the Effect of Cholecystokinin (CCK) on Neurons in the Periaqueductal Gray of the Rat: Immunocytochemical and in Vivo and in Vitro Electrophysiological Studies.” *Brain Research* 642 (1-2): 83–94.

Li, Yi, Jiawei Zeng, Juen Zhang, Chenyu Yue, Weixin Zhong, Zhixiang Liu, Qiru Feng, and Minmin Luo. 2018. “Hypothalamic Circuits for Predation and Evasion.” *Neuron* 0 (0). https://doi.org/10.1016/j.neuron.2018.01.005.

Lovick, T. A. 1993. “Integrated Activity of Cardiovascular and Pain Regulatory Systems: Role in

Adaptive Behavioural Responses." *Progress in Neurobiology* 40 (5): 631–44.
———. 1994. "Influence of the Dorsal and Median Raphe Nuclei on Neurons in the Periaqueductal Gray Matter: Role of 5-Hydroxytryptamine." *Neuroscience* 59 (4): 993–1000.
———. 2008. "Pro-Nociceptive Action of Cholecystokinin in the Periaqueductal Grey: A Role in Neuropathic and Anxiety-Induced Hyperalgesic States." *Neuroscience and Biobehavioral Reviews* 32 (4): 852–62.
Luppi, P. H., G. Aston-Jones, H. Akaoka, G. Chouvet, and M. Jouvet. 1995. "Afferent Projections to the Rat Locus Coeruleus Demonstrated by Retrograde and Anterograde Tracing with Cholera-Toxin B Subunit and Phaseolus Vulgaris Leucoagglutinin." *Neuroscience* 65 (1): 119–60.
Maekawa, Fumihiko, Ken Fujiwara, Shinji Tsukahara, and Toshihiko Yada. 2006. "Pituitary Adenylate Cyclase-Activating Polypeptide Neurons of the Ventromedial Hypothalamus Project to the Midbrain Central Gray." *Neuroreport* 17 (2): 221–24.
Maione, S., I. Marabese, F. Rossi, L. Berrino, E. Palazzo, and L. Trabace. 2000. "Effects of Persistent Nociception on Periaqueductal Gray Glycine Release." *Neuroscience* 97 (2): 311–16.
Mantyh, P. W. 1982. "The Midbrain Periaqueductal Gray in the Rat, Cat, and Monkey: A Nissl, Weil, and Golgi Analysis." *The Journal of Comparative Neurology* 204 (4): 349–63.
Marchand, J. E., and N. Hagino. 1983. "Afferents to the Periaqueductal Gray in the Rat. A Horseradish Peroxidase Study." *Neuroscience* 9 (1): 95–106.
Mar, Lynn, Fu-Chia Yang, and Qiufu Ma. 2012. "Genetic Marking and Characterization of Tac2-Expressing Neurons in the Central and Peripheral Nervous System." *Molecular Brain* 5 (1): 3.
Martin, M. (2011) Cutadapt Removes Adapter Sequences from High-Throughput Sequencing Reads. *EMBnet Journal*, 17, 10-12.
Martinez, R. C., E. F. Carvalho-Netto, E. R. Ribeiro-Barbosa, M. V. C. Baldo, and N. S. Canteras. 2011. "Amygdalar Roles during Exposure to a Live Predator and to a Predator-Associated Context." *Neuroscience* 172 (January): 314–28.
Masferrer, M. E., B. A. Silva, K. Nomoto, S. Q. Lima, and C. T. Gross. 2018. "Differential Encoding of Predator Fear in the Ventromedial Hypothalamus and Periaqueductal Grey." *bioRxiv*. https://www.biorxiv.org/content/early/2018/03/17/283820.abstract.
Mason, Peggy. 2005. "Ventromedial Medulla: Pain Modulation and beyond." *The Journal of Comparative Neurology* 493 (1): 2–8.
Matsumoto, Seiji, Mark C. Levendusky, Penelope A. Longhurst, Robert M. Levin, and William R. Millington. 2004. "Activation of Mu Opioid Receptors in the Ventrolateral Periaqueductal Gray Inhibits Reflex Micturition in Anesthetized Rats." *Neuroscience Letters* 363 (2): 116–19.
McCarthy, Davis J., Kieran R. Campbell, Aaron T. L. Lun, and Quin F. Wills. 2017. "Scater: Pre-Processing, Quality Control, Normalization and Visualization of Single-Cell RNA-Seq Data in R." *Bioinformatics* 33 (8): 1179–86.
McDonald, A. J. 1998. "Cortical Pathways to the Mammalian Amygdala." *Progress in Neurobiology* 55 (3): 257–332.
Meller, S. T., and B. J. Dennis. 1986. "Afferent Projections to the Periaqueductal Gray in the Rabbit." *Neuroscience* 19 (3): 927–64.
———. 1991. "Efferent Projections of the Periaqueductal Gray in the Rabbit." *Neuroscience* 40 (1): 191–216.
Michel, Stephan, Jason Itri, Jung H. Han, Kathryn Gniotczynski, and Christopher S. Colwell. 2006. "Regulation of Glutamatergic Signalling by PACAP in the Mammalian Suprachiasmatic Nucleus." *BMC Neuroscience* 7 (February): 15.
Miguel, Tarciso Tadeu, and Ricardo Luiz Nunes-de-Souza. 2011. "Anxiogenic and Antinociceptive Effects Induced by Corticotropin-Releasing Factor (CRF) Injections into the Periaqueductal Gray Are Modulated by CRF1 Receptor in Mice." *Hormones and Behavior* 60 (3): 292–300.

Min, B. I., C. J. Kim, J. S. Rhee, and N. Akaike. 1996. “Modulation of Glycine-Induced Chloride Current in Acutely Dissociated Rat Periaqueductal Gray Neurons by Mu-Opioid Agonist DAGO.” *Brain Research* 734 (1-2): 72–78.

Mobbs, Dean. 2018. “The Ethological Deconstruction of Fear(s).” *Current Opinion in Behavioral Sciences* 24 (December): 32–37.

Mobbs, Dean, Predrag Petrovic, Jennifer L. Marchant, Demis Hassabis, Nikolaus Weiskopf, Ben Seymour, Raymond J. Dolan, and Christopher D. Frith. 2007. “When Fear Is near: Threat Imminence Elicits Prefrontal-Periaqueductal Gray Shifts in Humans.” *Science* 317 (5841): 1079–83.

Mongeau, R., B. M. De Oca, M. S. Fanselow, and C. A. Marsden. 1998. “Differential Effects of Neurokinin-1 Receptor Activation in Subregions of the Periaqueductal Gray Matter on Conditional and Unconditional Fear Behaviors in Rats.” *Behavioral Neuroscience* 112 (5): 1125–35.

Morgan, M. M., P. K. Whitney, and M. S. Gold. 1998. “Immobility and Flight Associated with Antinociception Produced by Activation of the Ventral and Lateral/dorsal Regions of the Rat Periaqueductal gray1Published on the World Wide Web on 24 July 1998.1.” *Brain Research* 804 (1): 159–66.

Morley, J. E., M. Horowitz, P. M. Morley, and J. F. Flood. 1992. “Pituitary Adenylate Cyclase Activating Polypeptide (PACAP) Reduces Food Intake in Mice.” *Peptides* 13 (6): 1133–35.

Morrell, J. I., L. M. Greenberger, and D. W. Pfaff. 1981. “Hypothalamic, Other Diencephalic, and Telencephalic Neurons That Project to the Dorsal Midbrain.” *The Journal of Comparative Neurology* 201 (4): 589–620.

Motta, Simone C., Marina Goto, Flavia V. Gouveia, Marcus V. C. Baldo, Newton S. Canteras, and Larry W. Swanson. 2009. “Dissecting the Brain’s Fear System Reveals the Hypothalamus Is Critical for Responding in Subordinate Conspecific Intruders.” *Proceedings of the National Academy of Sciences of the United States of America* 106 (12): 4870–75.

Motta, Simone C., Cibele Carla Guimarães, Isadora Clivatti Furigo, Marcia Harumi Sukikara, Marcus V. C. Baldo, Joseph S. Lonstein, and Newton S. Canteras. 2013. “Ventral Premammillary Nucleus as a Critical Sensory Relay to the Maternal Aggression Network.” *Proceedings of the National Academy of Sciences of the United States of America* 110 (35): 14438–43.

Nasanbuyan, Naranbat, Masahide Yoshida, Yuki Takayanagi, Ayumu Inutsuka, Katsuhiko Nishimori, Akihiro Yamanaka, and Tatsushi Onaka. 2018. “Oxytocin-Oxytocin Receptor Systems Facilitate Social Defeat Posture in Male Mice.” *Endocrinology* 159 (2): 763–75.

Nashold, B. S., Jr, W. P. Wilson, and D. G. Slaughter. 1969. “Sensations Evoked by Stimulation in the Midbrain of Man.” *Journal of Neurosurgery* 30 (1): 14–24.

Netto, Cristina Ferreira, and Francisco Silveira Guimarães. 2004. “Anxiogenic Effect of Cholecystokinin in the Dorsal Periaqueductal Gray.” *Neuropsychopharmacology: Official Publication of the American College of Neuropsychopharmacology* 29 (1): 101–7.

Niederkofler, Vera, Tedi E. Asher, Benjamin W. Okaty, Benjamin D. Rood, Ankita Narayan, Lara S. Hwa, Sheryl G. Beck, Klaus A. Miczek, and Susan M. Dymecki. 2016. “Identification of Serotonergic Neuronal Modules That Affect Aggressive Behavior.” *Cell Reports* 17 (8): 1934–49.

Ogawa, Sonoko, Lee-Ming Kow, Margaret M. McCarthy, Donald W. Pfaff, and Susan Schwartz-Giblin. 1991. “Midbrain PAG Control of Female Reproductive Behavior: In Vitro Electrophysiological Characterization of Actions of Lordosis-Relevant Substances.” In *The Midbrain Periaqueductal Gray Matter: Functional, Anatomical, and Neurochemical Organization*, edited by Antoine Depaulis and Richard Bandler, 211–35. Boston, MA: Springer US.

Oh, Seung Wook, Julie A. Harris, Lydia Ng, Brent Winslow, Nicholas Cain, Stefan Mihalas, Quanxin Wang, et al. 2014. “A Mesoscale Connectome of the Mouse Brain.” *Nature* 508 (7495): 207–14.

Olson, Ian, Shreyas M. Suryanarayana, Brita Robertson, and Sten Grillner. 2017. “Griseum Centrale, a Homologue of the Periaqueductal Gray in the Lamprey.” *IBRO Reports* 2 (June):

24–30.
Ozawa, Takaaki, Edgar A. Ycu, Ashwani Kumar, Li-Feng Yeh, Touqeer Ahmed, Jenny Koivumaa, and Joshua P. Johansen. 2017. “A Feedback Neural Circuit for Calibrating Aversive Memory Strength.” *Nature Neuroscience* 20 (1): 90–97.
Park, Cheongdahm, Jong-Hyun Kim, Bo-Eun Yoon, Eui-Ju Choi, C. Justin Lee, and Hee-Sup Shin. 2010. “T-Type Channels Control the Opioidergic Descending Analgesia at the Low Threshold-Spiking GABAergic Neurons in the Periaqueductal Gray.” *Proceedings of the National Academy of Sciences of the United States of America* 107 (33): 14857–62.
Parker, David. 2006. “Complexities and Uncertainties of Neuronal Network Function.” *Philosophical Transactions of the Royal Society of London. Series B, Biological Sciences* 361 (1465): 81–99.
Petrovich, G. D., P. Y. Risold, and L. W. Swanson. 1996. “Organization of Projections from the Basomedial Nucleus of the Amygdala: A PHAL Study in the Rat.” *The Journal of Comparative Neurology* 374 (3): 387–420.
Picelli, Simone, Omid R. Faridani, Asa K. Björklund, Gösta Winberg, Sven Sagasser, and Rickard Sandberg. 2014. “Full-Length RNA-Seq from Single Cells Using Smart-seq2.” *Nature Protocols* 9 (1): 171–81.
Pinel, John P., Michael J. Mana, and J’anne A. Ward. 1989. “Stretched-Approach Sequences Directed at a Localized Shock Source by Rattus Norvegicus.” *Journal of Comparative Psychology* 103 (2): 140–48.
Puelles, L., and M. C. Bendala. 1978. “Differentiation of Neuroblasts in the Chick Optic Tectum up to Eight Days of Incubation: A Golgi Study.” *Neuroscience* 3 (3): 307–25.
Puelles, L., M. Martinez-De-La-Torre, G. Paxinos, C. Watson, and S. Martinez. 2007. “The Chick Brain in Stereotaxic Coordinates: An Atlas Correlating Avian and Mammalian Neuroanatomy.” Academic Press, San Diego.
Ramsköld, Daniel, Shujun Luo, Yu-Chieh Wang, Robin Li, Qiaolin Deng, Omid R. Faridani, Gregory A. Daniels, et al. 2012. “Full-Length mRNA-Seq from Single-Cell Levels of RNA and Individual Circulating Tumor Cells.” *Nature Biotechnology* 30 (8): 777–82.
Redgrave, P., P. Dean, I. J. Mitchell, A. Odekunle, and A. Clark. 1988. “The Projection from Superior Colliculus to Cuneiform Area in the Rat. I. Anatomical Studies.” *Experimental Brain Research. Experimentelle Hirnforschung. Experimentation Cerebrale* 72 (3): 611–25.
Ressler, Kerry J., Kristina B. Mercer, Bekh Bradley, Tanja Jovanovic, Amy Mahan, Kimberly Kerley, Seth D. Norrholm, et al. 2011. “Post-Traumatic Stress Disorder Is Associated with PACAP and the PAC1 Receptor.” *Nature* 470 (7335): 492–97.
Risold, P. Y., N. S. Canteras, and L. W. Swanson. 1994. “Organization of Projections from the Anterior Hypothalamic Nucleus: A Phaseolus Vulgaris-Leucoagglutinin Study in the Rat.” *The Journal of Comparative Neurology* 348 (1): 1–40.
Robertson, Brita, Andreas Kardamakis, Lorenza Capantini, Juan Pérez-Fernández, Shreyas M. Suryanarayana, Peter Wallén, Marcus Stephenson-Jones, and Sten Grillner. 2014. “The Lamprey Blueprint of the Mammalian Nervous System.” *Progress in Brain Research* 212: 337–49.
Ross, Rachel A., Silvia Leon, Joseph C. Madara, Danielle Schafer, Chrysanthi Fergani, Caroline A. Maguire, Anne Mj Verstegen, et al. 2018. “PACAP Neurons in the Ventral Premammillary Nucleus Regulate Reproductive Function in the Female Mouse.” *eLife* 7 (June). https://doi.org/10.7554/eLife.35960.
Rudy, B., and C. J. McBain. 2001. “Kv3 Channels: Voltage-Gated K+ Channels Designed for High-Frequency Repetitive Firing.” *Trends in Neurosciences* 24 (9): 517–26.
Ruiz-Torner, A., F. Olucha-Bordonau, A. A. Valverde-Navarro, and F. Martínez-Soriano. 2001. “The Chemical Architecture of the Rat’s Periaqueductal Gray Based on Acetylcholinesterase Histochemistry: A Quantitative and Qualitative Study.” *Journal of Chemical Neuroanatomy* 21 (4): 295–312.
Sakurai, Katsuyasu, Shengli Zhao, Jun Takatoh, Erica Rodriguez, Jinghao Lu, Andrew D. Leavitt, Min Fu, Bao-Xia Han, and Fan Wang. 2016. “Capturing and Manipulating Activated Neuronal Ensembles with CANE Delineates a Hypothalamic Social-Fear Circuit.” *Neuron* 92 (4): 739–

53.
Sandner, G., and G. Di Scala. 1991. “Periaqueductal Gray Spike Trains Recorded in Frontal or Horizontal Mesencephalic Brain Slices from the Rat.” *Neuroscience Letters* 121 (1-2): 147–50.
Sandner, G., G. Di Scala, B. Rocha, and M. J. Angst. 1992. “C-Fos Immunoreactivity in the Brain Following Unilateral Electrical Stimulation of the Dorsal Periaqueductal Gray in Freely Moving Rats.” *Brain Research* 573 (2): 276–83.
Sandner, G., P. Schmitt, and P. Karli. 1986. “Unit Activity Alterations Induced in the Mesencephalic Periaqueductal Gray by Local Electrical Stimulation.” *Brain Research* 386 (1-2): 53–63.
Saper, C. B., and A. D. Loewy. 1980. “Efferent Connections of the Parabrachial Nucleus in the Rat.” *Brain Research* 197 (2): 291–317.
Saper, C. B., L. W. Swanson, and W. M. Cowan. 1978. “The Efferent Connections of the Anterior Hypothalamic Area of the Rat, Cat and Monkey’.” *J. COMP. NEUR.* 182: 575–600.
Sasaki, Mitsuyoshi. 2005. “Role of Barrington’s Nucleus in Micturition.” *The Journal of Comparative Neurology* 493 (1): 21–26.
Satija, Rahul, Jeffrey A. Farrell, David Gennert, Alexander F. Schier, and Aviv Regev. 2015. “Spatial Reconstruction of Single-Cell Gene Expression Data.” *Nature Biotechnology* 33 (5): 495–502.
Scalia, F., and S. S. Winans. 1975. “The Differential Projections of the Olfactory Bulb and Accessory Olfactory Bulb in Mammals.” *The Journal of Comparative Neurology* 161 (1): 31–55.
Schenberg, L. C., E. C. Vasquez, and M. B. da Costa. 1993. “Cardiac Baroreflex Dynamics during the Defence Reaction in Freely Moving Rats.” *Brain Research* 621 (1): 50–58.
Selverston, A. I., D. F. Russell, and J. P. Miller. 1976. “The Stomatogastric Nervous System: Structure and Function of a Small Neural Network.” *Progress in Neurobiology* 7 (3): 215–90.
Selverston, Allen I. 1980. “Are Central Pattern Generators Understandable?” *The Behavioral and Brain Sciences* 3 (4): 535–40.
Severini, Cinzia, Giovanna Improta, Giuliana Falconieri-Erspamer, Severo Salvadori, and Vittorio Erspamer. 2002. “The Tachykinin Peptide Family.” *Pharmacological Reviews* 54 (2): 285–322.
Shaikh, M. B., N. C. De Lanerolle, and A. Siegel. 1997. “Serotonin 5-HT1A and 5-HT2/1C Receptors in the Midbrain Periaqueductal Gray Differentially Modulate Defensive Rage Behavior Elicited from the Medial Hypothalamus of the Cat.” *Brain Research* 765 (2): 198–207.
Shin, Min-Chul, Mi-Hyeon Jang, Hyun-Kyung Chang, Youn-Jung Kim, Ee-Hwa Kim, and Chang-Ju Kim. 2003. “Modulation of Cyclooxygenase-2 on Glycine- and Glutamate-Induced Ion Currents in Rat Periaqueductal Gray Neurons.” *Brain Research Bulletin* 59 (4): 251–56.
Shipley, M. T., J. H. McLean, and M. M. Behbehani. 1987. “Heterogeneous Distribution of Neurotensin-like Immunoreactive Neurons and Fibers in the Midbrain Periaqueductal Gray of the Rat.” *The Journal of Neuroscience: The Official Journal of the Society for Neuroscience* 7 (7): 2025–34.
Silva, Bianca A., Camilla Mattucci, Piotr Krzywkowski, Emanuele Murana, Anna Illarionova, Valery Grinevich, Newton S. Canteras, Davide Ragozzino, and Cornelius T. Gross. 2013. “Independent Hypothalamic Circuits for Social and Predator Fear.” *Nature Neuroscience* 16 (12): 1731–33.
Simerly, R. B., and L. W. Swanson. 1988. “Projections of the Medial Preoptic Nucleus: A PhaseoZus Vulgaris Leucoagglutinin Anterograde Tract-Tracing Study in the Rat.” *The Journal of Comparative Neurology* 270: 209–42.
Skinner, B. F. 1950. “Are Theories of Learning Necessary?” *Psychological Review* 57 (4): 193–216.
Smith, Tom, Andreas Heger, and Ian Sudbery. 2017. “UMI-Tools: Modeling Sequencing Errors in Unique Molecular Identifiers to Improve Quantification Accuracy.” *Genome Research* 27 (3): 491–99.

Stiedl, O., and J. Spiess. 1997. “Effect of Tone-Dependent Fear Conditioning on Heart Rate and Behavior of C57BL/6N Mice.” *Behavioral Neuroscience* 111 (4): 703–11.

Stotz-Potter, E. H., L. R. Willis, and J. A. DiMicco. 1996. “Muscimol Acts in Dorsomedial but Not Paraventricular Hypothalamic Nucleus to Suppress Cardiovascular Effects of Stress.” *The Journal of Neuroscience: The Official Journal of the Society for Neuroscience* 16 (3): 1173–79.

Sudré, E. C., M. R. de Barros, G. N. Sudré, and L. C. Schenberg. 1993. “Thresholds of Electrically Induced Defence Reaction of the Rat: Short- and Long-Term Adaptation Mechanisms.” *Behavioural Brain Research* 58 (1-2): 141–54.

Sukiasyan, N., H. Hultborn, and M. Zhang. 2009. “Distribution of Calcium Channel Ca(V)1.3 Immunoreactivity in the Rat Spinal Cord and Brain Stem.” *Neuroscience* 159 (1): 217–35.

Sukikara, Marcia Harumi, Sandra Regina Mota-Ortiz, Marcus Vinícius Baldo, Luciano Freitas Felicio, and Newton Sabino Canteras. 2010. “The Periaqueductal Gray and Its Potential Role in Maternal Behavior Inhibition in Response to Predatory Threats.” *Behavioural Brain Research* 209 (2): 226–33.

Sukikara, M. H., S. R. Mota-Ortiz, M. V. Baldo, L. F. Felício, and N. S. Canteras. 2006. “A Role for the Periaqueductal Gray in Switching Adaptive Behavioral Responses.” *The Journal of Neuroscience: The Official Journal of the Society for Neuroscience* 26 (9): 2583–89.

Svensson, Valentine, Kedar N. Natarajan, Lam-Ha Ly, Ricardo J. Miragaia, Charlotte Labalette, Iain C. Macaulay, Ana Cvejic, and Sarah A. Teichmann. 2016. “Power Analysis of Single Cell RNA-Sequencing Experiments.” *bioRxiv*. https://doi.org/10.1101/073692.

Swanson, L. W. 2000. “Cerebral Hemisphere Regulation of Motivated Behavior.” *Brain Research* 886 (1-2): 113–64.

Swanson, L. W., and G. D. Petrovich. 1998. “What Is the Amygdala?” *Trends in Neurosciences* 21 (8): 323–31.

Tan, Chan Lek, Elizabeth K. Cooke, David E. Leib, Yen-Chu Lin, Gwendolyn E. Daly, Christopher A. Zimmerman, and Zachary A. Knight. 2016. “Warm-Sensitive Neurons That Control Body Temperature.” *Cell* 167 (1): 47–59.e15.

Tang, Fuchou, Catalin Barbacioru, Yangzhou Wang, Ellen Nordman, Clarence Lee, Nanlan Xu, Xiaohui Wang, et al. 2009. “mRNA-Seq Whole-Transcriptome Analysis of a Single Cell.” *Nature Methods* 6 (5): 377–82.

Thompson, R. H., and L. W. Swanson. 1998. “Organization of Inputs to the Dorsomedial Nucleus of the Hypothalamus: A Reexamination with Fluorogold and PHAL in the Rat.” *Brain Research Reviews* 27 (2): 89–118.

Tinbergen, Nikolaas. 1951. *The Study of Instinct*. New York: Clarendon Press/Oxford University Press.

Todd, William D., Henning Fenselau, Joshua L. Wang, Rong Zhang, Natalia L. Machado, Anne Venner, Rebecca Y. Broadhurst, et al. 2018. “A Hypothalamic Circuit for the Circadian Control of Aggression.” *Nature Neuroscience* 21 (5): 717–24.

Tovote, Philip, Maria Soledad Esposito, Paolo Botta, Fabrice Chaudun, Jonathan P. Fadok, Milica Markovic, Steffen B. E. Wolff, et al. 2016. “Midbrain Circuits for Defensive Behaviour.” *Nature* 534 (7606): 206–12.

Treutlein, Barbara, Doug G. Brownfield, Angela R. Wu, Norma F. Neff, Gary L. Mantalas, F. Hernan Espinoza, Tushar J. Desai, Mark A. Krasnow, and Stephen R. Quake. 2014. “Reconstructing Lineage Hierarchies of the Distal Lung Epithelium Using Single-Cell RNA-Seq.” *Nature* 509 (7500): 371–75.

Vargas, L. C., T. A. Marques, and L. C. Schenberg. 2000. “Micturition and Defensive Behaviors Are Controlled by Distinct Neural Networks within the Dorsal Periaqueductal Gray and Deep Gray Layer of the Superior Colliculus of the Rat.” *Neuroscience Letters* 280 (1): 45–48.

Vaudry, David, Anthony Falluel-Morel, Steve Bourgault, Magali Basille, Delphine Burel, Olivier Wurtz, Alain Fournier, et al. 2009. “Pituitary Adenylate Cyclase-Activating Polypeptide and Its Receptors: 20 Years after the Discovery.” *Pharmacological Reviews* 61 (3): 283–357.

Vecino, E., C. Piñuela, R. Arévalo, J. Lara, J. R. Alonso, and J. Aijón. 1992. “Distribution of Enkephalin-like Immunoreactivity in the Central Nervous System of the Rainbow Trout: An Immunocytochemical Study.” *Journal of Anatomy* 180 (Pt 3) (June): 435–53.

Vertes, Robert P. 2004. “Differential Projections of the Infralimbic and Prelimbic Cortex in the Rat.” *Synapse* 51 (1): 32–58.

Vianna, Daniel M. L., and Pascal Carrive. 2005. “Changes in Cutaneous and Body Temperature during and after Conditioned Fear to Context in the Rat.” *The European Journal of Neuroscience* 21 (9): 2505–12.

Vianna, D. M. L., and M. L. Brandão. 2003. “Anatomical Connections of the Periaqueductal Gray: Specific Neural Substrates for Different Kinds of Fear.” *Brazilian Journal of Medical and Biological Research = Revista Brasileira de Pesquisas Medicas E Biologicas / Sociedade Brasileira de Biofisica ... [et Al.]* 36 (5): 557–66.

Wang, Li, Irene Z. Chen, and Dayu Lin. 2015. “Collateral Pathways from the Ventromedial Hypothalamus Mediate Defensive Behaviors.” *Neuron* 85 (6): 1344–58.

Watson, Charles, George Paxinos, and Luis Puelles. 2012. *The Mouse Nervous System*. Academic Press.

Weckowicz, T. E., and H. Liebel-Weckowicz. 1982. “Typologies of the Theory of Behaviorism since Descartes.” *Sudhoffs Archiv* 66 (2): 129–51.

Wei, Pengfei, Nan Liu, Zhijian Zhang, Xuemei Liu, Yongqiang Tang, Xiaobin He, Bifeng Wu, et al. 2015. “Processing of Visually Evoked Innate Fear by a Non-Canonical Thalamic Pathway.” *Nature Communications* 6 (April): 6756.

Wheatley, M. D. 1944. “The Hypothalamus and Affective Behavior in Cats. A Study of the Effects of Experimental Lesions with Anatomic Correlations” 52: 296–316.

Wolters, J. G., H. J. ten Donkelaar, and A. A. Verhofstad. 1986. “Distribution of Some Peptides (substance P, [Leu]enkephalin, [Met]enkephalin) in the Brain Stem and Spinal Cord of a Lizard, Varanus Exanthematicus.” *Neuroscience* 18 (4): 917–46.

Wscieklica, Tatiana, Mariana S. C. F. Silva, Jéssica A. Lemes, Liana Melo-Thomas, Isabel C. Céspedes, and Milena B. Viana. 2017. “Deep Brain Stimulation of the Dorsal Raphe Inhibits Avoidance and Escape Reactions and Activates Forebrain Regions Related to the Modulation of Anxiety/panic.” Behavioural Brain Research 321 (March): 193–200.

Wu, Ye Emily, Lin Pan, Yanning Zuo, Xinmin Li, and Weizhe Hong. 2017. “Detecting Activated Cell Populations Using Single-Cell RNA-Seq.” *Neuron* 96 (2): 313–29.e6.

Xing, Jihong, De-Pei Li, and Jianhua Li. 2008. “Role of GABA Receptors in Nitric Oxide Inhibition of Dorsolateral Periaqueductal Gray Neurons.” Neuropharmacology 54 (4): 734–44.

Xu, Chen, and Zhengchang Su. 2015. “Identification of Cell Types from Single-Cell Transcriptomes Using a Novel Clustering Method.” *Bioinformatics* 31 (12): 1974–80.

Yamashita, Paula Shimene de Melo, Valquiria Camin de Bortoli, and Helio Zangrossi Jr. 2011. “5-HT2C Receptor Regulation of Defensive Responses in the Rat Dorsal Periaqueductal Gray.” *Neuropharmacology* 60 (2-3): 216–22.

Yang, Jun, Peng Li, Jin-Ying Liang, Yan-Juan Pan, Xi-Qin Yan, Fu-Lin Yan, Fang Hao, et al. 2011. “Oxytocin in the Periaqueductal Grey Regulates Nociception in the Rat.” *Regulatory Peptides* 169 (1-3): 39–42.

Yilmaz, Melis, and Markus Meister. 2013. “Rapid Innate Defensive Responses of Mice to Looming Visual Stimuli.” *Current Biology: CB* 23 (20): 2011–15.

Yin, Jun-Bin, Huang-Hui Wu, Yu-Lin Dong, Ting Zhang, Jian Wang, Yong Zhang, Yan-Yan Wei, et al. 2014. “Neurochemical Properties of BDNF-Containing Neurons Projecting to Rostral Ventromedial Medulla in the Ventrolateral Periaqueductal Gray.” *Frontiers in Neural Circuits* 8 (November): 137.

Zeisel, Amit, Hannah Hochgerner, Peter Lonnerberg, Anna Johnsson, Fatima Memic, Job van der Zwan, Martin Haring, et al. 2018. “Molecular Architecture of the Mouse Nervous System.” *bioRxiv*. https://doi.org/10.1101/294918.

Zeisel, Amit, Ana B. Muñoz-Manchado, Simone Codeluppi, Peter Lönnerberg, Gioele La Manno, Anna Juréus, Sueli Marques, et al. 2015. “Brain Structure. Cell Types in the Mouse Cortex and Hippocampus Revealed by Single-Cell RNA-Seq.” *Science* 347 (6226): 1138–42.

Zelikowsky, Moriel, May Hui, Tomomi Karigo, Andrea Choe, Bin Yang, Mario R. Blanco, Keith Beadle, Viviana Gradinaru, Benjamin E. Deverman, and David J. Anderson. 2018. “The Neuropeptide Tac2 Controls a Distributed Brain State Induced by Chronic Social Isolation

Stress." *Cell* 173 (5): 1265–79.e19.
Zhong, Suijuan, Shu Zhang, Xiaoying Fan, Qian Wu, Liying Yan, Ji Dong, Haofeng Zhang, et al. 2018. "A Single-Cell RNA-Seq Survey of the Developmental Landscape of the Human Prefrontal Cortex." *Nature*, March. https://doi.org/10.1038/nature25980.

Supplementary Figures

Supplementary Figure 1. FACS gating strategy for sorting NeuN+ nuclei. (A) Side scatter against DAPI level of single nuclei suspension from cortex, stained with DAPI and anti-NeuN-AF4988 (see methods); Gate P1 contains single nuclei. (B) Histogram of AF-488 levels shows two distinct peaks; Gate P5 contains NeuN+ nuclei. Both graphs are generated with BD FACSDiva 8.0.1

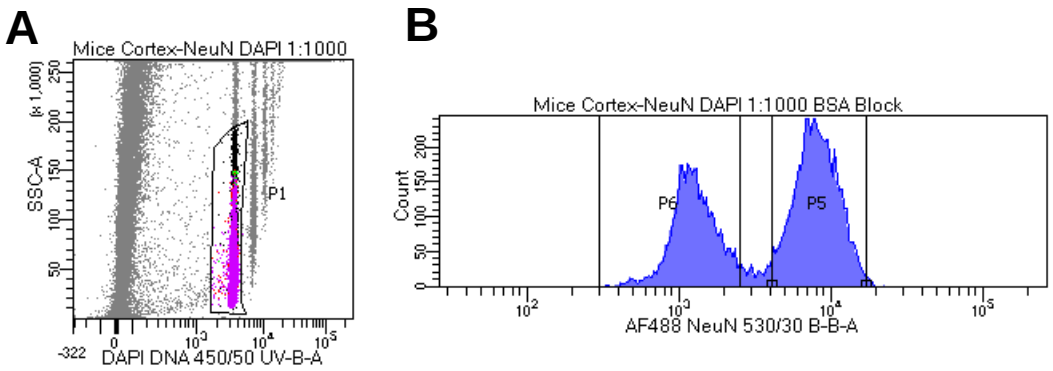

Supplementary Figure 2. Quality control for single nuclei RNA-seq experiments and a comparison with the literature. Violin Plots showing (A) number of counts (transcripts) and (B) number of genes detected sorted by experiment and sample types. cor: FACS sorted cortical neurons; Unsorted_cor: unsorted cortical neurons; Neg_Ctrl: empty wells upon imaging. The reference literature data is obtained from Habib et al. 2017. Dots at the extremes of the violins indicate outliers

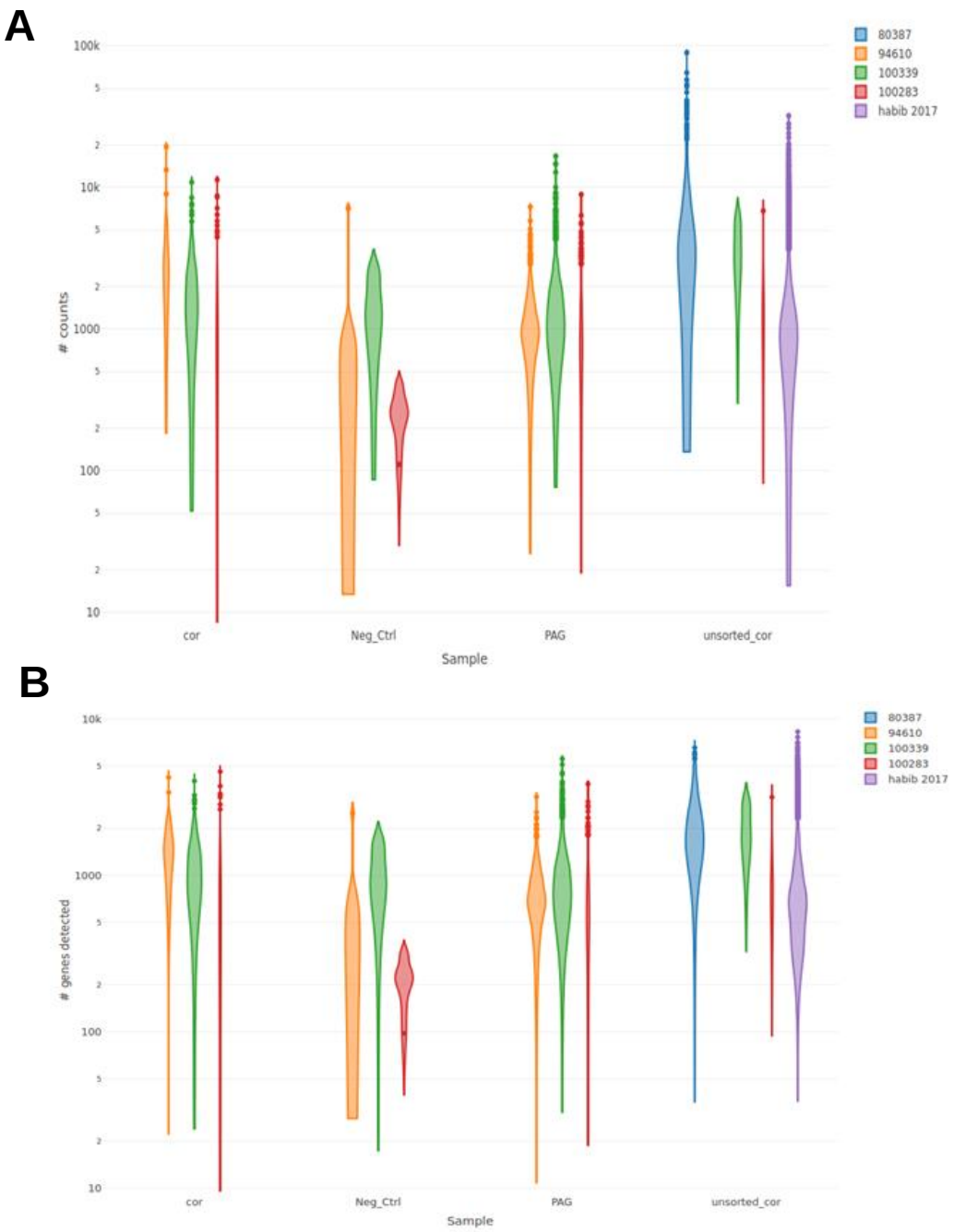

Supplementary Figure 3. Parameter optimisation for identification of highly variable genes (HVG). With each combination of threshold for mean expression and threshold for variance, a number of HVGs were selected (indicated at the top right of each t-SNE plot). PCA was performed with these genes and top 13PCs were selected for t-SNE visualisation. The t-SNE plots shown here, overlaid with colours identifying (A) source experiment and (B) sample, were used to qualitatively assess batch effects.

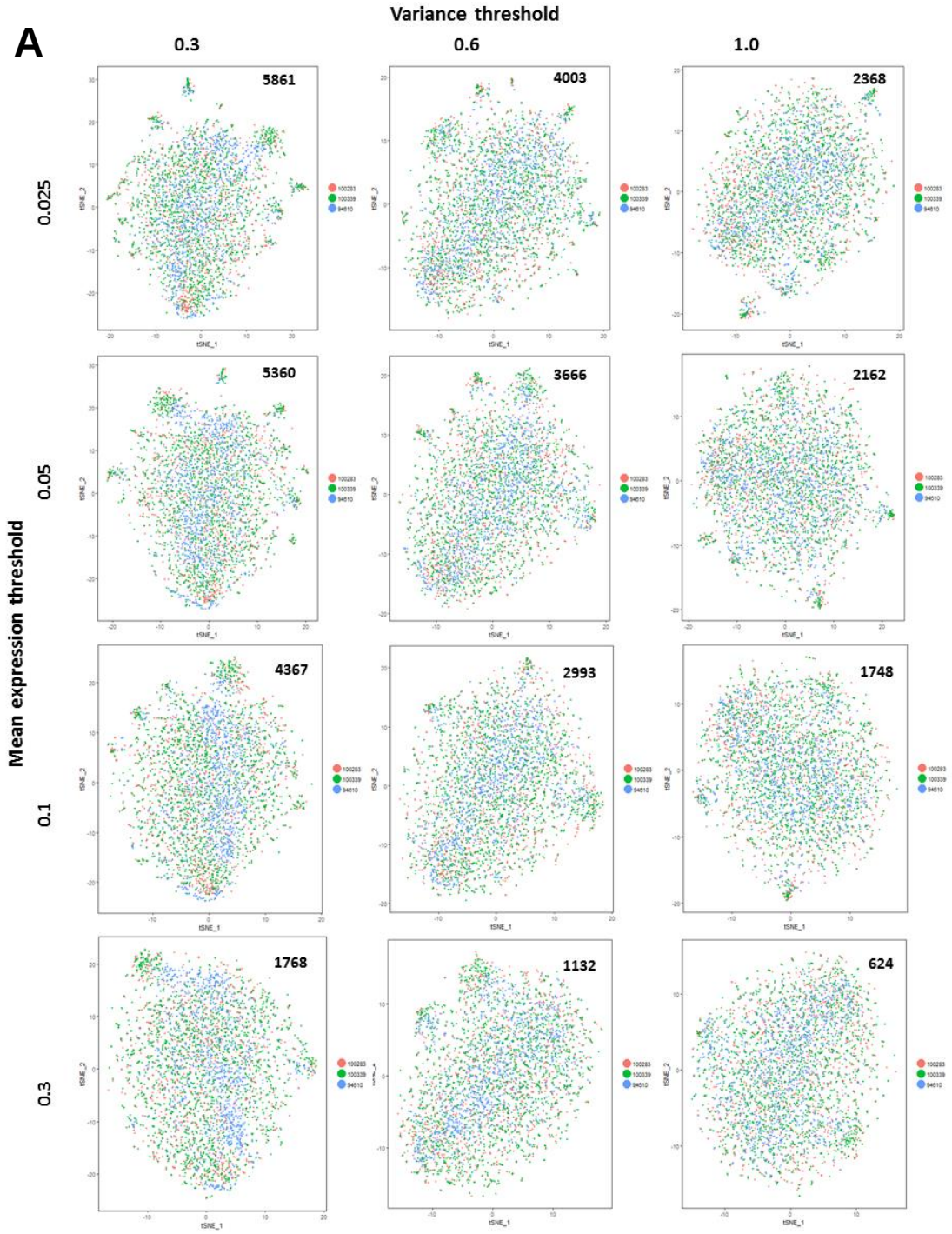

B

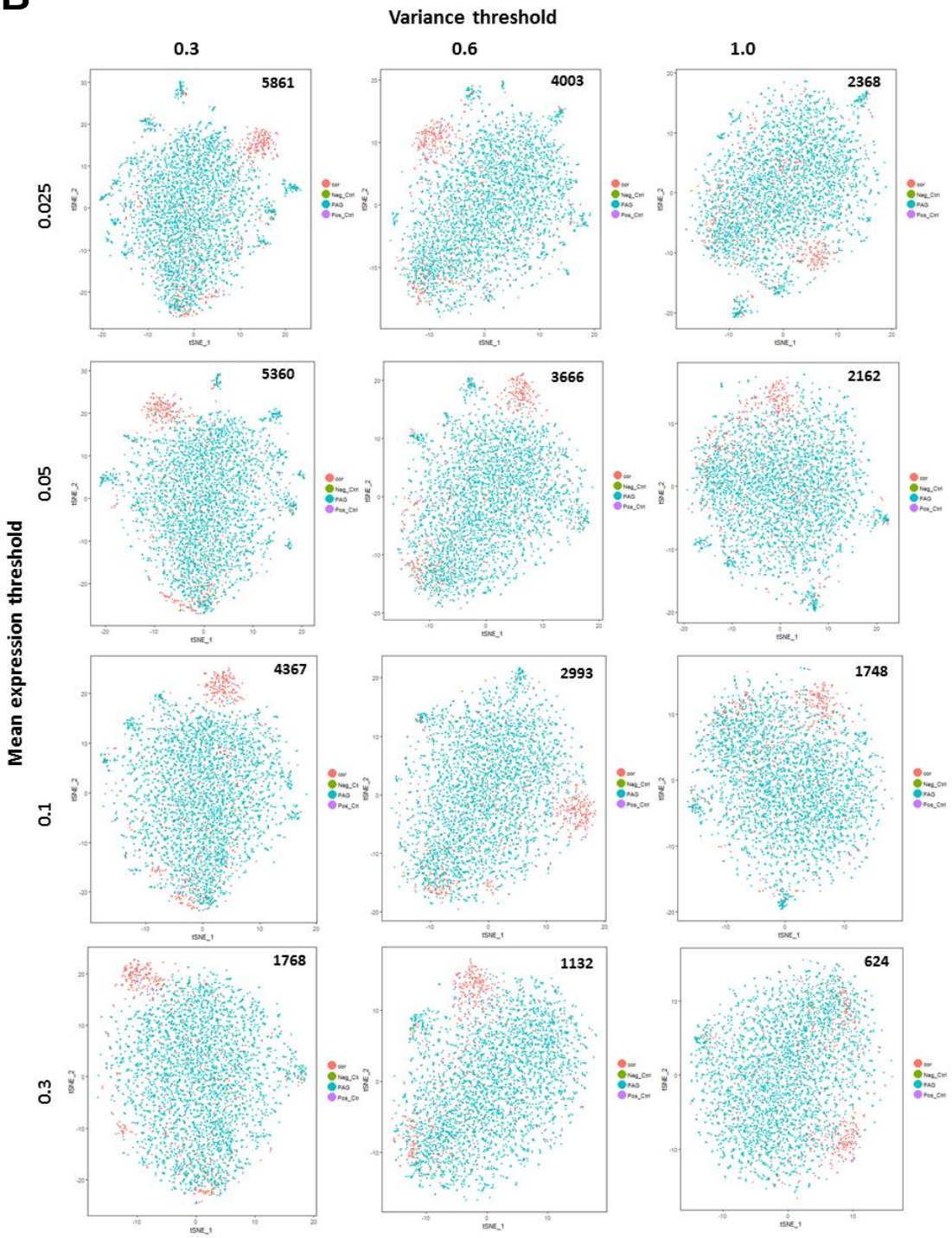
Variance threshold
0.3
0.6
1.0
Mean expression threshold
0.025
0.05
0.1
0.3
5861
4003
2368
5360
3666
2162
4367
2993
1748
1768
1132
624
tSNE_1
tSNE_2
cor
Neg_Ctrl
PAG
Pos_Ctrl

Supplementary Figure 4. Obtaining clutsering consensus with parameter space sampling. (A) t-SNE plots coloured with clustering results generated using each combination of resolution and k (no. of nearest neighbour). Number of resulting clusters vary between 6-16. (B) Heatmap showing dissimilarity score between each pair of nuclei; red: low dissimilarity (nuclei were always in the same cluster for all 20 of the clustering parameter sets sampled), yellow: high dissimilarity (nuclei were never in the same cluster). Dendrogram shows the result of hierarchical clustering based on dssimilarity matrix.

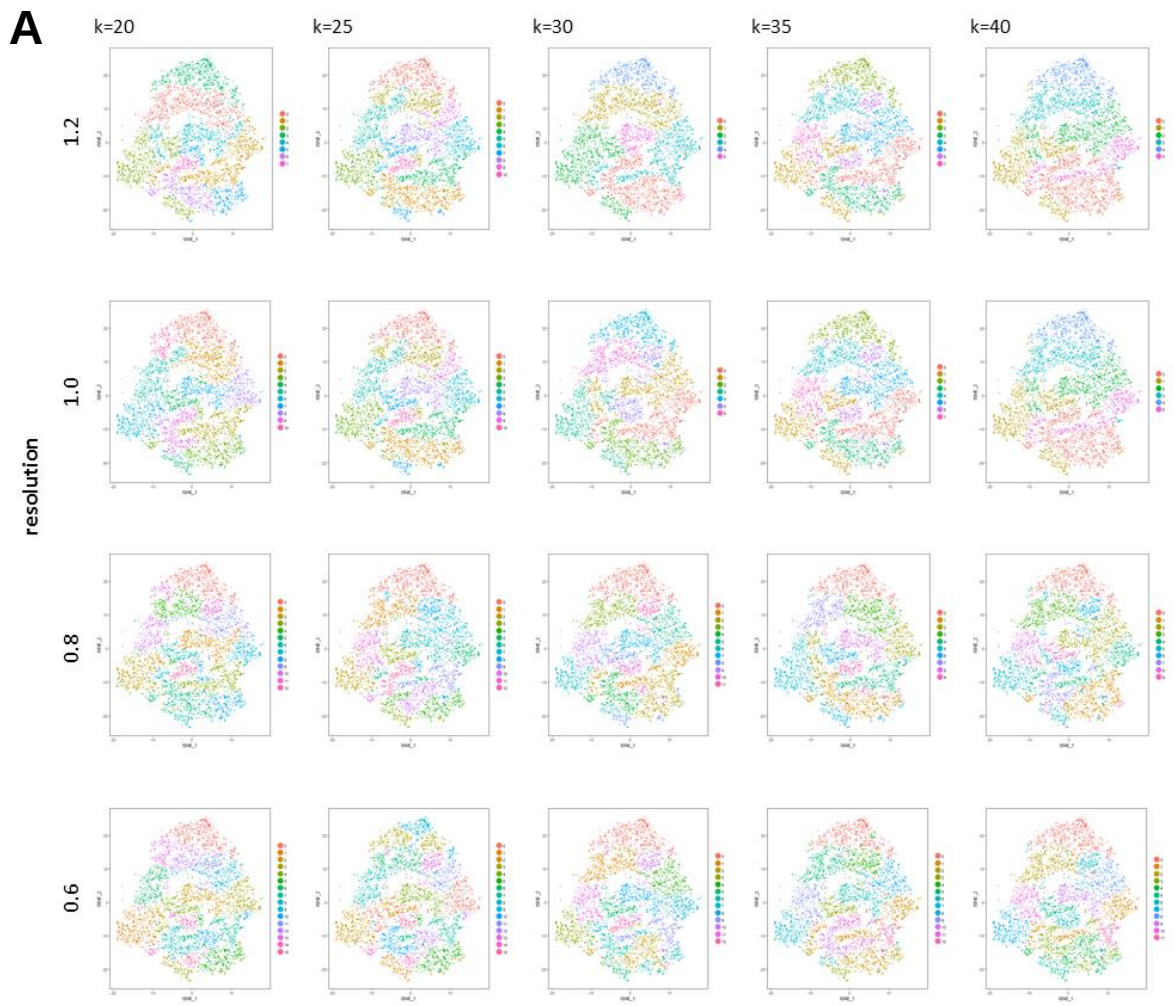

B

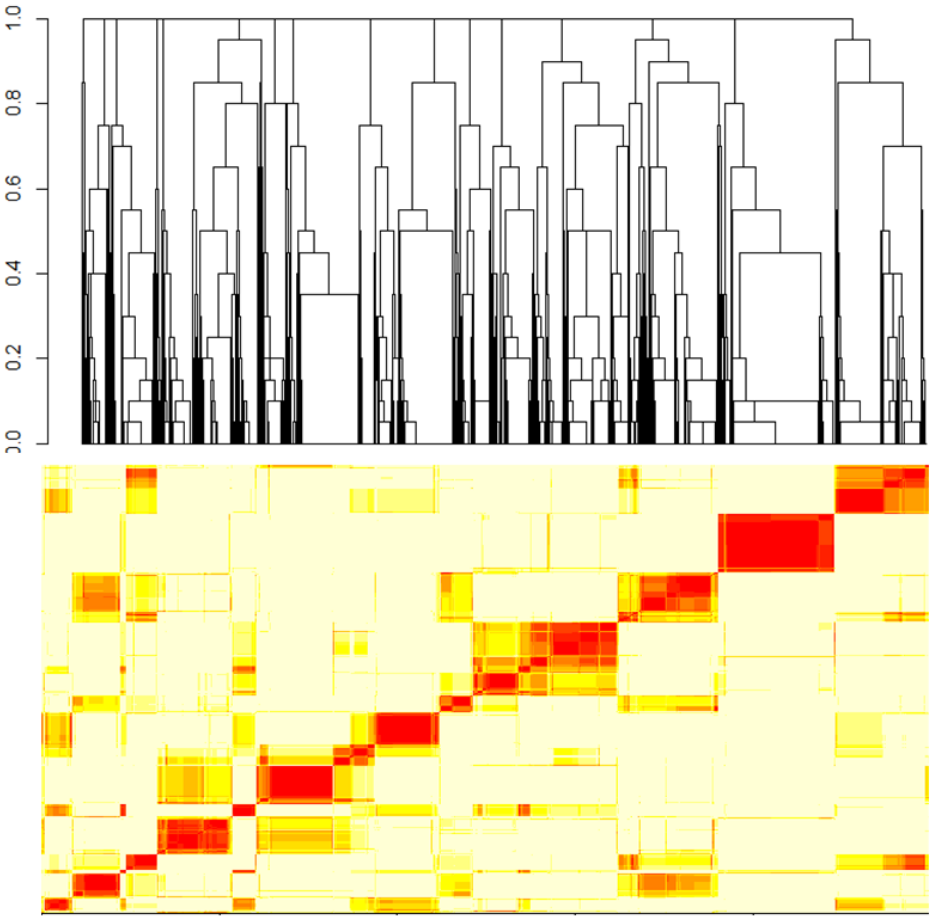

Supplementary Tables

Supplementary table 1. Experimental details for single nucleus RNA-seq experiments

Chip ID	80387	94610	100339	100283
Sample	428 unsorted cortical nuclei	148 FACS cortical neuronal nuclei 818 FACS PAG neuronal nuclei 10 -ve controls (empty)	178 FACS cortical neuronal nuclei 1431 FACS PAG neuronal nuclei 7 unsorted cortical nuclei 8 -ve controls (empty)	266 FACS cortical neuronal nuclei 763 FACS PAG neuronal nuclei 19 unsorted cortical nuclei 10 -ve controls (empty)
Total # reads	590,448,762	390,702,678	453,718,283	616,964,111
# assigned reads (% total reads)	387,662,992 (65.7%)	152,191,937 (39.0%)	238,859,771 (52.6%)	426,306,369 (69.1%)
Total # counts	4,647,859	5,445,545	3,171,520	1,343,813
# genes detected (detected in 2+ samples)	10,853	27,155	25,196	22,237

Supplementary table 2. Differentially expressed (positively and negatively) genes in clusters from unsupervised clustering, identified with the Wilcoxon rank sum test (see Methods). avg_logFC: average log fold change, p_val_adj: adjusted p-value; sorted by decreasing average log fold change for each cluster.

Gene	cluster	avg_logFC	p_val_adj
Ttc27	1	-0.2502751	8.78E-08
Gm44560	1	-0.2511775	0.0001535
BC018473	1	-0.2546092	3.67E-13
Gm26917	1	-0.2555185	3.96E-11
Gnao1	1	-0.2589773	0.0030615
Snrnp70	1	-0.261498	0.0316533
Fstl5	1	-0.2661952	1.48E-10
Klhl1	1	-0.2695991	7.12E-07
Rnf157	1	-0.2710031	0.0261414
Rnpc3	1	-0.2712517	0.0077909
Hs3st4	1	-0.2749809	2.62E-09
AW554918	1	-0.2839934	0.0121008
Ano4	1	-0.294864	4.32E-07
A330008L17Rik	1	-0.2962985	4.04E-05
Znhit1	1	-0.3002701	3.05E-14
Yeats2	1	-0.3076794	0.047005
Rbm6	1	-0.3173092	1.00E-06
Sema6d	1	-0.3312103	1.94E-10
Nfx1	1	-0.3795803	0.0225933
Gm12153	1	-0.5104025	0.0497444
Rgs7bp	3	-0.2700615	0.0414332
Gm12153	3	-0.7762041	6.48E-05
Khdrbs3	4	1.1072378	7.82E-25
Celf2	4	1.0023953	1.96E-49
Cnksr2	4	0.9860698	2.97E-44
Gm28928	4	0.9179439	6.36E-21
R3hdm1	4	0.8699126	1.49E-26
Camk2a	4	0.8096821	3.49E-33
Kctd16	4	0.7782876	7.23E-28
Phactr1	4	0.7730265	3.60E-26
Arpp21	4	0.7631238	1.69E-21
Homer1	4	0.7537475	1.10E-12
Mef2c	4	0.7492071	5.97E-15
Slit3	4	0.7106649	3.29E-26
Atp2b1	4	0.6821892	7.40E-22
Kalrn	4	0.6819554	4.74E-28
Pex5l	4	0.6626168	1.09E-09
Grin2a	4	0.660825	1.05E-25
Tcf4	4	0.6331361	8.93E-15
Mapk4	4	0.6313243	0.0116711
Ptprd	4	0.6037924	6.54E-21
Slc1a2	4	0.5964186	1.72E-19
Pde1a	4	0.594408	2.59E-11
Dlgap2	4	0.5817038	6.15E-20
Gpm6b	4	0.5689473	2.66E-12
Zeb2	4	0.5596588	7.97E-11
Kcnq5	4	0.5515329	2.80E-11
Fam19a1	4	0.5385901	6.61E-05
Nav3	4	0.5354676	3.44E-18
Kcnh7	4	0.5120035	6.72E-15
Sipa1l1	4	0.5065104	6.70E-07
Ankrd33b	4	0.4871822	1.53E-07
Syt1	4	0.4824627	1.40E-18
Grin2b	4	0.480558	1.03E-17
Pdzrn3	4	0.4772204	5.63E-07

Gene	cluster	avg_logFC	p_val_adj
Nell2	4	0.4152294	3.66E-06
Lrrk2	4	0.4133478	0.0004474
Mapk10	4	0.4131412	4.88E-08
Nlk	4	0.4099983	1.21E-06
Slc8a1	4	0.39938	2.12E-07
Dlgap1	4	0.3989807	2.11E-16
Wdr17	4	0.3972731	0.0028895
Iqgap2	4	0.3970351	4.32E-06
Mical2	4	0.3945663	0.0018401
Neto1	4	0.3945031	0.0001029
Sv2b	4	0.3874784	6.21E-06
Chsy3	4	0.3873538	3.57E-05
Grm3	4	0.386166	0.0132527
Dclk1	4	0.3857699	0.0004832
Nwd2	4	0.3832581	9.02E-08
Kcnb1	4	0.37156	0.00133
Arhgef37	4	0.3706433	1.26E-07
Kcnq3	4	0.3689806	0.0003576
Slc24a2	4	0.3667126	7.80E-06
Nfix	4	0.3654761	0.0005627
Fam81a	4	0.3639759	6.27E-13
Gria2	4	0.3618739	5.40E-12
Acap2	4	0.3616233	5.97E-07
Adcy2	4	0.3608753	2.17E-05
Prmt8	4	0.3595903	0.0062909
Erc2	4	0.3595203	2.68E-09
Hivep2	4	0.3594313	0.0007398
Lrrc7	4	0.3593581	2.23E-09
Braf	4	0.3588746	0.0003232
St3gal5	4	0.358101	0.0120866
Gria3	4	0.3561679	4.16E-05
Trim9	4	0.3529497	2.10E-06
Setbp1	4	0.347279	4.95E-09
Dlgap3	4	0.3455095	1.17E-05
Rnf165	4	0.3439329	0.0010772
Itga8	4	0.3430395	0.0002858
Opcml	4	0.339988	2.07E-06
Sept7	4	0.3361248	0.0002973
Nin	4	0.3356889	0.0005025
Large1	4	0.3346977	1.51E-07
Nrp1	4	0.3280298	3.83E-06
Nrgn	4	0.3271589	1.21E-09
Nfib	4	0.3265856	0.0067195
Nptn	4	0.3247719	0.0437189
Prkag2	4	0.3190671	3.78E-05
Lmo4	4	0.3186224	1.13E-05
Cdh10	4	0.3175909	0.0133925
Hcn1	4	0.3160117	0.0024599
Rock2	4	0.3100529	0.0249368
Iqsec2	4	0.3088445	0.0010647
Dlg2	4	0.3085584	7.89E-09
Nckap1	4	0.3073091	0.0002163
Snap25	4	0.3070251	1.87E-05
Prickle1	4	0.3056761	0.0060619
Plcl2	4	0.3031303	9.00E-10

Supplementary Tables

Gene	cluster	avg_logFC	p_val_adj
Sorbs2	4	0.4752616	2.66E-11
Tspan5	4	0.4686743	1.01E-07
Msra	4	0.4678344	2.12E-06
Satb2	4	0.4668447	1.36E-09
Ppm1e	4	0.4640744	5.29E-09
Brinp1	4	0.4605164	4.83E-12
Kcnip4	4	0.4567301	7.21E-14
Slc17a7	4	0.445936	2.48E-22
Cdh11	4	0.4198904	0.0019645
3110035E14Rik	4	0.4189534	6.20E-22
Plcb1	4	0.4183795	3.47E-11
Lhfp	4	0.3023766	0.0004038
Ltn1	4	0.3010706	0.006086
Baiap2	4	0.301005	0.0144225
Arap2	4	0.2981753	1.03E-05
Gda	4	0.2964938	0.0092552
Fam212b	4	0.2926101	4.81E-07
Dgkg	4	0.2913764	0.0273832
Lmo7	4	0.2896711	0.0005685
Itpr1	4	0.2895224	0.0124871
Cfap77	4	0.2866457	6.29E-05
Kctd1	4	0.2851996	0.0196319
Frmd6	4	0.2850412	0.0006923
Rasgrp1	4	0.2841451	0.0007894
Phf24	4	0.2818949	0.0144908
Mir9-3hg	4	0.2814144	0.0050164
Pcsk2	4	0.2806848	9.07E-08
Csmd1	4	0.280132	4.15E-12
Nrxn3	4	0.279792	5.25E-08
Nrcam	4	0.2781316	0.0130272
Cap2	4	0.2765362	0.0298945
Etl4	4	0.2765228	0.0002149
Arsb	4	0.2756174	0.0005714
Adcy9	4	0.2737349	2.37E-06
Fbxw7	4	0.273628	0.0294576
Man1c1	4	0.2734209	0.0002527
Kcnt2	4	0.2697415	0.0056632
Tnrc6c	4	0.2681827	3.75E-06
Gabra4	4	0.2679248	0.0041164
Kcnj3	4	0.2667561	0.0004222
Xylt1	4	0.2653296	0.0041757
Vwa1	4	0.2652377	0.0008857
Rap1gds1	4	0.2636445	0.0296404
Olfm1	4	0.2620744	4.12E-06
Senp2	4	0.2620588	0.04808
Anks1b	4	0.2612828	9.59E-06
Camk4	4	0.2591621	0.0005794
Prickle2	4	0.2590068	0.0001166
Pde10a	4	0.2588254	0.0022546
Cdh12	4	0.2584627	0.0308964
Dlg1	4	0.2561646	0.008198
Kcnma1	4	0.2553957	0.0003215
Calm2	4	0.2517096	0.0002398
Meg3	4	-0.2575136	7.71E-12
Cdh18	4	-0.4508105	1.59E-08
Htr2c	4	-0.5774612	0.0072315
C130073E24Rik	4	-0.8357395	0.0001975
Gm12153	5	2.6821681	2.70E-84
Gm38058	5	2.3399981	7.68E-63

Gene	cluster	avg_logFC	p_val_adj
Spsb4	5	2.1213391	3.23E-23
Gm26641	5	2.0998845	9.70E-116
Rspo1	5	1.7953555	2.93E-32
4921507P07Rik	5	1.4236715	5.89E-50
Dock1	5	1.2409093	1.80E-12
Map4k1	5	1.2385917	6.63E-22
Mfsd4a	5	1.2330872	1.58E-09
Lnx2	5	1.1145493	1.70E-08
Hipk3	5	1.0501361	1.05E-09
Stxbp3-ps	5	0.9924418	7.18E-24
Ephx2	5	0.9312901	2.27E-28
Slc25a26	5	0.9146774	6.32E-06
Trim39	5	0.8614655	1.10E-11
Tsc22d4	5	0.7387553	0.0332947
Adk	5	0.6977548	1.92E-08
Scn2b	5	0.659001	0.0202255
Etohd2	5	0.5288426	1.55E-17
Dnaaf1	5	0.5187507	2.88E-05
Prkar2b	5	0.4711469	7.99E-06
Stxbp3	5	0.4510653	4.58E-09
Abcg2	5	0.4122517	3.77E-11
Fgf6	5	0.3914275	1.32E-14
Cwc22	5	0.3502902	0.0005339
Clec2g	5	0.3389498	5.39E-09
Lipc	5	0.337229	0.0010633
Plekhh1	5	0.3172077	0.0291356
Fam222a	5	0.3150393	7.55E-09
Gm45470	5	0.3086277	0.0041593
Tnp1	5	0.2972928	7.03E-22
Capn13	5	0.2670704	3.53E-05
Gm20658	5	0.2584553	6.41E-06
Mypopos	5	0.2542453	1.04E-12
Rps14	6	2.220813	1.51E-201
Gm6204	6	2.1370159	0
Gm5805	6	2.0832601	0
Gm12025	6	1.153802	1.70E-169
Rpl35	7	2.0645903	0
Gm10269	7	1.9649423	0
Gm2000	7	1.723789	0
Gm8444	7	1.2463165	7.61E-185
Gm15607	7	1.0924615	5.95E-181
Pinx1	7	0.5497858	0.0060102

Supplementary Table 3. List of neuronal function related candidate genes used for supervised clustering

Ache	Chga	Gad1	Htr2c	Kcnq5	Rxfp3	Slc41a2	Vipr2
Adcyap1	Chgb	Gad2	Htr3a	Kcns1	Ryr1	Slc44a5	Wnt4
Adcyap1r1	Chrm1	Gal	Htr3b	Kcns2	Ryr2	Slc45a1	
Adra1a	Chrm2	Galp	Htr4	Kcns3	Ryr3	Slc4a10	
Adra1d	Chrm3	Galr1	Htr5a	Kcnt2	Scg2	Slc4a3	
Adra2a	Chrm4	Galr2	Htr5b	Kcnv1	Scn1a	Slc5a5	
Adra2b	Chrm5	Gast	Htr7	Kcnv2	Scn1b	Slc5a7	
Adra2c	Chrna1	Gcg	Itpr1	Kiss1r	Scn2b	Slc6a1	
Adrb1	Chrna2	Gcgr	Kcna1	Mc4r	Scn3a	Slc6a11	
Adrbk2	Chrna3	Gjd2	Kcna4	Mchr1	Scn3b	Slc6a15	
Ano3	Chrna4	Glp1r	Kcna6	Mmd	Scn4b	Slc6a17	
Asic1	Chrna5	Glra1	Kcnab1	Mtch1	Scn5a	Slc6a2	
Asic2	Chrna6	Glra2	Kcnab2	Nalcn	Scn8a	Slc6a3	
Avp	Chrna7	Glra3	Kcnab3	Nenf	Scn9a	Slc6a4	
Avpr1a	Chrna8	Glra4	Kcnb1	Nos1	Scnn1a	Slc6a7	
Avpr1b	Chrna9	Glrb	Kcnb2	Npffr1	Slc12a5	Slc6a9	
Cacna1a	Chrnb1	Gls2	Kcnc1	Nppc	Slc16a11	Slc7a14	
Cacna1b	Chrnb2	Got1	Kcnc2	Npy	Slc16a14	Slc7a4	
Cacna1c	Chrnb3	Gria1	Kcnc3	Npy1r	Slc17a6	Slc8a2	
Cacna1d	Chrnd	Gria2	Kcnc4	Npy2r	Slc17a7	Slc8a3	
Cacna1e	Chrng	Gria3	Kcnd2	Npy5r	Slc17a8	Slc9a5	
Cacna1g	Clcn1	Gria4	Kcnd3	Nts	Slc18a1	Sst	
Cacna1g	Clic6	Grik1	Kcnf1	Ntsr1	Slc18a2	Sstr2	
Cacna1h	Cngb1	Grik2	Kcng1	Nxph2	Slc18a3	Sstr3	
Cacna1i	Cnr1	Grik3	Kcng2	Nxph3	Slc1a2	Sstr4	
Cacna2d1	Cntn1	Grik4	Kcng3	Nxph4	Slc1a3	Sstr5	
Cacna2d2	Cort	Grik5	Kcng4	Oprd1	Slc1a6	Tac1	
Cacna2d3	Crh	Grin1	Kcnh1	Oprk1	Slc24a1	Tac2	
Cacnb1	Crhr1	Grin2b	Kcnh2	Oprl1	Slc24a3	Tacr1	
Cacnb2	Crhr2	Grin2d	Kcnh3	Oprm1	Slc25a16	Tacr3	
Cacnb3	Cx3cl1	Grin3a	Kcnh4	Oxt	Slc25a18	Th	
Cacnb4	Drd1a	Grin3b	Kcnh5	Oxtr	Slc25a22	Trh	
Cacng2	Drd2	Grm1	Kcnh7	P2ry12	Slc25a23	Trhr	
Cacng3	Drd3	Grm2	Kcnh8	Paqr9	Slc25a25	Trpc1	
Cacng4	Drd4	Grm4	Kcnj14	Pdyn	Slc25a39	Trpc3	
Cacng5	Fgf1	Grm5	Kcnj3	Penk	Slc27a2	Trpc4	
Cacng7	Fgf2	Grm7	Kcnj4	Pgrmc1	Slc29a4	Trpc5	
Calm2	Fgf9	Grm8	Kcnj5	Pmch	Slc2a13	Trpc6	
Calm3	Gabbr1	Gucy2g	Kcnj6	Pnoc	Slc2a6	Trpc7	
Cartpt	Gabra1	Hcn1	Kcnj9	Pomc	Slc30a3	Trpm2	
Cbln1	Gabra2	Hcn2	Kcnk1	Prokr2	Slc30a9	Trpv1	
Cbln2	Gabra3	Hcn3	Kcnk12	Ptger4	Slc32a1	Trpv2	
Cbln4	Gabra4	Hcn4	Kcnk2	Pthlh	Slc35d3	Trpv3	
Cck	Gabra5	Hcrtr1	Kcnk3	Qrfpr	Slc35f3	Trpv4	
Cckar	Gabrb2	Hcrtr2	Kcnk4	Rac3	Slc35f4	Ubl5	
Cckbr	Gabrb3	Hrh1	Kcnma1	Retn	Slc36a4	Ucn3	
Ccl17	Gabrd	Hrh2	Kcnmb4	Rimkla	Slc37a1	Vdac1	
Ccl25	Gabrg2	Hrh3	Kcnq2	Rln1	Slc38a1	Vgf	
Ccl27a	Gabrg3	Htr1a	Kcnq3	Rspo1	Slc38a4	Vip	
Cd274	Gabrq	Htr1b	Kcnq4	Rspo3	Slc3a1	Vipr1	

Supplementary Table 4. Candidate genes differentially expressed (positively and negatively) in clusters from supervised clustering. avg_logFC: average log fold change, p_val_adj: adjusted p-value; sorted by decreasing average log fold change for each cluster.

Gene	Cluster	avg_logFC	p_val_adj
Grm4	1	-0.271133213	0.04611428
Chrm3	1	-0.275100471	3.95E-12
Cacna1b	1	-0.279665949	1.37E-09
Trpc6	1	-0.284261141	0.03055465
Slc44a5	1	-0.286568763	7.06E-05
Cacna1c	1	-0.299650546	5.90E-25
Ryr2	1	-0.314709085	8.65E-24
Glra2	1	-0.323842451	0.02093158
Grm1	1	-0.328107133	2.02E-15
Nos1	1	-0.329854955	0.00012207
Oprm1	1	-0.36171249	5.90E-05
Grm8	1	-0.381472662	1.05E-21
Scg2	1	-0.398100042	0.00200604
Slc24a3	1	-0.406112951	1.36E-17
Kcnc2	1	-0.436457396	1.27E-24
Glra3	1	-0.498345076	2.02E-11
Grik2	1	-0.551382636	3.51E-48
Cacna1d	1	-0.552386341	4.03E-26
Trpc4	1	-0.577324365	1.29E-13
Tacr1	2	0.736377516	2.01E-11
Kcnc2	2	0.551920491	9.49E-08
Glra3	2	0.499073611	1.12E-05
Gad2	2	0.482804013	9.56E-07
Nos1	2	0.475320954	2.23E-06
Fgf9	2	0.389635633	9.42E-05
Vipr2	2	0.36860857	1.29E-10
Grm1	2	0.355429273	0.00708389
Cbln1	2	0.318864652	2.84E-06
Cacna1d	2	0.314686748	0.00087273
Ano3	2	0.290921916	0.00606097
Cacna1i	2	0.289369206	0.00332353
Cacna1g	3	0.442406845	2.44E-05
Trpm2	3	0.411192297	0.00041671
Glra1	3	0.333622204	0.01013062
Glrb	3	0.316046776	0.01221213
Scn5a	3	0.313030948	1.13E-06
Htr2c	3	0.308779266	0.00060771
Gabra2	3	0.292072702	6.52E-05
Grm7	3	0.261430662	5.63E-07
Gria4	4	-0.449699713	0.00023484
Cacna1d	5	-0.402398067	0.00793805
Kcnh7	5	-0.423778654	0.00134667
Ryr2	5	-0.455006493	5.60E-06
Kcnq5	5	-0.513525675	0.00656946
Grin2b	5	-0.651676598	6.23E-06
Slc6a4	9	1.493905672	7.93E-53
Slc18a2	9	1.021245425	9.42E-79
Scn9a	9	0.53359565	2.64E-08
Slc17a8	9	0.499445018	2.73E-11
Slc37a1	9	0.48475827	2.49E-09
Glra2	9	0.477814315	2.25E-05
Scg2	9	0.416158141	0.00796005
Kcns3	9	0.384102047	4.78E-05
Gria4	9	0.33110175	0.00553615
Cntn1	9	0.310246751	0.00042661
Grik2	9	0.283659958	0.00027473
Gria3	9	-0.49989525	0.00386102
Chrm3	9	-0.591598881	0.0012179
Adcyap1r1	11	0.458598271	0.00061502
Cacna1d	11	0.402884294	0.00672772
Slc1a2	12	0.577964586	3.19E-20
Slc17a7	12	0.569782688	9.80E-27
Hcn1	12	0.555200475	7.06E-12
Kcnq5	12	0.532623088	1.28E-13

Gene	Cluster	avg_logFC	p_val_adj
Gria3	12	0.5109062	4.26E-15
Kcnh7	12	0.5027072	1.08E-14
Grin2b	12	0.4557411	6.24E-17
Kcnb1	12	0.4419423	1.17E-06
Gabbr1	12	0.4205838	9.98E-06
Kcnq3	12	0.4132489	4.01E-08
Gabra4	12	0.4075009	0.0012685
Gria2	12	0.3812466	1.56E-16
Cacna1e	12	0.3530218	7.43E-09
Gria1	12	0.3513094	1.02E-05
Kcnj9	12	0.3500128	1.56E-05
Ryr3	12	0.3495989	0.0002584
Itpr1	12	0.334162	0.016251
Kcnma1	12	0.332967	9.46E-07
Kcnt2	12	0.3180017	0.0044526
Grm5	12	0.3120652	5.04E-08
Ryr2	12	0.276443	3.38E-07
Cacnb4	12	0.2688833	0.0137425
Scn2b	12	-0.5527984	0.0015373
Htr2c	12	-0.6501452	0.0130931
Scg2	13	0.8042828	0.0029551
Itpr1	14	0.3467101	2.35E-06
Kcnmb4	14	0.3392197	1.36E-06
Kcnc2	14	-0.4872601	0.0108152
Gad2	16	0.5463407	0.0005631
Scn9a	16	0.5454588	0.0323833
Htr2c	16	0.4576824	0.0307387
Kcnh2	16	0.4363855	6.50E-09
Glra3	17	0.5179974	0.0085421
Kcng3	17	0.4981029	1.80E-06
Htr2c	17	0.3850092	0.0099214
Kcnc2	17	0.3695433	0.0001511
Gabra3	17	0.3564226	0.0166226
Chrm3	17	0.326552	0.0190615
Grik2	17	0.2980376	0.0088926
Grm5	17	0.2838142	0.0001796
Glrb	19	0.4542228	0.0002365
Grm8	19	0.4083768	3.46E-05
Cacna1b	19	0.3982328	0.0017381
Kcnc2	19	0.356771	0.0114109
Scn1a	19	0.3548762	7.84E-06
Grm5	19	0.3415635	1.27E-05
Asic2	19	0.3211978	1.18E-05
Kcnh7	19	0.2872754	0.0036827
Ryr2	19	0.2724328	0.0023532
Kcnj3	19	0.2722744	0.0073418
Scn2b	20	0.8183231	9.67E-12
Rspo1	20	0.7305368	3.76E-05
Cacna1d	20	0.6432573	5.41E-11
Glra3	20	0.6036954	8.51E-07
Glra2	20	0.5999233	0.0153815
Trpc4	20	0.5457199	0.000118
Grm1	20	0.4582889	1.36E-05
Grm4	20	0.4477537	5.64E-08
Slc1a3	20	0.4011131	0.0039166
Slc44a5	20	0.3987389	0.0158658
Nos1	20	0.3867655	0.000419
Drd3	20	0.3830986	1.94E-07
Hcn4	20	0.2947751	0.0135375
Vipr2	20	0.2934019	0.000305
Adra1d	20	0.2900361	1.29E-06
Drd2	20	0.2660132	0.0238335
Cacna2d3	20	0.2630336	0.0287692
Fgf9	20	0.2573767	0.0009836

Supplementary Table 5. Non-candidate genes positively enriched in clusters from supervised clustering; due to large numbers this list only shows, for each cluster, top 10 genes of highest average log fold change. avg_logFC: average log fold change, p_val_adj: adjusted p-value; sorted by decreasing average log fold change for each cluster.

Gene	cluster	avg_logFC	p_val_adj
Cask	1	0.407046097	0.0313004
Tmem161b	1	0.395577829	0.00631211
2010111I01Rik	1	0.389765825	0.02181285
Zcchc18	1	0.385723285	0.02432402
2410089E03Rik	1	0.372682852	0.0013903
Xpo7	1	0.363387918	0.00088086
Atp8a1	1	0.360404058	0.00697682
Ssbp2	1	0.345611427	0.00019077
Snap91	1	0.335349707	0.00026082
Mapk10	1	0.325880517	1.56E-06
Wdr49	3	0.301067492	0.00667717
Mrap	4	0.40405961	0.00086753
Gm31135	4	0.39911057	0.02970752
Npdc1	4	0.334688398	0.04578635
Gm11823	7	0.348327804	0.02115154
Olfm3	8	0.394435506	0.02339812
Fnip2	8	0.380859056	0.01451583
Tph2	9	0.938693537	0.00015334
Dach1	9	0.454538481	0.00578412
Megf8	9	0.450999544	0.01121482
Vwa5b1	9	0.334038565	0.00965336
3300002A11Rik	9	0.331232165	4.40E-05
Maob	9	0.317867714	0.00033205
Celf2	12	0.812367444	1.12E-28
Cnksr2	12	0.76733642	2.81E-15
Gm28928	12	0.717599598	1.57E-11
Phactr1	12	0.664378559	2.35E-16
Grin2a	12	0.651078331	6.66E-19
R3hdm1	12	0.640627011	2.71E-10
Camk2a	12	0.636664106	1.85E-15
Pex5l	12	0.626540619	1.73E-07
Kalrn	12	0.559381378	2.39E-13
Arpp21	12	0.558878114	3.39E-09
Crb1	13	0.584097488	0.04941206
Dyrk4	13	0.324857482	0.02351834
Xpnpep1	14	0.268267496	0.00042455
Ncald	14	0.260412389	0.0449692
Fam186a	16	0.362625502	0.000677
Tmem132c	17	0.39915642	0.03236239
Gm8098	17	0.317681096	0.01913915
Shisa7	19	0.429480438	0.04449747
Erbb4	19	0.388195818	0.01401343
Znhit1	19	0.335909136	3.84E-05
Gdpd4	19	0.316389666	0.04786344
Gm26871	19	0.312898382	0.00178823
Gm42826	19	0.29218716	0.00203392
Cntnap2	19	0.27656149	0.00027659
Mgat4c	19	0.276042854	0.02111107
Lingo2	19	0.26462373	5.29E-05
Gbp7	19	0.263561174	0.00218357
Ak7	20	0.966591747	0.02635967
Gzmm	20	0.757485153	1.69E-09
Ckm	20	0.75570413	5.24E-09
Gm40123	20	0.747962898	1.08E-09
Ypel5	20	0.746284935	1.21E-12
D830032E09Rik	20	0.73243605	9.91E-08
Kyat3	20	0.729662284	2.19E-07
Fyb2	20	0.708828278	9.84E-06
Lhx5	20	0.708626197	9.67E-06
2810471M01Rik	20	0.706676687	2.08E-06